Article

Cell

Slow Delivery Immunization Enhances HIV Neutralizing Antibody and Germinal Center Responses via Modulation of Immunodominance

Graphical Abstract

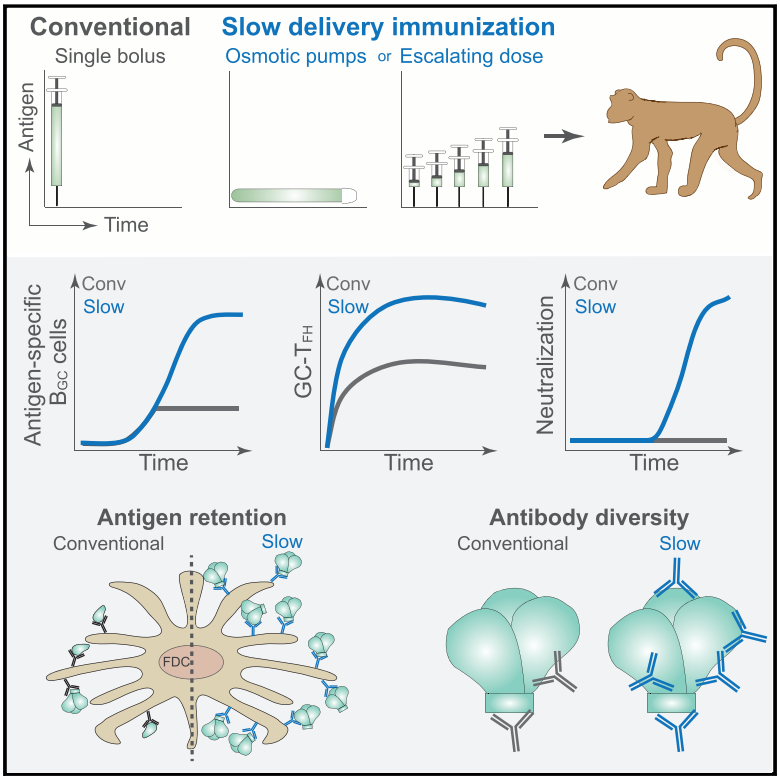

Authors

Kimberly M. Cirelli, Diane G. Carnathan, Bartek Nogal, ..., Guido Silvestri, Darrell J. Irvine, Shane Crotty

Correspondence

shane@lji.org

In Brief

An integrated immunological, bioinformatic and imaging approach demonstrates how slow delivery immunization enhances neutralizing antibody and germinal center reactions over conventional strategies in response to HIV Env protein immunization in non-human primates.

Highlights

- Slow delivery immunization enhances HIV neutralizing antibody development in monkeys
- Slow delivery immunization alters immunodominance of the responding B cells
- Weekly longitudinal germinal center (GC) B and T_{FH} analyses provides new GC insights
- High-resolution rhesus immunoglobulin locus genomic reference sequence

Cirelli et al., 2019, Cell *177*, 1–19
May 16, 2019
https://doi.org/10.1016/j.cell.2019.04.012

CellPress

Please cite this article in press as: Cirelli et al., Slow Delivery Immunization Enhances HIV Neutralizing Antibody and Germinal Center Responses via Modulation of Immunodominance, Cell (2019), https://doi.org/10.1016/j.cell.2019.04.012

Cell

Slow Delivery Immunization Enhances HIV Neutralizing Antibody and Germinal Center Responses via Modulation of Immunodominance

Kimberly M. Cirelli,[1,2] Diane G. Carnathan,[2,3,4] Bartek Nogal,[2,5] Jacob T. Martin,[2,6] Oscar L. Rodriguez,[7] Amit A. Upadhyay,[3] Chiamaka A. Enemuo,[3,4] Etse H. Gebru,[3,4] Yury Choe,[3,4] Federico Viviano,[3,4] Catherine Nakao,[1] Matthias G. Pauthner,[2,8] Samantha Reiss,[1,2] Christopher A. Cottrell,[2,5] Melissa L. Smith,[7] Raiza Bastidas,[2,8] William Gibson,[9] Amber N. Wolabaugh,[3] Mariane B. Melo,[2,6] Benjamin Cossette,[6] Venkatesh Kumar,[10] Nirav B. Patel,[11] Talar Tokatlian,[2,6] Sergey Menis,[2,8] Daniel W. Kulp,[2,8,12] Dennis R. Burton,[2,8,13] Ben Murrell,[10,14] William R. Schief,[2,8,13] Steven E. Bosinger,[3,11] Andrew B. Ward,[2,5] Corey T. Watson,[9] Guido Silvestri,[2,3,4] Darrell J. Irvine,[2,6,13,15] and Shane Crotty[1,2,10,16,*]

[1]Division of Vaccine Discovery, La Jolla Institute for Immunology (LJI), La Jolla, CA 92037, USA
[2]Center for HIV/AIDS Vaccine Immunology and Immunogen Discovery (Scripps CHAVI-ID), The Scripps Research Institute, La Jolla, CA 92037, USA
[3]Yerkes National Primate Research Center, Emory University, Atlanta, GA 30322, USA
[4]Emory Vaccine Center, Emory University School of Medicine, Atlanta, GA 30322, USA
[5]Department of Integrative Structural and Computational Biology, The Scripps Research Institute, La Jolla, CA 92037, USA
[6]Koch Institute for Integrative Cancer Research, Massachusetts Institute of Technology, Cambridge, MA 02139, USA
[7]Department of Genetics and Genomic Sciences, Icahn School of Medicine at Mount Sinai, New York, NY 10029, USA
[8]Department of Immunology and Microbiology, The Scripps Research Institute, La Jolla, CA 92037, USA
[9]Department of Biochemistry and Molecular Genetics, University of Louisville School of Medicine, Louisville, KY 40202, USA
[10]Department of Medicine, University of California, San Diego, La Jolla, CA 92037, USA
[11]Yerkes NHP Genomics Core Laboratory, Yerkes National Primate Research Center, Atlanta, GA 30329, USA
[12]Vaccine and Immunotherapy Center, Wistar Institute, Philadelphia, PA 19104, USA
[13]Ragon Institute of Massachusetts General Hospital, Massachusetts Institute of Technology, and Harvard University, Cambridge, MA 02139, USA
[14]Department of Microbiology, Tumor and Cell Biology, Karolinska Institutet, Stockholm, Sweden
[15]Departments of Biological Engineering and Materials Science and Engineering, Massachusetts Institute of Technology, Cambridge, MA 02139, USA
[16]Lead Contact
*Correspondence: shane@lji.org
https://doi.org/10.1016/j.cell.2019.04.012

SUMMARY

Conventional immunization strategies will likely be insufficient for the development of a broadly neutralizing antibody (bnAb) vaccine for HIV or other difficult pathogens because of the immunological hurdles posed, including B cell immunodominance and germinal center (GC) quantity and quality. We found that two independent methods of slow delivery immunization of rhesus monkeys (RMs) resulted in more robust T follicular helper (T_{FH}) cell responses and GC B cells with improved Env-binding, tracked by longitudinal fine needle aspirates. Improved GCs correlated with the development of >20-fold higher titers of autologous nAbs. Using a new RM genomic immunoglobulin locus reference, we identified differential IgV gene use between immunization modalities. Ab mapping demonstrated targeting of immunodominant non-neutralizing epitopes by conventional bolus-immunized animals, whereas slow delivery-immunized animals targeted a more diverse set of epitopes. Thus, alternative immunization strategies can enhance nAb development by altering GCs and modulating the immunodominance of non-neutralizing epitopes.

INTRODUCTION

The majority of licensed vaccines provide protection through induction of protective antibodies (Plotkin, 2010). Isolation of HIV-1 broadly neutralizing antibodies (bnAbs) from HIV-infected individuals and the finding that passive transfer of bnAbs can protect non-human primates (NHPs) from simian/human immunodeficiency virus (SHIV) infection support the feasibility of an antibody-based HIV vaccine (Burton and Hangartner, 2016; Nishimura and Martin, 2017). Elicitation of neutralizing antibodies (nAbs) against clinically relevant HIV strains (i.e., tier 2 and tier 3 strains) by immunization has been difficult (Montefiori et al., 2018). Much of that challenge centers on structural features of the HIV envelope (Env), which have complex and incompletely understood immunological implications. Env consists of gp120 and gp41 components that form a trimeric spike that is the only viral protein on HIV virions and the only target for

nAbs (Burton and Hangartner, 2016). Human immunization with monomeric gp120 has failed to elicit tier 2 nAbs in clinical trials (Haynes et al., 2012; Mascola et al., 1996; Rerks-Ngarm et al., 2009). The reasons for this are not obvious because nAb epitopes are present on gp120. Key developments in protein design have been made toward the expression of soluble native-like HIV Env trimers (Julien et al., 2013; Kulp et al., 2017; Lyumkis et al., 2013; Sanders et al., 2013). Immunization with these Env trimers elicited substantial strain-specific tier 2 nAbs in rabbits and guinea pigs but failed to elicit nAbs in mice (Feng et al., 2016; Hu et al., 2015; Sanders et al., 2015). Trimer immunization of NHPs has been sporadically successful (Havenar-Daughton et al., 2016a; Pauthner et al., 2017; Sanders et al., 2015; Zhou et al., 2017). For some regimes in NHPs, autologous tier 2 nAbs have been elicited within 10 weeks, which is comparable with the speed of nAb development in HIV-infected individuals (Pauthner et al., 2017; Richman et al., 2003; Wei et al., 2003). Thus, although nAb epitopes are presented on native-like trimers, the immunological parameters controlling the development of nAbs to Env remain to be elucidated. These parameters are also likely important for nAbs to other pathogens.

Germinal centers (GCs) are essential for HIV nAb development, which requires antibody (Ab) somatic hypermutation (SHM) (Klein et al., 2013; West et al., 2014). GCs are sites where B cells compete for antigen and undergo repeated rounds of SHM of their B-cell receptors (BCRs) and selection by GC T follicular helper (GC-T_{FH}) cells to evolve high-affinity Abs (Crotty, 2014; Mesin et al., 2016). B cells with higher affinity to antigen (Ag) present more peptide:major histocompatibility complex (MHC) complexes to GC-T_{FH} cells and receive more help (Crotty, 2014; Gitlin et al., 2014; Victora et al., 2010). GC-T_{FH} cell help signals to GC B (B_{GC}) cells result in proliferation and further SHM (Gitlin et al., 2015). T_{FH} cell help quality is associated with HIV nAb development in trimer-immunized rhesus monkeys (RMs) (Havenar-Daughton et al., 2016a). Frequencies of highly functional memory T_{FH} cells in the blood are associated with bnAb development in HIV-infected humans (Locci et al., 2013; Moody et al., 2016). GC-T_{FH} cells are also positively correlated with nAb development in simian immunodeficiency virus positive (SIV^+) RMs and $SHIV^+$ RMs (Chowdhury et al., 2015; Petrovas et al., 2012; Yamamoto et al., 2015).

B cell responses to protein Ags are polyclonal, targeting several epitopes across an Ag. The composition of the Ag-specific B cell repertoire can be complex. B cells initially engage in interclonal competition and then in interclonal and intraclonal competition, resulting in complex outcomes (Kuraoka et al., 2016; Tas et al., 2016). Theoretically, the surface of a protein represents a continuum of epitopes. In reality, the Ab response to a protein predominantly targets a limited number of epitopic sites. Immunodominance is the phenomenon in which B cells that recognize an epitopic site dominate a response at the expense of B cells that recognize other sites. Immunodominance is well-described for influenza hemagglutinin (HA), in which the epitopes are recognized in a hierarchical manner (Angeletti and Yewdell, 2018; Angeletti et al., 2017). Immunodominance appears to be a key immunological process limiting the development of broad nAb responses to influenza (Andrews et al., 2018; Angeletti and Yewdell, 2018; Angeletti et al., 2017; Victora and Wilson, 2015) and may also be important for nAb development against other refractory pathogens, including HIV (Havenar-Daughton et al., 2017). The soluble Env trimer can be subject to *in vivo* degradation, resulting in breakdown products that are not exposed on the virion surface. These non-native epitopes are likely "dark antigen" and can be immunodominant (Kuraoka et al., 2016). Evidence of immunodominance impairing HIV nAb development includes the lack of tier 2 nAb responses by gp120-immunized humans, the lack of autologous tier 2 nAb responses in non-native Env trimer-immunized RMs, the sporadic nature of tier 2 nAb development in Env trimer-immunized RMs, and the role of immunodominance in the response of rare and low-affinity HIV CD4 binding site-specific B cells in a mouse model (Abbott et al., 2018; Havenar-Daughton et al., 2017).

Much of the focus in HIV vaccine development is on the choice of antigen and adjuvant, but another parameter is the kinetics of antigen availability. Slow delivery immunization is an attractive vaccine strategy because it more closely mimics a natural acute infection (Cirelli and Crotty, 2017). Although the adjuvanticity of alum has been believed to be in part due to a "depot" effect of antigen, many antigens rapidly elute from alum *in vivo* (Hogenesch, 2002; Shi et al., 2001; Weissburg et al., 1995), and several studies have reported that this depot does not affect Ab responses (Hogenesch, 2013; Hutchison et al., 2012; Noe et al., 2010), suggesting that alum adjuvanticity does not primarily function via a slow release mechanism. In contrast, 2-week slow release immunization using nonmechanical osmotic pumps (OPs) and a soluble adjuvant resulted in enhanced B_{GC} and T_{FH} cell responses in mouse models (Hu et al., 2015; Tam et al., 2016). Two-week escalating dose (ED) immunization resulted in similar outcomes and enhanced deposition of immune complexes onto follicular dendritic cells (FDCs) (Tam et al., 2016).

Understanding the importance of different aspects of B and T cell biology in the development of HIV nAbs has been limited by the fact that wild-type mice do not develop tier 2 nAbs in response to trimer immunization. Although NHPs are important animal models for HIV vaccine design because of their close evolutionary relationship to humans, it has been difficult to study the early response to Env immunization because of the inaccessible nature of lymph nodes (LNs). As a first proof of concept in NHPs, RMs were immunized with soluble native-like Env trimers in a soluble immune stimulating complex (ISCOM)-class saponin adjuvant delivered via OPs (Pauthner et al., 2017). OP-immunized RMs responded with the most robust autologous tier 2 nAb responses in the study, which developed by week 10 in all animals. The rapidity and magnitude of the nAb response suggested that improved affinity maturation, B cell lineage recruitment, Env-specific T_{FH} cell responses, or other factors may be responsible for the improved nAb response. Antigen-specific B cell and T_{FH} cells were not examined. Here we examined the early B and T cell responses to Env trimers in RMs using new tools and comparative immunology between conventional and slow release concepts to gain insights into the development of HIV nAbs, which may also be applicable to other refractory pathogens.

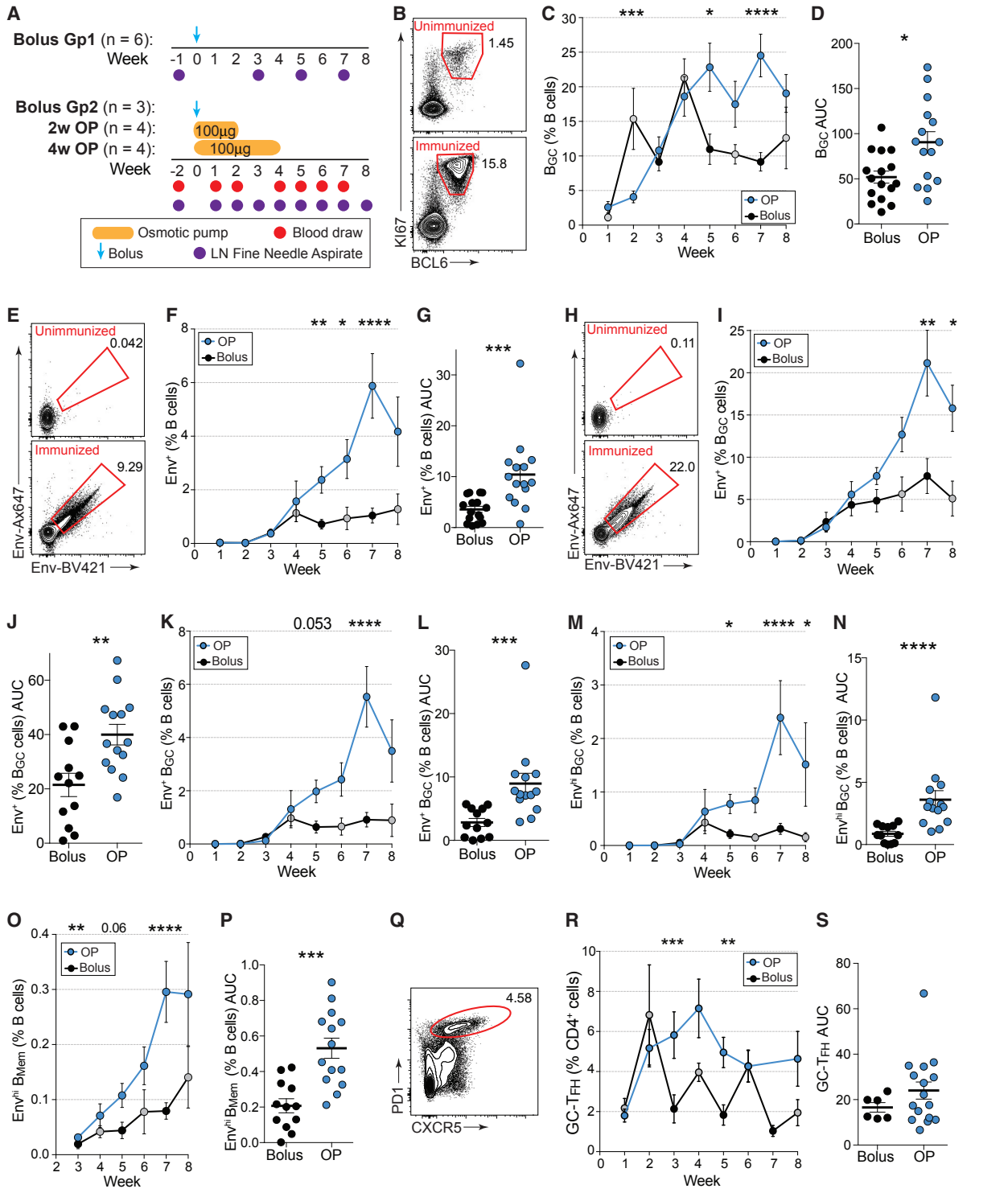

Figure 1. Sustained Delivery Immunization Enhances B_{GC} Cell Responses

(A) Immunization and sampling schedule of the first immunization. Bolus group 2 (Gp2), 2-week osmotic pump (OP), and 4-week OP RMs were immunized and sampled at the same time. Bolus Gp1 RMs were immunized and sampled separately. Bolus Gp1 and Gp2 data were pooled.

(B) Representative B_{GC} cell flow cytometry, gated on viable $CD20^+$ B cells pre- and post-immunization. See Figure S1 for the full gating strategy.

(C) B_{GC} cell frequencies over time. Black circles, pooled bolus Gp1 and Gp2; gray circles, bolus Gp2.

(D) Cumulative B_{GC} cell responses (AUC of C) to immunization within individual LNs at weeks 1 and 3–7 (AUC).

(legend continued on next page)

RESULTS

Env-Specific GC Responses Are More Robust upon Slow Release Immunization

Three groups of RMs were immunized with soluble native-like Env trimer BG505 Olio6$_{CD4ko}$ protein (Kulp et al., 2017) in a soluble ISCOM-class saponin adjuvant. Three delivery strategies were tested: conventional bolus immunization via subcutaneous (s.c.) injection (n = 9), 2-week s.c. nonmechanical OPs (n = 4) and 4-week s.c. OPs (n = 4) (Figure 1A). All immunizations were given bilaterally in the left and right thighs. To determine the kinetics of the GC response to primary immunization, longitudinal LN fine needle aspirates (FNAs) were employed to sample the draining inguinal LNs weekly in each hindlimb. This study is the first longitudinal (i.e., the same individuals were sampled) weekly kinetic analysis of a GC response in any species. Previous work demonstrated that LN FNAs well represented the cellular composition of the whole LN and were well-tolerated (Havenar-Daughton et al., 2016a).

GCs developed slower than expected, based on comparison with mouse data of LN GC kinetics after protein immunization, with almost no B_{GC} cells (BCL6$^+$KI67$^+$ or CD38$^-$CD71$^+$ of CD20$^+$CD3$^-$) detectable at week 1 post-immunization (Figures 1B, 1C, S1A, and S1B). Substantially greater B_{GC} cell frequencies were present at week 2 in both groups (week 1 versus week 2, p = 0.0015). No differences were observed in GC kinetics between the OP groups, so data from these groups were pooled in subsequent analyses (n = 8 animals, n = ~16 LN FNAs per time point; Figures S1C and S1D). Total B_{GC} cells in the LNs peaked at week 7 in OP-immunized RMs after a single immunization, substantially later than after bolus immunization (Figure 1C). OP animals had significantly more B_{GC} cells throughout the first immunization (p = 0.017, area under the curve [AUC]); Figures 1D and S1D).

Given that RMs are not kept in a sterile environment, interpretation of B_{GC} cell kinetics in the absence of antigen-specific probes is confounded by uncertainty regarding the antigenic targets of the GCs. In previous studies, total B_{GC} cell responses were measured, but antigen specificity was not determined (Havenar-Daughton et al., 2016a; Pauthner et al., 2017). Detection of antigen-specific B_{GC} cells is a challenge because B_{GC} cells express less BCR than non-B_{GC} cells (Figure S1E). Using Olio6 Env trimers conjugated to two fluorochromes as probes (Env$_{Ax647}$ and Env$_{BV421}$), we measured the kinetics and magnitude of the Env trimer-specific B and B_{GC} cell response (Env$_{Ax647}^+$ Env$_{BV421}^+$ BCL6$^+$KI67$^+$ or CD38$^-$ CD71$^+$ of CD20$^+$ CD3$^-$; Figures 1E–1N and S1F–S1O). This method was specific, with little experimental "noise," because naive B cells and B_{GC} cells from unimmunized animals did not bind these probes (Figures 1E, 1H, S1H, and S1M; Data S1). Despite observing considerable GCs at weeks 2–3, Env-specific B_{GC} cells with detectable affinity to the probes were rare at weeks 2–3 but consistently detectable at week 4 in both groups (Figures 1I–1K and S1H–S1O). Env-specific B_{GC} cell frequencies were relatively stable between weeks 4–8 in bolus RMs. In OP animals, frequencies of Env-specific B_{GC} cells increased over time (p = 0.006 compared with bolus as percent Env$^+$ of B_{GC} cells over time [AUC] and p = 0.0001 compared with bolus as percent Env$^+$ B_{GC} of total B cells over time [AUC]; Figures 1H–1L). Enhanced B_{GC} cell binding of Env by OP animals was not due to an increase in BCR expression (Figure S1I). High binding Env-specific B_{GC} cells became more abundant in OP animals over time (p < 0.0001 compared with bolus [AUC]; Figures 1M, 1N, S1J–S1O, and S1R), suggesting that OP administration resulted in more affinity maturation compared with conventional bolus immunization.

Env trimer-specific memory B (B_{Mem}) cells (BCL6$^-$ KI67$^-$ or CD38$^+$CD71$^-$ Env$_{Ax647}^{+/hi}$ Env$_{BV421}^{+/hi}$ CD20$^+$ cells) developed in draining LNs in each group (Figures 1O, 1P, S1P, and S1Q). OP animals developed higher frequencies of high-affinity Env trimer-specific B_{Mem} cells. Overall, these data demonstrate that slow immunization delivery resulted in more robust GCs and suggested substantially greater affinity maturation to Env after a single immunization than upon conventional bolus immunization.

Slow Release Immunization Enhanced Env-Specific GC-T_{FH} Cell Responses

Although OP RMs had higher total GC-T_{FH} cell (CXCR5$^+$PD1^{hi} of CD4$^+$CD8$^-$) frequencies than bolus RMs at several points during the first immunization, GC-T_{FH} cells did not differ between groups overall (Figures 1Q–1S and S2A). The specificity of

(E) Representative flow cytometry of Env trimer-specific B cells pre- and post-immunization.
(F) Env trimer-specific B cell frequencies over time.
(G) Cumulative Env trimer-specific B cells (AUC of F) in each LN.
(H) Representative flow cytometry Env trimer-specific B_{GC} cells pre- and post-immunization.
(I) Env trimer-specific B_{GC} cell frequencies over time.
(J) Cumulative Env trimer-specific B_{GC} cells (AUC of I) in each LN.
(K) Env trimer-specific B_{GC} cells over time.
(L) Cumulative Env trimer-specific B_{GC} cells (AUC of K) in each LN.
(M) Frequencies of high-affinity Env trimer-specific B_{GC} cells over time.
(N) Cumulative high-affinity Env trimer-specific B_{GC} cells (AUC of M) in each LN.
(O) High-affinity Env trimer-specific B_{Mem} cells over time.
(P) Cumulative high-affinity Env trimer-specific B_{Mem} cell responses in individual LNs.
(Q) Representative flow cytometry of GC-T_{FH} cells, gated on CD4$^+$ T cells. See Figure S2 for the full gating strategy.
(R) GC-T_{FH} cells over time.
(S) Cumulative GC-T_{FH} cell response (AUC of R) between week 1 and weeks 3–6.
Mean ± SEM are graphed. Statistical significance was tested using unpaired, two-tailed Mann-Whitney *U* tests. *p ≤ 0.05, **p ≤ 0.01, ***p ≤ 0.001, ****p ≤ 0.0001. See also Figures S1 and S2 and Data S1.

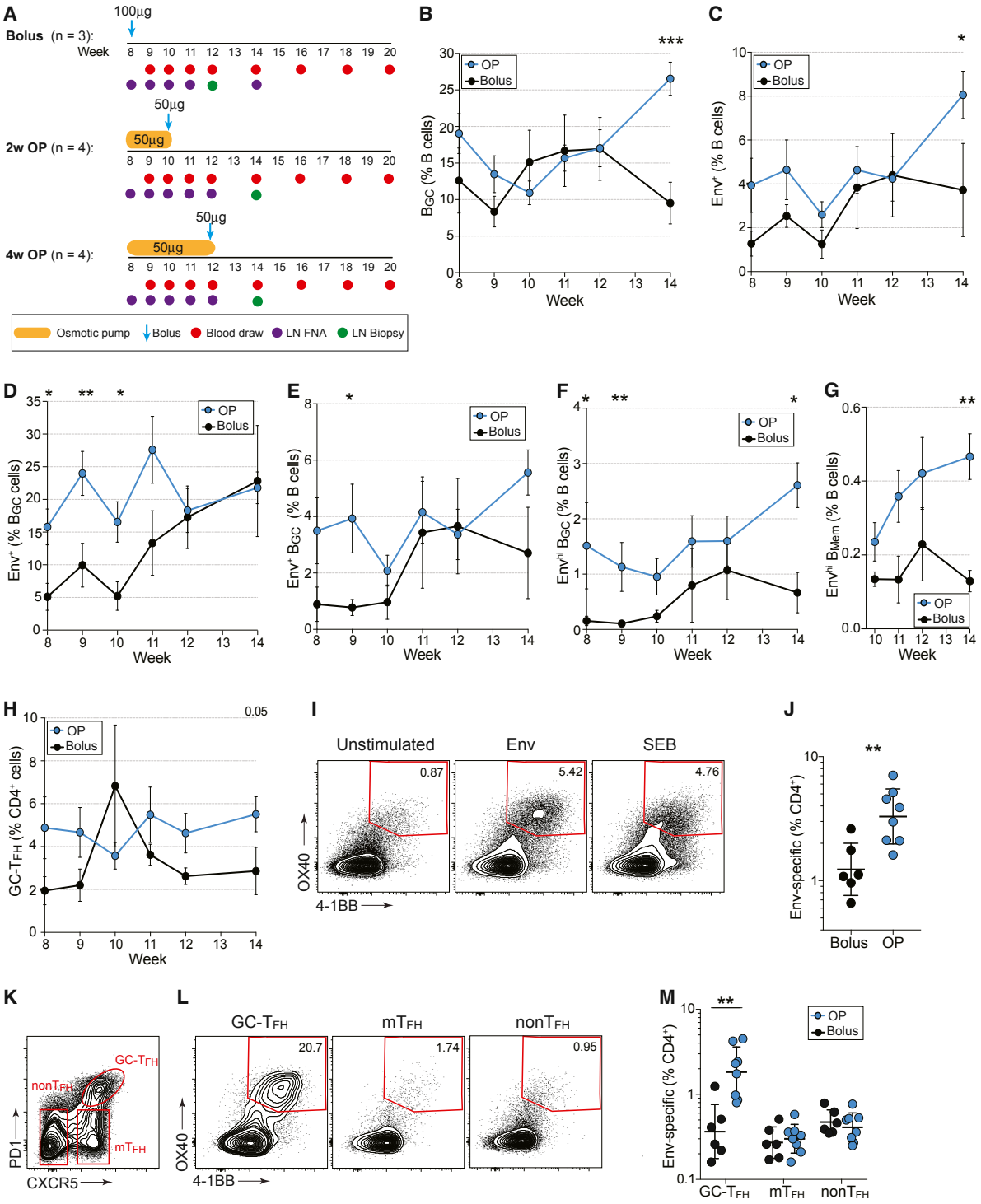

Figure 2. GC Responses following the Second Env Trimer Immunization

(A) Immunization and sampling schedule of the second immunization. Groups were immunized and sampled contemporaneously.

(B) Frequencies of total B_{GC} cells over time.

(C) Env trimer-specific B cell frequencies over time.

(D) Env trimer-specific B_{GC} cells over time.

(E) Env trimer-specific B_{GC} cells (as % of total B cells) over time.

(F) High-affinity Env trimer-specific B_{GC} cells over time.

(legend continued on next page)

GC-T_{FH} cells at these time points could not be measured because of limited cell numbers and experimental prioritization of the B cell assays.

Based on previous immunization regimens (Pauthner et al., 2017), we administered a second immunization at week 8 (Figure 2A). For OP groups, the immunization was split evenly between pumps and a bolus administered at the end of OP delivery to simulate an escalating dose immunization. We hypothesized that a bolus immunization at the end of the slow release delivery may enhance plasma (B_{PC}) cell differentiation and Ab titers. The total dose of Env trimer was matched between groups (100 μg; Figure 2A). Draining LN GC responses observed after the second immunization were relatively flat (Figure 2B), perhaps because of ongoing GC reactions immediately prior to the second immunization (Figures 1C and 2B). OP RMs had significantly larger B_{GC} cell responses at week 14 (Figure 2B). Env-specific B and B_{GC} cell frequencies in bolus RMs increased after the second immunization (Figures 2C–2F). High-affinity Env-specific B_{GC} cell recall responses were largely comparable between OP- and bolus-immunized animals (Figure 2G). Overall, the kinetics of the secondary GC responses differed from those in the primary GC responses.

Total GC-T_{FH} cell frequencies were similar in response to the second Env trimer immunization (Figure 2H). To identify Env-specific GC-T_{FH} cells, we performed cytokine-agnostic activation-induced marker (AIM) flow cytometry assays with biopsied LN cells. Higher frequencies of Env-specific $CD4^+$ T cells were present in OP animals compared with bolus RMs (Figures 2I, 2J, and S2B). The Env-specific $CD4^+$ T cell response enhancement was selective for Env-specific GC-T_{FH} cells (Figures 2K–2M). Thus, OP immunization elicited an immune response that generated substantially more Env-specific GC-T_{FH} cells, commensurate with the development of significantly higher frequencies of high-affinity Env-specific B_{GC} cells.

Slow Release Immunization Enhanced Humoral Responses

Antibody responses to the immunization approaches were examined in light of the differences in GC responses. A single bolus immunization failed to elicit detectable BG505 Env trimer-specific plasma immunoglobulin G (IgG) titers (Figures 3A, S2C, and S2D). In contrast, a single OP immunization elicited modest but significant Env-specific plasma IgG titers (week 7, $p = 0.048$). The $Olio6_{CD4ko}$ Env trimer design included a His tag, which elicited a strong Ab response after one OP immunization (Figures 3B, S2E, and S2F), whereas bolus RMs made anti-His IgG after the booster immunization. A fraction of the Env-specific B and B_{GC} cells likely recognized the His tag epitope. The second Env trimer immunization induced anamnestic Env IgG responses in both groups, with OP outperforming bolus immunization (Figure 3A). Env-specific IgG titers increased in response to the second OP immunization prior to the end-of-regimen bolus injection, demonstrating that OP immunization alone was sufficient for substantial anamnestic B_{PC} development (week 7 versus week 10, $p = 0.008$). Env-binding IgG titers between bolus groups and between OP groups were similar to the previous RM study (Figure S2G).

To assess the development of tier 2 nAb titers over time, sera were tested for autologous neutralization of BG505 N332 pseudovirus using TZM-bl neutralization assays (Figures 3C, 3D, and S2H–S2J). By week 10, 5 of 8 OP animals developed nAbs, in contrast to 0 of 3 bolus animals (1:99 versus less than 1:10 geometric mean titer [GMT]). All OP RMs developed nAbs by week 18. Peak neutralization titers of OP RMs were ~20-fold higher than those of bolus animals (1:202 versus 1:10 GMT, $p = 0.01$). Neutralization breadth was assessed using a 12-virus panel of tier 2 isolates. 6 of 8 OP RMs demonstrated partial neutralization breadth, neutralizing one to three heterologous isolates (Figures 3E and S2K). No heterologous nAbs were detected in bolus animals. Thus, slow release immunization enhanced the magnitude and quality of the Ab response to Env immunization, which was associated with the enhanced Env-specific B_{GC} and GC-T_{FH} cell responses.

Slow Delivery Immunization Alters the Antigen-Specific B Cell Repertoire

Because of the higher frequencies of high-affinity B cells and nAb titers observed in the OP animals, we hypothesized that slow release immunization delivery may affect several aspects of B cell responses. First, slow delivery immunization may activate (direct effect) or recruit (via T cell help) more diverse B cell lineages. Inclusion of more independent B cell lineages would increase the likelihood that B cells with rarer and/or lower-affinity BCRs capable of developing into nAbs will be expanded. Second, slow delivery may increase immune complex formation, affecting GC development and maintenance. Third, slow delivery may result in the generation of more B_{Mem} cells capable of recirculating and reseeding new GCs among multiple LNs upon booster immunization. Finally, slow delivery immunization may drive higher rates of SHM. A major technical challenge for testing several of these hypotheses was the lack of a complete reference sequence of the RM Ig gene locus, which is required for proper B cell lineage assignment and identification of authentic SHM. Although an RM genome sequence was available (Gibbs et al., 2007), the Ig genes were largely unmapped. Ig genes reside within highly complex genomic regions that are

(G) High-affinity Env trimer-specific B_{Mem} cells over time.
(H) GC-T_{FH} cell frequencies after the second immunization.
(I) Representative flow cytometry of Env-specific $CD4^+$ T cells from LNs. Cells were left unstimulated or stimulated with a peptide pool spanning $Olio6_{CD4ko}$.
(J) Env-specific $CD4^+$ T cells at week 12 (bolus) or week 14 (OP).
(K) Representative flow cytometry of GC-T_{FH}, mantle (m)T_{FH}, and non-T_{FH} cell subsets.
(L) Flow cytometry of the AIM_{OB} assay using $OX40^+4\text{-}1BB^+$, gated on GC-T_{FH}, mT_{FH}, or non-T_{FH} cells.
(M) Quantification of Env-specific $CD4^+$ T cells by subset.
Mean ± SEM are graphed. Statistical significance was tested using unpaired, two-tailed Mann-Whitney *U* test. *$p \leq 0.05$, **$p \leq 0.01$, ***$p \leq 0.00$. See also Figure S2.

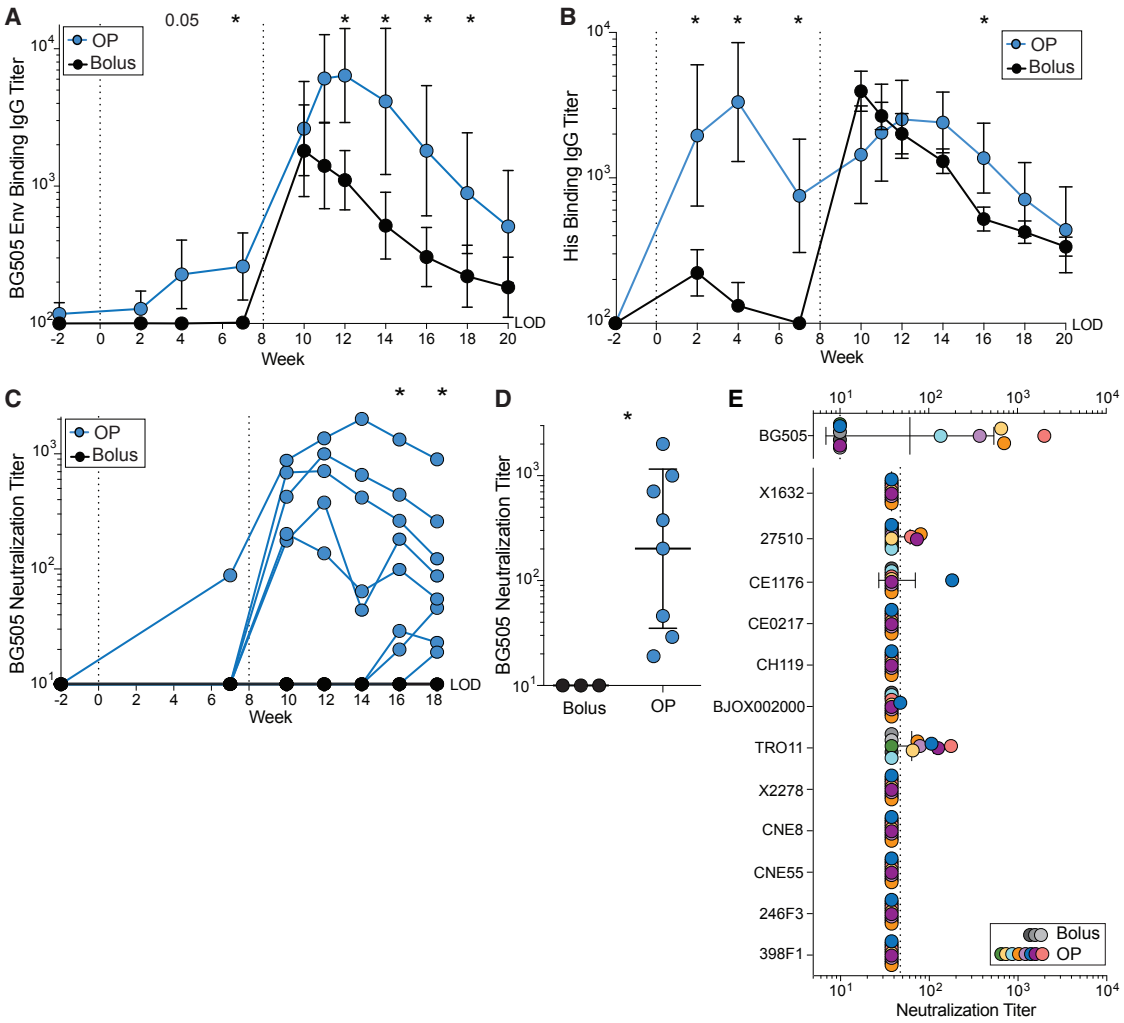

Figure 3. Sustained Delivery Immunization Induces Higher nAb Titers

(A) BG505 Env trimer IgG binding endpoint titers over time.

(B) His IgG binding endpoint titers over time.

(C) BG505 (autologous) nAb titers over time.

(D) Peak BG505 nAb titers after two immunizations.

(E) Neutralization breadth on a 12-virus panel.

GMT and ± geometric SD; statistical significance was tested using unpaired, two-tailed Mann-Whitney *U* test. *p ≤ 0.05.

See also Figure S2.

characterized by high levels of repetitive sequences and inter-individual haplotype variation, which make genomic characterization and Ig gene annotation challenging (Watson and Breden, 2012; Watson et al., 2017). Most next-generation sequencing techniques use short-read technologies (~150 bp), which can be insufficient for resolving large (>15 kb) repetitive segments (Alkan et al., 2011). Therefore, we sequenced the genome of an RM using Pacific Biosciences long-read sequencing technology to 60-fold coverage. Overall, reads had a median length of 16.6 kb and a maximum individual read length of 69.4 kb. Genome assembly was conducted using FALCON/FALCON-Unzip, resulting in a total of 1,633 primary contigs with a median length of 8.4 Mb (2.83 Gb total bases).

Contigs containing the Ig locus were identified, and V, D, and J genes were annotated via a combination of bioinformatics and manual curation (Figure 4A). 66 IGHV, 41 IGHD, 6 IGHJ, 68 IGKV, 5 IGKJ, 62 IGLV, and 7 IGLJ genes were identified by focusing on gene segments with open reading frames (ORFs; Figure 4A). Notably, the long reads allowed characterization of regions that were unresolved in previous assemblies, including the current RM reference genome (rheMac8), facilitating identification of novel gene loci (Figure 4B). It was also possible to identify heterozygous allelic variants at loci identified in primary contigs by using a combination of raw read data and alternate contigs from FALCON-Unzip (Figures 4C–4E). We determined that 37 of 66 IGHV, 31 of 68 IGKV, and 12 of 65 IGLV genes

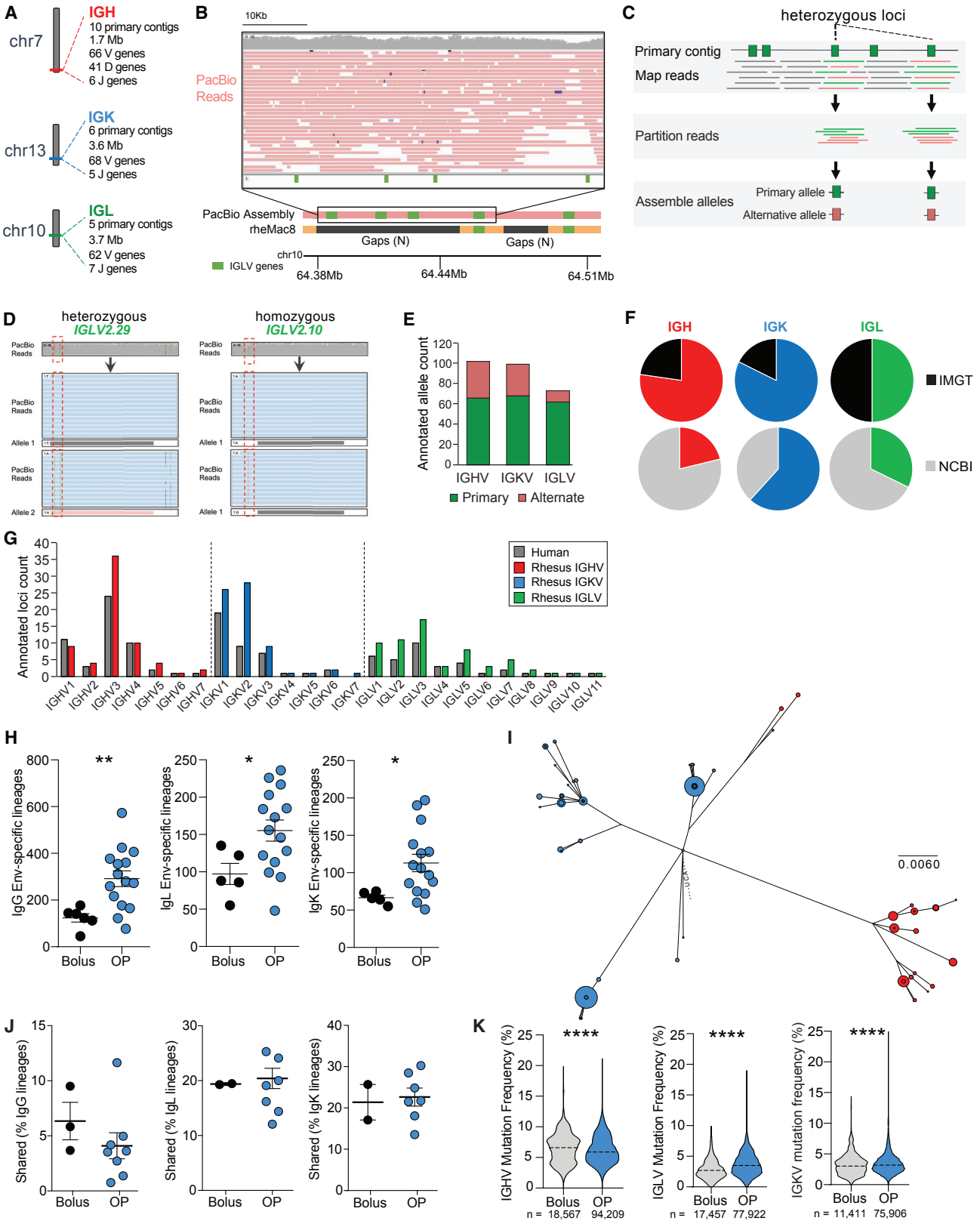

(legend on next page)

were heterozygous, amounting to a germline database of 103, 99, and 77 V alleles for each respective locus (Figure 4E; Table S1). Sequencing BCRs of mature B cells from the same animal and close relatives supported the presence of these annotated ORF sequences (data not shown). A significant fraction of alleles identified in the assemblies were not represented by sequences in either the international ImMunoGeneTics information system (IMGT) database or NCBI Ig gene repositories, highlighting the utility of this approach for improving existing genomic databases (Figure 4F). Ig gene family sizes are comparable in humans and RMs (Figure 4G).

To assess how slow delivery immunization affected the Env-specific B cell repertoire, we isolated and sequenced BCRs from Env-specific B cells in the biopsied draining LNs after the second immunization (Figures 2A and S3A). The majority of the sequenced Env-specific B cells were B_{GC} cells (77%), providing a window into this difficult-to-study cell type (Table S2). More Env-specific B cells were isolated from OP animals compared with bolus RMs (303,644 versus 52,302 cells [total]; 20,242 versus 8,717 cells [mean], p = 0.029; Data S1), consistent with the higher frequencies identified by flow cytometry (Figures 1 and 2). Utilizing the new RM Ig genomic reference, we assigned each unique Env-specific BCR sequence to the V and J genes with most similarity, performed lineage analysis, and determined SHMs. Larger numbers of Env-specific BCR sequences were isolated from OP animals than from bolus animals, both for heavy chains (*IgG*: 94,209 versus 18,567 [total], 5,691 versus 2,846 [mean]) and light chains (*IgL*: 77,922 versus 17,457 [total], 5,240 versus 3,643 [mean]; *IgK*: 75,906 versus 11,411 [total], 4,827 versus 2,261 [mean]). Furthermore, significantly more unique *IgG*, *IgL*, and *IgK* B cell lineages were identified in LNs of OP animals compared with bolus-immunized animals (Figures 4H and S3B). Clonal abundance and Shannon H index analyses confirmed increased clonal diversity in pump animals (Figures S3C and S3D). Although most BCR lineages were found in only one LN (Figure S3E), 0.7%–30.2% were found in both right (R) and left (L) LNs (Figures 4I and 4J). SHM rates in variable (V) genes and across the BCR were largely similar between groups, as were CDR3 lengths (Figures 4K, S3F, and S3G). Thus, substantially more Env-specific B cell lineages were recruited and sustained in animals receiving a slow release immunization, whereas SHM rates were comparable.

Slow Delivery Immunization Results in Greater Ab Diversity

Given that slow delivery immunization resulted in more Env-specific B cell lineage diversity, we sought to determine whether differential IgV gene usage occurred, which may suggest differences in the epitopes targeted on the Env trimer. Bolus RMs utilized *IGLV3-15*01* (IGLV3-15) significantly more frequently than OP RMs (q = 0.00003; Figures 5A, 5B, and S4A). 18.75% and 2.6% of Env-specific B cells from LNs of bolus and OP animals, respectively, utilized IGLV3-15. Using IMGT for similar analysis, a difference in IGLV3-15 (aka *IGLV3-10*01*) was also identified between groups (Figures S4B–S4D). Env-specific B cells that used IGLV3-15 were phylogenetically diverse (bolus, 11.4 mean per LN; OP, 6.4) and could be found in both draining LNs in a single animal (Figure 5C).

The differential use of IGLV3-15 suggested that the Env-specific B cells elicited by bolus immunization preferentially targeted epitopes distinct from the Env-specific B cells elicited by OP immunization. Taken together with the lack of nAbs in the bolus animals, we hypothesized that B cells that utilized IGLV3-15 recognized the base of the trimer. This region is normally hidden on full-length Env expressed on HIV virions. In contrast, the base is the largest proteinaceous region exposed on the soluble Env trimer because of the unusually dense glycans covering most of the remainder of the surface of Env (Stewart-Jones et al., 2016; Figure 5D). The base is a major non-neutralizing Ab target in mice and RMs immunized with the soluble Env trimer, and base-specific B cells are proposed to be immunodominant to nAb epitope-specific B cells (Havenar-Daughton et al., 2017; Hu et al., 2015; Kulp et al., 2017). To test this hypothesis, we sequenced Env-specific single B cells from the draining LNs of two bolus-immunized animals at week 7 to obtain paired BCR sequences utilizing IGLV3-15. We synthesized a panel of IGLV3-15$^+$ mAbs, termed BDA1-11, representing 11 unique B cell lineages (Table S3). Almost all of the IGLV3-15$^+$ mAbs bound the BG505 Env trimer but not monomeric BG505 gp120 or His peptide (Figures 5E and S5A–S5C). Binding of several base-directed antibody (BDA) mAbs to Env was selectively

Figure 4. Immunoglobulin Gene Germline Annotations Using Long-Read Genomic DNA Sequencing

(A) Locus and assembly summaries for the RM Ig locus. Lengths refer to sum of contig lengths.

(B) A representative region where PacBio primary contigs resolved gaps in the current RM reference genome. PacBio reads span these gaps (inset).

(C) Overview of the V gene allelic variant discovery process. Reads overlapping annotations on primary contigs were assessed for the presence of SNPs, which were used to partition reads for allele-specific assemblies.

(D) SNPs (green and red) within or near genes (red boxes) were used to partition reads to each respective haplotype, allowing for identification of heterozygous (pink) and homozygous (gray) gene segments.

(E) Primary and alternate contig allele counts.

(F) Variable (V) genes from PacBio assembly that were present in the IMGT or NCBI V gene repositories.

(G) V gene counts from PacBio primary contig assemblies compared with human gene loci.

(H) Quantification of Env-specific B cell lineages from individual LNs.

(I) Phylogenetic analysis of a lineage found in both LNs in one animal. Blue, left LN; red, right LN. Dot size represents the number of reads with that sequence.

(J) Lineages shared between R and L LNs in an animal.

(K) Mutation frequencies in IGHV, IGLV, or IGKV. Violin plots; dash = mean.

Mean ± SEM; statistical significance in (H) and (J) was tested using unpaired two-tailed Mann-Whitney *U* test. Significance in (K) was tested using Student's t test. $^*p \leq 0.05$, $^{**}p \leq 0.01$, $^{***}p \leq 0.001$.

See also Figure S3 and Tables S1 and S2.

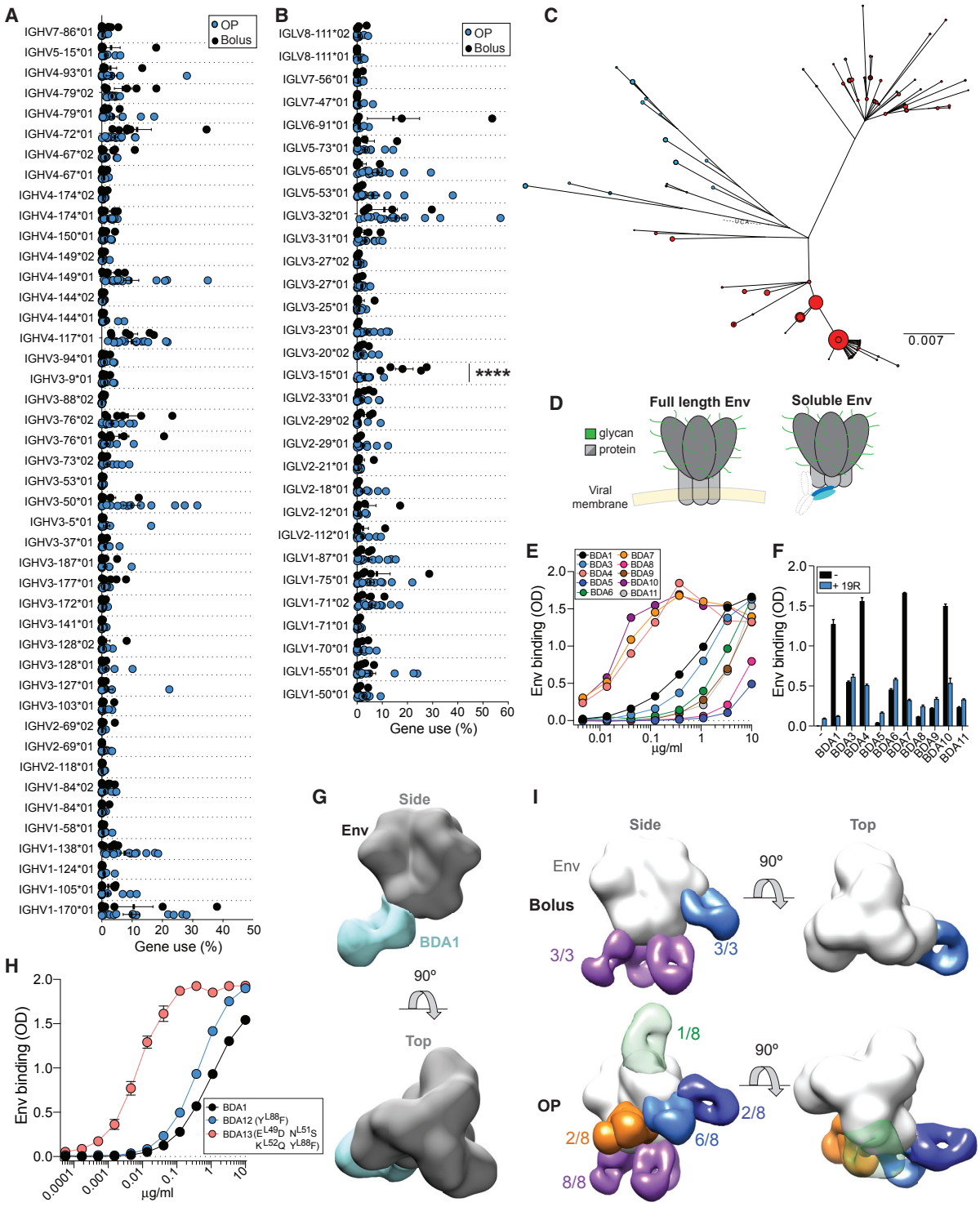

Figure 5. Slow Delivery Immunization Shifts Immunodominance

(A and B) IGHV (A) or IGLV (B) used by antigen-specific B cells within a LN. Each data point represents a single LN. Statistical significance was tested using multiple t tests with a false discovery rate (FDR) of 5%; ****$q < 0.0001$.

(C) Phylogenetic tree of an IGLV3-15^{+} lineage. Blue, left LN; red, right LN. Dot size represents the number of reads with that sequence.

(D) The base of Env is hidden on the virion surface. The soluble trimer allows access of the base to B cells. Glycans restrict access to the main Env trimer surface.

(E) Binding curves of mAbs isolated from week 7 to the BG505 Env trimer.

(F) Cross-competition ELISA assay. Data are representative of two experiments, each performed in duplicate.

(legend continued on next page)

blocked by 19R, a high-affinity Env base-binding mAb, demonstrating that IGLV3-15$^+$ Abs recognize the Env trimer base (Figure 5F). Electron microscopy (EM) analysis of a BDA mAb Fab complex with the Env trimer confirmed binding of BDA1 to the trimer base (Figure 5G). We next sought to determine how BDA1 is related to the Env-specific B cells isolated from the same LN after booster immunization with the Env trimer (week 12). Alignment and phylogenetic analysis of the BDA1 lineage consisted of BDA1, three related week 12 sequences, and the inferred germline sequence (Figures S5D and S5E). The BDA1-lineage heavy and light chains accumulated more mutations at week 12, indicating recall GC responses of IGLV3-15$^+$ cells and ongoing SHM. Introduction of week 12 IgL mutations into BDA1 resulted in an increase in Env binding, suggesting that the BDA1 light chain contacts the Env trimer base (Figures 5H and S5D–S5F).

We utilized polyclonal EM serological analysis as an independent approach to assess the Ab responses to the Env trimer between the immunization strategies. This technique allows simultaneous visualization of Abs targeting distinct epitopes from polyclonal serum (Bianchi et al., 2018). Ab responses in bolus animals targeted two sites on Env: the trimer base (3 of 3 animals) and the glycan hole I region (GH-1; 3 of 3) (Figures 5I and S6). In contrast, the Ab responses in OP animals were more diverse. In addition to the base and GH-1 regions, three potential nAb epitopes, the fusion peptide, V1/V3-glycan, and C3/V5 regions (Klasse et al., 2018; Kong et al., 2016), were targeted by OP animals. In sum, slow release immunization resulted in a substantial shift in the B_{GC} cell and Ab response toward Env epitopes that are more diverse than those targeted by bolus animals. The shifted response was toward nAb epitopes, which are likely immunorecessive relative to the Env trimer base, indicating that slow delivery immunization modulates immunodominance or changes the immunodominance hierarchy.

Escalating Dose Immunization Enhances GC and nAb Responses

Escalating dose (ED) immunization is a strategy to achieve extended antigen exposure that is an approach distinct from OP administration (Tam et al., 2016). ED immunization has the added advantage of mimicking the antigen dose dynamics of an acute infection. Therefore, an RM ED study was performed with the Env trimer as an independent assessment of the immunological implications of extended antigen delivery in a vaccine setting. The control group was given conventional bolus immunizations at week 0, week 10, and week 24, totaling 100 μg, 100 μg, and 300 μg of Olio6 native-like Env trimer protein, respectively, mixed with an ISCOM-class adjuvant. ED immunizations were administered as 7 injections over 2 weeks (Figure 6A), with a total antigen dose equivalent to that of the conventional bolus immunization group. Significantly higher frequencies of B_{GC} cells in draining LNs were observed at week 5 in the ED group compared with the conventional bolus immunization group (Figures 6B, 6C, and S7A). ED immunization resulted in significantly more Env-specific B and B_{GC} cells after the first immunization ($p = 0.0002$ [AUC]; Figures 6D, 6E, and S7B–S7F; Data S2). Bolus-immunized animals had significantly higher frequencies of Env-specific B_{GC} cells than ED animals after the second immunization. These frequencies were comparable after the third immunization. ED immunization elicited improved affinity maturation, as indicated by the enhanced development of Env^{hi} B_{GC} cells compared with conventional immunization after the first immunization (Figures S7G–S7L). Additionally, ED immunization resulted in significantly more Env-specific B_{Mem} cells compared with conventional immunization after the first immunization (Figures S7M–S7P). Total B_{GC} cell frequencies and Env-specific B_{GC} and B_{Mem} cell frequencies increased upon the second and third ED immunizations, but not above the peak frequencies observed in response to the first ED regimen. Analysis of CD4$^+$ T cells in the draining LNs revealed that ED resulted in significantly higher total GC-T_{FH} and Env-specific GC-T_{FH} cells after the first immunization (Figures 6F–6H, S7Q, and S7R). ED-immunized animals showed a higher ratio of Env$^+$ B_{GC}:Env-specific GC-T_{FH} cells, suggesting that ED immunization resulted in greater antigen-specific help to B cells than conventional immunization (Figure 6I). The magnitude of the improved primary Env-specific B_{GC} cell response, the increased GC-T_{FH} cell response, and the enhanced Env^{hi} B_{GC} cells upon ED immunization were comparable with those observed after OP immunization.

A single ED immunization regimen was sufficient to elicit a BG505 Env-specific IgG response (Figure 6J). Anamnestic Env-binding plasma Ab responses were observed after the second and third ED and conventional immunizations. All ED-immunized animals developed autologous tier 2 nAbs after the second immunization, whereas only 3 of 6 conventionally immunized animals developed nAbs (Figure 6K). Peak autologous nAb titers after the third immunization were ~30-fold higher in ED RMs, significantly greater than in bolus animals (1:615 versus 1:18 GMT, $p = 0.009$; Figure 6L; see heterologous nAb breadth in Figure S7S).

Bolus animals targeted three regions on Env (base, GH-I, and fusion peptide), whereas ED-immunized animals targeted four (base, GH-I, C3/V5-I, and II) (Figure 6M). 6 of 6 ED animals had Ab responses against multiple regions of Env, whereas 2 of 6 bolus animals targeted a single site (Figures 6M and S8A). Thus, ED immunization resulted in greater Ab diversity.

Total GC-T_{FH} cell frequencies correlated with total B_{GC} cell frequencies during the first immunization ($r = 0.773$, $p = < 0.0001$ [peak of first immunization]; Figure 6N). In a previous study, total B_{GC} cell frequencies correlated with nAb development (Pauthner

(G) 3D EM reconstruction of the BDA1 Fab (blue) in complex with the BG505 Env trimer.
(H) Binding curves of BDA1 and related mutants to the BG505 Env trimer. BDA12 has a single week 12 mutation in L-CDR3. BDA13 contains this mutation and three additional week 12 mutations in L-CDR2. Data are representative of two experiments, each performed in duplicate.
(I) Composite 3D reconstruction of the Env trimer bound to Fabs isolated from all animals, as determined by polyclonal EM analysis. Numbers of individuals with a Fab that binds the region are listed. Base, purple; glycan hole I (GH-I), light blue; C3/V5, dark blue; fusion peptide, orange; V1/V3 apex, green. The apex-specific Fab is transparent to represent rarity.
Mean ± SEM. See also Figures S4–S6 and Table S3.

Please cite this article in press as: Cirelli et al., Slow Delivery Immunization Enhances HIV Neutralizing Antibody and Germinal Center Responses via Modulation of Immunodominance, Cell (2019), https://doi.org/10.1016/j.cell.2019.04.012

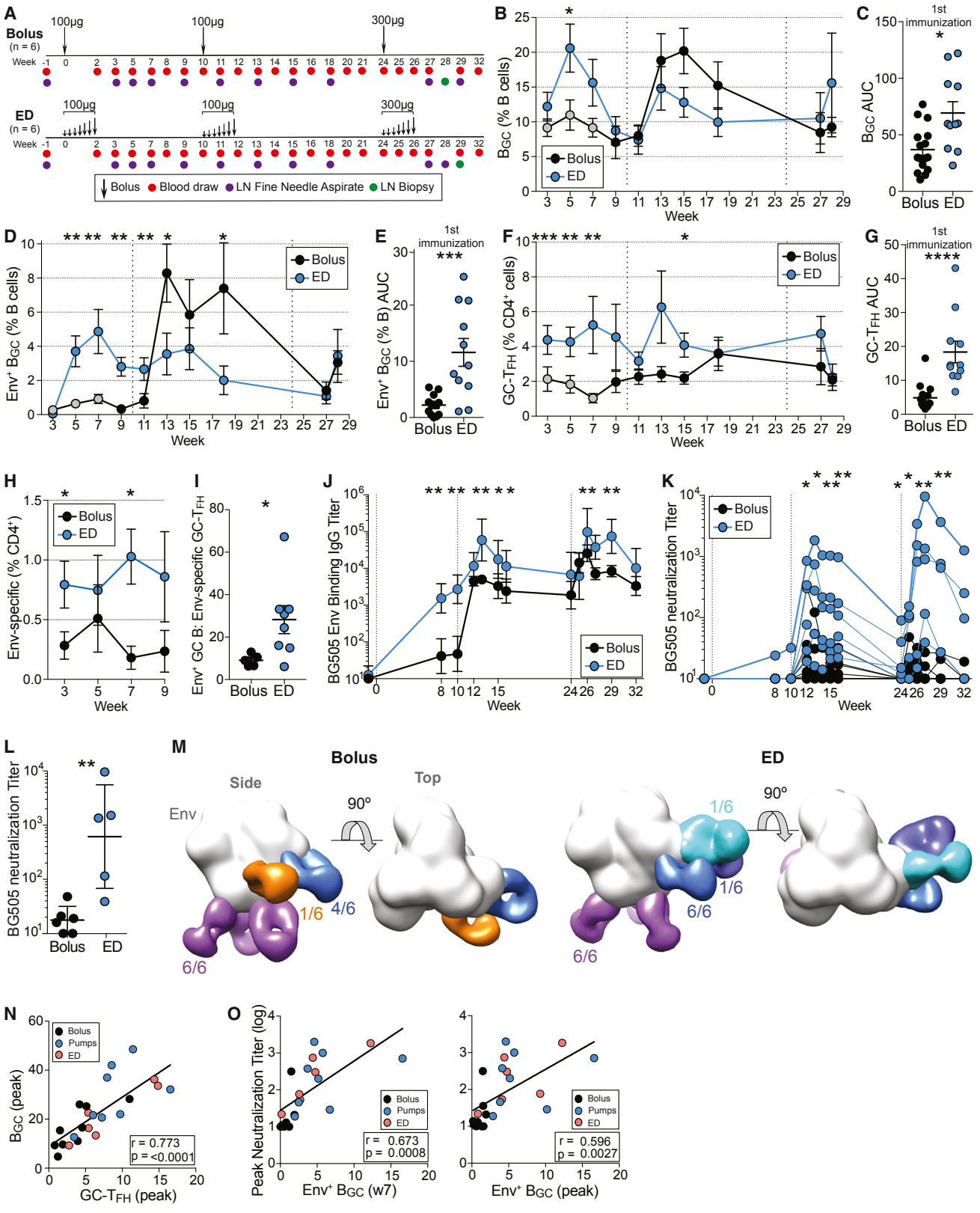

(legend on next page)

et al., 2017). A primary hypothesis of this study was that the magnitude of Env-specific B_{GC} cells to the first immunization might predict autologous nAb development. Peak Env-specific B_{GC} frequencies to the first immunization correlated with peak autologous nAb titers in response to the second immunization ($r = 0.673$, $p = 0.0008$ [week 7]; $r = 0.596$, $p = 0.0027$ [peak of first immunization]; Figure 6O), indicating that Env-specific B_{GC} and GC-T_{FH} cell responses can predict subsequent nAb development.

Taken together, the data show that the ED immunization modality generated greater GC and humoral responses than dose-matched conventional immunization, recapitulating the immune responses elicited to OP immunization, indicating that modulation of B_{GC} and T_{FH} cell responses is a general property of slow delivery immunization strategies that can result in dramatically different B cell specificities and nAb development.

An ED regimen resulted in enhanced FDC deposition of antigen in mice (Tam et al., 2016). We hypothesized that the enhanced GC responses observed in Env trimer-immunized RMs with both slow delivery immunization modalities were, at least in part, due to increased availability of antigen to B_{GC} and GC-T_{FH} cells (Cirelli and Crotty, 2017). An *in vivo* antigen tracking study was performed with fluorescently labeled Env trimer and ISCOM-class adjuvant administered via a conventional bolus, 2-week OP, or an ED regimen. LNs of OP- and ED-immunized animals contained significantly more Env trimer on day 2, as measured by laser-scanning imaging (Figures 7A and S8B). Light sheet microscopy of whole LNs revealed substantially more Env-containing B cell follicles in animals immunized with either slow delivery regimen (Figure 7B; Video S1). Histological analyses of LNs confirmed that Env colocalized with FDCs and GC-adjacent cells after OP or ED immunization (Figures 7C; S8C). Thus, slow delivery immunization leads to enhanced antigen retention within LNs in NHPs.

DISCUSSION

Understanding the underlying immunological challenges to nAb development against difficult pathogens may be important for understanding why protective immunity to such pathogens is elusive. Direct examination of primary immune responses in lymphoid tissue is required to develop such an understanding. Strategies to enhance humoral and GC responses to immunization are likely needed for the development of vaccines against some complex pathogens, particularly HIV. Using two independent methods, we demonstrated that slow delivery immunization resulted in enhanced autologous tier 2 nAb development in NHPs. We found that several aspects of GC biology were affected by slow delivery immunization. OP and ED immunization induced higher frequencies of total and Env-specific GC-T_{FH} cells. Greater availability of GC-T_{FH} cell help and antigen to B cells was accompanied by larger and more enduring B_{GC} responses. Both slow delivery strategies resulted in substantially more Env-specific B_{GC} cells. The B_{GC} cells were more diverse, as defined by unique Env-specific B cell lineages, which may be a consequence of broader initial activation of antigen-specific B cells and/or of sustaining larger GCs over time. The biological relevance of those processes is reinforced by the observation of more diverse nAb Env-binding specificities generated in slow delivery-immunized RMs compared with conventional bolus immunization.

To examine the immune responses directly in the draining LNs, we employed weekly LN FNAs. From this, we found that bolus immunization elicited a robust GC response but that slow delivery immunization altered the kinetics and overall magnitude of the GC response. Larger Env-specific B cell responses during the primary immunization were positively correlated with the larger nAb response that subsequently developed in OP- and ED-immunized animals, suggesting that much of the failure of a bolus immunization to a difficult antigen is intrinsic to early B cell events associated with immunodominance features of multiepitope complex antigens. Strikingly, slow delivery modulated the immunodominance of the B cell response to non-neutralizing epitopes on the Env trimer. OP and bolus RMs had comparable Env-binding ELISA titers at week 10. Nevertheless, OP animals had considerably higher autologous nAb titers at that same time point. This was also observed in ED and bolus RMs at week 11 and week 25. These data strongly suggested that the

Figure 6. The Dose Escalating Immunization Strategy Results in Higher nAb Titers

(A) Immunization and sampling schedule. Groups were immunized and sampled contemporaneously.
(B) Total B_{GC} frequencies over time. Data from bolus Gp2 (Figure 1) are included in these analyses (gray circles).
(C) Cumulative B_{GC} cell response to the first immunization, calculated between weeks 3–7 (AUC of B).
(D) Env trimer-specific B_{GC} cell frequencies over time.
(E) Cumulative Env trimer-specific B_{GC} cell responses to one immunization (AUC of D).
(F) Total GC-T_{FH} cell frequencies over time.
(G) Cumulative GC-T_{FH} responses to one immunization (AUC of F).
(H) Env-specific $CD4^+$ responses after one immunization.
(I) Ratio of Env^+ B_{GC} to Env-specific GC-T_{FH} cells at week 5, calculated as Env^+ B_{GC} (percent of B cells)/Env-specific GC-T_{FH} (percent of $CD4^+$).
(J) BG505 Env trimer-binding IgG endpoint titers over time.
(K) Autologous BG505 nAb titers over time.
(L) Peak BG505 nAb titers after three immunizations.
(M) Composite 3D reconstruction of the Env trimer bound to Fabs isolated from all animals after two immunizations. 3D EM reconstructions from individual animals can be seen in Figure S8A.
(N) Correlation between peak GC-T_{FH} and B_{GC} cell percent during the first immunization from both studies.
(O) Correlation between Env^+ B_{GC} cells (percent of B cells) and peak neutralization titers. Env^+ B_{GC} cell values are from week 7 or peak frequencies during the first immunization. Peak nAb titers are after the second immunization.
Serological data represent GMT ± geometric SD. Cell frequency data represent mean ± SEM. Statistical significance was tested using unpaired two-tailed Mann-Whitney *U* tests. *$p < 0.05$, **$p < 0.01$, ***$p < 0.001$, ****$p < 0.0001$. See also Figures S7 and S8 and Data S2.

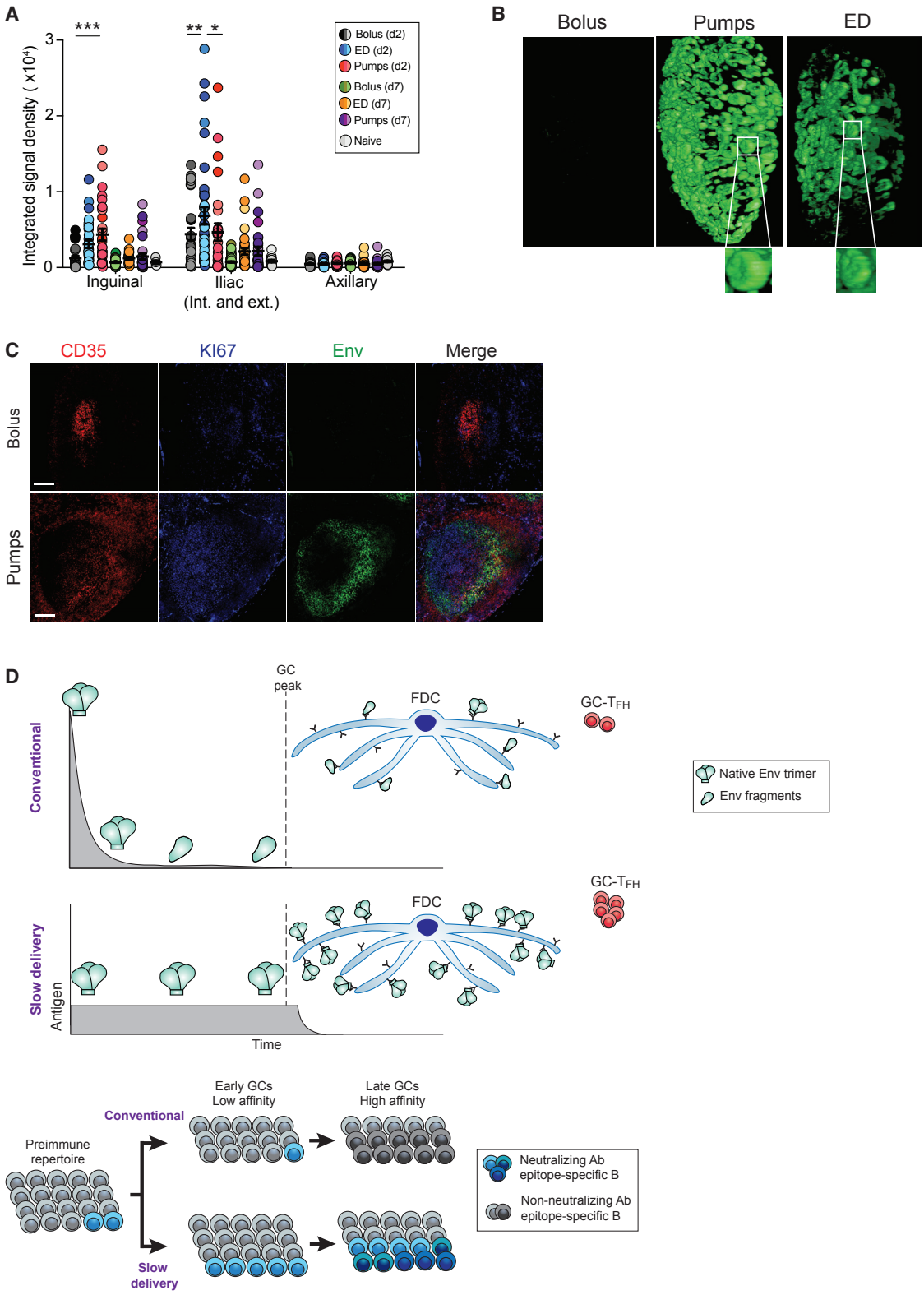

Figure 7. Slow Delivery Immunization Results in Enhanced Antigen Retention in LNs

(A) Quantitation of fluorescent Env in draining inguinal and iliac and non-draining axillary LNs. Mean ± SEM; statistical significance was tested using two-way ANOVA. *adjusted $p < 0.05$, **$p < 0.01$, ***$p < 0.001$.

(legend continued on next page)

composition of the Ab response was altered by slow delivery so that nAbs were a significantly greater fraction of the responses. The data show that slow delivery immunization does not simply elicit a larger total Ab response.

Nearly 20% of Env trimer-specific B cells in bolus-immunized animals were IGLV3-15^{+}. Several IGLV3-15^{+} Abs targeted the non-neutralizing base of the Env trimer. The base is a major site recognized by Abs of soluble trimer-immunized animals. The trimer base appears to be immunodominant because it is a large exposed protein surface with many potential epitopes and acceptable BCR angles of approach compared with the other surfaces of the Env trimer, which are predominantly shielded by large glycans (Havenar-Daughton et al., 2017). Taken together, the differences in the Env-specific B cell repertoire, nAb titers, and polyclonal Ab EM mapping demonstrate substantial immunodominance of non-neutralizing B cells that outcompete B cells specific for neutralizing epitopes after a conventional bolus injection.

Slow delivery immunization altered the repertoire of the responding Env-specific B cells and the range of Ab and nAb specificities. The simplest explanation for this outcome is that slow delivery increases the likelihood that rare and/or lower-affinity immunorecessive nAb precursors are recruited into the B cell response, resulting in more diversity in the epitopes targeted among the B_{GC} cells. We reiterate that the antigen dose was equal between the bolus and OP or ED animals; thus, total dose is not the driver of these differential outcomes. It has been reported that naive antigen-specific B cells normally have a narrow window of time of a few days to be recruited into a GC response (Turner et al., 2017). A narrow window of time for B cell recruitment disproportionately affects B cells with rare precursor frequencies. Slow delivery immunization may substantially expand the pool of recruited B cells by extending that window, increasing the breadth of the B cell repertoire sampled by the draining LN. Additionally, T_{FH} cell selection of B cells based on affinity may be most stringent prior to the GC response (Schwickert et al., 2011; Yeh et al., 2018); slow antigen delivery may reduce that stringency by substantially broadening the time window for T_{FH} cell interactions with Env-specific B cells of differing epitope specificities at the border of the follicle. The diversity of the B cell response would then likely be greater at the end of the immunization.

Despite a considerable apparent difference in affinity maturation (Env^{hi} B_{GC} and B_{Mem} cells), SHM rates were largely equivalent between OP and bolus groups at the times measured. The data suggest that differential rates of SHM were not the cause of the improved affinity maturation and improved nAb responses. A study examining SHM in B_{Mem} cells after RM immunizations with non-native Env trimers and a range of adjuvants (which did not elicit tier 2 nAbs) did not observe differences in SHM between groups (Francica et al., 2015). The SHM data here are consistent with a model where the primary cause of the difference in the nAb outcomes was the altered immunodominance profile of the B cell response.

A small fraction of Env-specific B cells from OP RMs utilized IGLV3-15, but Abs isolated from OP animals still targeted the base, consistent with diverse epitopes accessible on the base allowing BCRs targeting this site to utilize diverse *IGHV* and *IGLV* genes. Although the Env trimer base was exposed in both contexts, differences in epitope accessibility on the Env trimer may exist between immunization strategies (Figure 7D). Immune complexes (ICs), composed of the Env trimer and Abs, are bound by FDCs for presentation to B cells. Binding of an Ab to its cognate epitope, however, may block access to that epitope by B_{GC} cells undergoing selection. We speculate that a large fraction of the early Ab response targets the base. During a slow delivery immunization, early base-specific non-neutralizing Abs may form ICs with newly available Env trimers, enhancing presentation on FDCs and possibly increasing the likelihood that nAb epitope-specific B_{GC} cells will be selected for survival because of increased antigen availability in the GC and the orientation of the Env trimer on FDCs occluding the base.

We predicted that slow release immunization would reduce the B cell response to protein breakdown products and fragments that occur *in vivo*, such as the internal face of gp120 and V3, by protecting the antigen in its native form, thus having a greater percentage of intact Env trimer antigen on FDCs 2–10 weeks post-immunization (Cirelli and Crotty, 2017; Tam et al., 2016). B_{GC} cell responses to breakdown products are surely present in each immunization group. These cells likely make up a substantial fraction of the "dark antigen" GC response (Kuraoka et al., 2016) and may have immunodominant specificities because a majority of B_{GC} cells did not bind the intact native Env trimer with measurable affinity (Figures 1I and S7E). Adjuvant alone does not induce a B_{GC} cell response, consistent with the conclusion that the B_{GC} cells elicited in these immunizations are predominantly specific for Env (Havenar-Daughton et al., 2016a). Although those specificities are of interest, experiments here focused on the Env trimer-binding B cells because of limited cell numbers per sample.

Despite their enhanced and more diverse responses to immunization, slow delivery-immunized animals still targeted non-neutralizing epitopes. Immunogens should therefore be optimized to focus the response toward neutralizing epitopes and minimize responses against non-neutralizing epitopes. OPs have been used in humans for drug delivery and are feasible for early human vaccine trials. However, OPs are impractical for large-scale vaccination efforts because immunization requires a simple surgery. Nevertheless, ED is technically available immediately as a GC enhancing alternative to conventional bolus

(B) Light sheet microscopy visualizing Env in intact draining LNs on day 2. 360° views are available in Video S1.

(C) Histology of draining LNs on day 7. Green, Env; red, CD35; blue, KI67. Scale bars, 100 μm.

(D) Model of the GC response in conventional immunization versus slow delivery. Slow delivery immunization likely alters early (~days 1–7) activation and differentiation of T_{FH} cells and activation and recruitment of a diverse set of B cells. Greater GC-T_{FH} help supports a wider repertoire of B cells, which is more likely to contain nAb precursors, later in the response (weeks 3–7). Antigen delivered via conventional bolus immunization can be subject to degradative processes, and nonnative forms of antigen can be presented by FDCs late in the response, whereas OPs protect the antigen prior to release. Immune complex (IC) formation is enhanced by slow delivery immunization. See also Figure S8 and Video S1.

immunization. Less cumbersome slow delivery immunization technologies are worthy of further development, including degradable encapsulating biomaterials and depot-forming adjuvants that make antigen available over time (i.e., not rendered inert in the depot) in ways that sustain GCs (Demuth et al., 2013, 2014). Such technologies may be able to rescue protective immune responses to antigens that have previously failed by conventional bolus immunization if immunodominance of non-neutralizing epitopes was a factor in their failure.

STAR★METHODS

Detailed methods are provided in the online version of this paper and include the following:

- KEY RESOURCES TABLE
- CONTACT FOR REAGENT AND RESOURCE SHARING
- EXPERIMENTAL MODEL AND SUBJECT DETAILS
  - Rhesus Macaques
- METHOD DETAILS
  - Immunizations
  - Lymph node fine needle aspirates, whole LN biopsy tissue, blood collection and processing
  - ISCOMs-class saponin adjuvant
  - Immunogen and probe generation
  - Flow cytometry and cellular analyses
  - Antigen-specific $CD4^+$ T cell assay
  - Whole genome sequencing and genome assembly
  - Immunoglobulin loci annotation
  - Bulk BCR sequencing
  - Single cell RNA-seq
  - V gene and somatic hypermutation analyses
  - Lineage analysis
  - ELISAs
  - Pseudovirus neutralization assay
  - 19R
  - Monoclonal EM analysis
  - Polyclonal EM analysis
  - Whole LN Imaging
  - Histology
- QUANTIFICATION AND STATISTICAL ANALYSIS
- DATA AND SOFTWARE AVAILABILITY

SUPPLEMENTAL INFORMATION

Supplemental Information can be found online at https://doi.org/10.1016/j.cell.2019.04.012.

ACKNOWLEDGMENTS

We thank A. Fungtammasan and B. Hannigan for genome assembly, S. Gumber of the Yerkes National Primate Research Center (YNPRC) for tissue isolation assistance, T. Diefenbach of the Ragon Institute Imagine Core for assistance, the Harvard Neurobiology Imaging Facility for consultation (NS072030), and J. Crotty for graphical assistance. This study was funded by NIH grants AI125068 (to D.J.I. and S.C.), AI100663 (Scripps CHAVI-ID to S.C., G.S., D.J.I., W.S., A.B.W., and D.R.B.), RR00165/OD011132 (to the YNPRC), AI124436 (to S.C., G.S., and S.B.), AI136621 (to A.B.W.), and F31AI131873 (to C.A.C.) and by the Ragon Institute and Howard Hughes Medical Institute (to D.J.I.).

AUTHOR CONTRIBUTIONS

K.M.C. performed AIM assays, ELISAs, and flow cytometry and analyzed data. D.G.C., C.A.E., E.H.G., Y.C., and F.V. performed animal work and flow cytometry. A.A.U., A.N.W., V.K., B.M., and S.E.B. performed BCR sequence analyses. C.N. and M.B.M. performed ELISAs. M.G.P., R.B., and D.R.B. performed and analyzed neutralization assays. C.A.C., B.N., and A.B.W. performed EM. S.R. performed flow cytometry. J.T.M., B.C., and D.J.I. performed antigen imaging. S.C. and M.L.S. designed the RM genome sequencing study. W.G., O.L.R., and C.T.W. assembled and annotated the germline Ig locus. N.B.P. and S.E.B. provided RM tissue. T.T. and D.J.I. provided the ISCOM-type adjuvant. S.M., D.W.K., and W.R.S. provided immunogens and proteins. K.M.C. and S.C. wrote the manuscript. D.J.I. and S.C. conceived the study. S.C. and G.S. supervised the study.

DECLARATION OF INTERESTS

The authors declare no competing interests.

Received: October 5, 2018
Revised: February 26, 2019
Accepted: April 5, 2019
Published: May 9, 2019

REFERENCES

Abbott, R.K., Lee, J.H., Menis, S., Skog, P., Rossi, M., Ota, T., Kulp, D.W., Bhullar, D., Kalyuzhniy, O., Havenar-Daughton, C., et al. (2018). Precursor Frequency and Affinity Determine B Cell Competitive Fitness in Germinal Centers, Tested with Germline-Targeting HIV Vaccine Immunogens. Immunity *48*, 133–146.e6.

Alkan, C., Sajjadian, S., and Eichler, E.E. (2011). Limitations of next-generation genome sequence assembly. Nat. Methods *8*, 61–65.

Andrew, S. (2010). FastQC: A quality control tool for high throughput sequence data. http://www.bioinformatics.babraham.ac.uk/projects/fastqc/.

Andrews, S.F., Graham, B.S., Mascola, J.R., and McDermott, A.B. (2018). Is It Possible to Develop a "Universal" Influenza Virus Vaccine? Immunogenetic Considerations Underlying B-Cell Biology in the Development of a Pan-Subtype Influenza A Vaccine Targeting the Hemagglutinin Stem. Cold Spring Harb. Perspect. Biol. *10*, a029413.

Angeletti, D., and Yewdell, J.W. (2018). Understanding and Manipulating Viral Immunity: Antibody Immunodominance Enters Center Stage. Trends Immunol. *39*, 549–561.

Angeletti, D., Gibbs, J.S., Angel, M., Kosik, I., Hickman, H.D., Frank, G.M., Das, S.R., Wheatley, A.K., Prabhakaran, M., Leggat, D.J., et al. (2017). Defining B cell immunodominance to viruses. Nat. Immunol. *18*, 456–463.

Bianchi, M., Turner, H.L., Nogal, B., Cottrell, C.A., Oyen, D., Pauthner, M., Bastidas, R., Nedellec, R., McCoy, L.E., Wilson, I.A., et al. (2018). Electron-Microscopy-Based Epitope Mapping Defines Specificities of Polyclonal Antibodies Elicited during HIV-1 BG505 Envelope Trimer Immunization. Immunity *49*, 288–300.e8.

Bolger, A.M., Lohse, M., and Usadel, B. (2014). Trimmomatic: a flexible trimmer for Illumina sequence data. Bioinformatics *30*, 2114–2120.

Burton, D.R., and Hangartner, L. (2016). Broadly Neutralizing Antibodies to HIV and Their Role in Vaccine Design. Annu. Rev. Immunol. *34*, 635–659.

Chaisson, M.J., and Tesler, G. (2012). Mapping single molecule sequencing reads using basic local alignment with successive refinement (BLASR): application and theory. BMC Bioinformatics *13*, 238.

Chin, C.S., Peluso, P., Sedlazeck, F.J., Nattestad, M., Concepcion, G.T., Clum, A., Dunn, C., O'Malley, R., Figueroa-Balderas, R., Morales-Cruz, A., et al. (2016). Phased diploid genome assembly with single-molecule real-time sequencing. Nat. Methods *13*, 1050–1054.

Chowdhury, A., Del Rio Estrada, P.M., Tharp, G.K., Trible, R.P., Amara, R.R., Chahroudi, A., Reyes-Teran, G., Bosinger, S.E., and Silvestri, G. (2015).

Decreased T Follicular Regulatory Cell/T Follicular Helper Cell (TFH) in Simian Immunodeficiency Virus-Infected Rhesus Macaques May Contribute to Accumulation of TFH in Chronic Infection. J. Immunol. *195*, 3237–3247.

Cirelli, K.M., and Crotty, S. (2017). Germinal center enhancement by extended antigen availability. Curr. Opin. Immunol. *47*, 64–69.

Corcoran, M.M., Phad, G.E., Vázquez Bernat, N., Stahl-Hennig, C., Sumida, N., Persson, M.A.A., Martin, M., and Karlsson Hedestam, G.B. (2016). Production of individualized V gene databases reveals high levels of immunoglobulin genetic diversity. Nat. Commun. *7*, 13642.

Crotty, S. (2014). T follicular helper cell differentiation, function, and roles in disease. Immunity *41*, 529–542.

Dan, J.M., Lindestam Arlehamn, C.S., Weiskopf, D., da Silva Antunes, R., Havenar-Daughton, C., Reiss, S.M., Brigger, M., Bothwell, M., Sette, A., and Crotty, S. (2016). A Cytokine-Independent Approach To Identify Antigen-Specific Human Germinal Center T Follicular Helper Cells and Rare Antigen-Specific CD4+ T Cells in Blood. J. Immunol. *197*, 983–993.

deCamp, A., Hraber, P., Bailer, R.T., Seaman, M.S., Ochsenbauer, C., Kappes, J., Gottardo, R., Edlefsen, P., Self, S., Tang, H., et al. (2014). Global panel of HIV-1 Env reference strains for standardized assessments of vaccine-elicited neutralizing antibodies. J. Virol. *88*, 2489–2507.

Demuth, P.C., Garcia-Beltran, W.F., Ai-Ling, M.L., Hammond, P.T., and Irvine, D.J. (2013). Composite dissolving microneedles for coordinated control of antigen and adjuvant delivery kinetics in transcutaneous vaccination. Adv. Funct. Mater. *23*, 161–172.

DeMuth, P.C., Min, Y., Irvine, D.J., and Hammond, P.T. (2014). Implantable silk composite microneedles for programmable vaccine release kinetics and enhanced immunogenicity in transcutaneous immunization. Adv. Healthc. Mater. *3*, 47–58.

Edgar, R.C. (2004). MUSCLE: multiple sequence alignment with high accuracy and high throughput. Nucleic Acids Res. *32*, 1792–1797.

Ehrenmann, F., and Lefranc, M.P. (2011). IMGT/DomainGapAlign: IMGT standardized analysis of amino acid sequences of variable, constant, and groove domains (IG, TR, MH, IgSF, MhSF). Cold Spring Harb. Protoc. *2011*, 737–749.

Ehrenmann, F., Kaas, Q., and Lefranc, M.P. (2010). IMGT/3Dstructure-DB and IMGT/DomainGapAlign: a database and a tool for immunoglobulins or antibodies, T cell receptors, MHC, IgSF and MhcSF. Nucleic Acids Res. *38*, D301–D307.

Feng, Y., Tran, K., Bale, S., Kumar, S., Guenaga, J., Wilson, R., de Val, N., Arendt, H., DeStefano, J., Ward, A.B., and Wyatt, R.T. (2016). Thermostability of Well-Ordered HIV Spikes Correlates with the Elicitation of Autologous Tier 2 Neutralizing Antibodies. PLoS Pathog. *12*, e1005767.

Francica, J.R., Sheng, Z., Zhang, Z., Nishimura, Y., Shingai, M., Ramesh, A., Keele, B.F., Schmidt, S.D., Flynn, B.J., Darko, S., et al.; NISC Comparative Sequencing Program (2015). Analysis of immunoglobulin transcripts and hypermutation following SHIV(AD8) infection and protein-plus-adjuvant immunization. Nat. Commun. *6*, 6565.

Fu, L., Niu, B., Zhu, Z., Wu, S., and Li, W. (2012). CD-HIT: accelerated for clustering the next-generation sequencing data. Bioinformatics *28*, 3150–3152.

Gibbs, R.A., Rogers, J., Katze, M.G., Bumgarner, R., Weinstock, G.M., Mardis, E.R., Remington, K.A., Strausberg, R.L., Venter, J.C., Wilson, R.K., et al.; Rhesus Macaque Genome Sequencing and Analysis Consortium (2007). Evolutionary and biomedical insights from the rhesus macaque genome. Science *316*, 222–234.

Gitlin, A.D., Shulman, Z., and Nussenzweig, M.C. (2014). Clonal selection in the germinal centre by regulated proliferation and hypermutation. Nature *509*, 637–640.

Gitlin, A.D., Mayer, C.T., Oliveira, T.Y., Shulman, Z., Jones, M.J.K., Koren, A., and Nussenzweig, M.C. (2015). HUMORAL IMMUNITY. T cell help controls the speed of the cell cycle in germinal center B cells. Science *349*, 643–646.

Grabherr, M.G., Haas, B.J., Yassour, M., Levin, J.Z., Thompson, D.A., Amit, I., Adiconis, X., Fan, L., Raychowdhury, R., Zeng, Q., et al. (2011). Full-length transcriptome assembly from RNA-Seq data without a reference genome. Nat. Biotechnol. *29*, 644–652.

Gupta, N.T., Vander Heiden, J.A., Uduman, M., Gadala-Maria, D., Yaari, G., and Kleinstein, S.H. (2015). Change-O: a toolkit for analyzing large-scale B cell immunoglobulin repertoire sequencing data. Bioinformatics *31*, 3356–3358.

Havenar-Daughton, C., Carnathan, D.G., Torrents de la Peña, A., Pauthner, M., Briney, B., Reiss, S.M., Wood, J.S., Kaushik, K., van Gils, M.J., Rosales, S.L., et al. (2016a). Direct Probing of Germinal Center Responses Reveals Immunological Features and Bottlenecks for Neutralizing Antibody Responses to HIV Env Trimer. Cell Rep. *17*, 2195–2209.

Havenar-Daughton, C., Reiss, S.M., Carnathan, D.G., Wu, J.E., Kendric, K., Torrents de la Peña, A., Kasturi, S.P., Dan, J.M., Bothwell, M., Sanders, R.W., et al. (2016b). Cytokine-Independent Detection of Antigen-Specific Germinal Center T Follicular Helper Cells in Immunized Nonhuman Primates Using a Live Cell Activation-Induced Marker Technique. J. Immunol. *197*, 994–1002.

Havenar-Daughton, C., Lee, J.H., and Crotty, S. (2017). Tfh cells and HIV bnAbs, an immunodominance model of the HIV neutralizing antibody generation problem. Immunol. Rev. *275*, 49–61.

Haynes, B.F., Gilbert, P.B., McElrath, M.J., Zolla-Pazner, S., Tomaras, G.D., Alam, S.M., Evans, D.T., Montefiori, D.C., Karnasuta, C., Sutthent, R., et al. (2012). Immune-correlates analysis of an HIV-1 vaccine efficacy trial. N. Engl. J. Med. *366*, 1275–1286.

Hogenesch, H. (2002). Mechanisms of stimulation of the immune response by aluminum adjuvants. Vaccine *20* (*Suppl 3*), S34–S39.

Hogenesch, H. (2013). Mechanism of immunopotentiation and safety of aluminum adjuvants. Front. Immunol. *3*, 406.

Hu, J.K., Crampton, J.C., Cupo, A., Ketas, T., van Gils, M.J., Sliepen, K., de Taeye, S.W., Sok, D., Ozorowski, G., Deresa, I., et al. (2015). Murine Antibody Responses to Cleaved Soluble HIV-1 Envelope Trimers Are Highly Restricted in Specificity. J. Virol. *89*, 10383–10398.

Huang, J., Kang, B.H., Ishida, E., Zhou, T., Griesman, T., Sheng, Z., Wu, F., Doria-Rose, N.A., Zhang, B., McKee, K., et al. (2016). Identification of a CD4-Binding-Site Antibody to HIV that Evolved Near-Pan Neutralization Breadth. Immunity *45*, 1108–1121.

Hutchison, S., Benson, R.A., Gibson, V.B., Pollock, A.H., Garside, P., and Brewer, J.M. (2012). Antigen depot is not required for alum adjuvanticity. FASEB J. *26*, 1272–1279.

Julien, J.P., Cupo, A., Sok, D., Stanfield, R.L., Lyumkis, D., Deller, M.C., Klasse, P.J., Burton, D.R., Sanders, R.W., Moore, J.P., et al. (2013). Crystal structure of a soluble cleaved HIV-1 envelope trimer. Science *342*, 1477–1483.

Katoh, K., and Standley, D.M. (2013). MAFFT multiple sequence alignment software version 7: improvements in performance and usability. Mol. Biol. Evol. *30*, 772–780.

Kent, W.J. (2002). BLAT–the BLAST-like alignment tool. Genome Res. *12*, 656–664.

Klasse, P.J., Ketas, T.J., Cottrell, C.A., Ozorowski, G., Debnath, G., Camara, D., Francomano, E., Pugach, P., Ringe, R.P., LaBranche, C.C., et al. (2018). Epitopes for neutralizing antibodies induced by HIV-1 envelope glycoprotein BG505 SOSIP trimers in rabbits and macaques. PLoS Pathog. *14*, e1006913.

Klein, F., Mouquet, H., Dosenovic, P., Scheid, J.F., Scharf, L., and Nussenzweig, M.C. (2013). Antibodies in HIV-1 vaccine development and therapy. Science *341*, 1199–1204.

Kong, R., Xu, K., Zhou, T., Acharya, P., Lemmin, T., Liu, K., Ozorowski, G., Soto, C., Taft, J.D., Bailer, R.T., et al. (2016). Fusion peptide of HIV-1 as a site of vulnerability to neutralizing antibody. Science *352*, 828–833.

Kubota, S.I., Takahashi, K., Nishida, J., Morishita, Y., Ehata, S., Tainaka, K., Miyazono, K., and Ueda, H.R. (2017). Whole-Body Profiling of Cancer Metastasis with Single-Cell Resolution. Cell Rep. *20*, 236–250.

Kulp, D.W., Steichen, J.M., Pauthner, M., Hu, X., Schiffner, T., Liguori, A., Cottrell, C.A., Havenar-Daughton, C., Ozorowski, G., Georgeson, E., et al. (2017). Structure-based design of native-like HIV-1 envelope trimers to silence non-neutralizing epitopes and eliminate CD4 binding. Nat. Commun. *8*, 1655.

Kumar, V., Vollbrecht, T., Chernyshev, M., Mohan, S., Hanst, B., Bavafa, N., Lorenzo, A., Ketteringham, R., Eren, K., Golden, M., et al. (2018). Long-read amplicon denoising. bioRxiv. https://doi.org/10.1101/383794.

Kuraoka, M., Schmidt, A.G., Nojima, T., Feng, F., Watanabe, A., Kitamura, D., Harrison, S.C., Kepler, T.B., and Kelsoe, G. (2016). Complex Antigens Drive Permissive Clonal Selection in Germinal Centers. Immunity *44*, 542–552.

Lander, G.C., Stagg, S.M., Voss, N.R., Cheng, A., Fellmann, D., Pulokas, J., Yoshioka, C., Irving, C., Mulder, A., Lau, P.W., et al. (2009). Appion: an integrated, database-driven pipeline to facilitate EM image processing. J. Struct. Biol. *166*, 95–102.

Langmead, B., and Salzberg, S.L. (2012). Fast gapped-read alignment with Bowtie 2. Nat. Methods *9*, 357–359.

Lefranc, M.P., and Lefranc, G. (2001). The Immunoglobulin Factsbook, First Edition (Academic Press).

Locci, M., Havenar-Daughton, C., Landais, E., Wu, J., Kroenke, M.A., Arlehamn, C.L., Su, L.F., Cubas, R., Davis, M.M., Sette, A., et al.; International AIDS Vaccine Initiative Protocol C Principal Investigators (2013). Human circulating PD-1+CXCR3-CXCR5+ memory Tfh cells are highly functional and correlate with broadly neutralizing HIV antibody responses. Immunity *39*, 758–769.

Lyumkis, D., Julien, J.P., de Val, N., Cupo, A., Potter, C.S., Klasse, P.J., Burton, D.R., Sanders, R.W., Moore, J.P., Carragher, B., et al. (2013). Cryo-EM structure of a fully glycosylated soluble cleaved HIV-1 envelope trimer. Science *342*, 1484–1490.

Mascola, J.R., Snyder, S.W., Weislow, O.S., Belay, S.M., Belshe, R.B., Schwartz, D.H., Clements, M.L., Dolin, R., Graham, B.S., Gorse, G.J., et al.; The National Institute of Allergy and Infectious Diseases AIDS Vaccine Evaluation Group (1996). Immunization with envelope subunit vaccine products elicits neutralizing antibodies against laboratory-adapted but not primary isolates of human immunodeficiency virus type 1. J. Infect. Dis. *173*, 340–348.

Mesin, L., Ersching, J., and Victora, G.D. (2016). Germinal Center B Cell Dynamics. Immunity *45*, 471–482.

Montefiori, D.C., Roederer, M., Morris, L., and Seaman, M.S. (2018). Neutralization tiers of HIV-1. Curr. Opin. HIV AIDS *13*, 128–136.

Moody, M.A., Pedroza-Pacheco, I., Vandergrift, N.A., Chui, C., Lloyd, K.E., Parks, R., Soderberg, K.A., Ogbe, A.T., Cohen, M.S., Liao, H.X., et al. (2016). Immune perturbations in HIV-1-infected individuals who make broadly neutralizing antibodies. Sci. Immunol. *1*, aag0851.

Nakane, T., Kimanius, D., Lindahl, E., and Scheres, S.H. (2018). Characterisation of molecular motions in cryo-EM single-particle data by multi-body refinement in RELION. eLife *7*, 1485.

Nishimura, Y., and Martin, M.A. (2017). Of Mice, Macaques, and Men: Broadly Neutralizing Antibody Immunotherapy for HIV-1. Cell Host Microbe *22*, 207–216.

Noe, S.M., Green, M.A., HogenEsch, H., and Hem, S.L. (2010). Mechanism of immunopotentiation by aluminum-containing adjuvants elucidated by the relationship between antigen retention at the inoculation site and the immune response. Vaccine *28*, 3588–3594.

Pauthner, M., Havenar-Daughton, C., Sok, D., Nkolola, J.P., Bastidas, R., Boopathy, A.V., Carnathan, D.G., Chandrashekar, A., Cirelli, K.M., Cottrell, C.A., et al. (2017). Elicitation of Robust Tier 2 Neutralizing Antibody Responses in Nonhuman Primates by HIV Envelope Trimer Immunization Using Optimized Approaches. Immunity *46*, 1073–1088.e6.

Petrovas, C., Yamamoto, T., Gerner, M.Y., Boswell, K.L., Wloka, K., Smith, E.C., Ambrozak, D.R., Sandler, N.G., Timmer, K.J., Sun, X., et al. (2012). CD4 T follicular helper cell dynamics during SIV infection. J. Clin. Invest. *122*, 3281–3294.

Picelli, S., Faridani, O.R., Björklund, A.K., Winberg, G., Sagasser, S., and Sandberg, R. (2014). Full-length RNA-seq from single cells using Smart-seq2. Nat. Protoc. *9*, 171–181.

Plotkin, S.A. (2010). Correlates of protection induced by vaccination. Clin. Vaccine Immunol. *17*, 1055–1065.

Potter, C.S., Chu, H., Frey, B., Green, C., Kisseberth, N., Madden, T.J., Miller, K.L., Nahrstedt, K., Pulokas, J., Reilein, A., et al. (1999). Leginon: a system for fully automated acquisition of 1000 electron micrographs a day. Ultramicroscopy *77*, 153–161.

Price, M.N., Dehal, P.S., and Arkin, A.P. (2010). FastTree 2–approximately maximum-likelihood trees for large alignments. PLoS ONE *5*, e9490.

Ramesh, A., Darko, S., Hua, A., Overman, G., Ransier, A., Francica, J.R., Trama, A., Tomaras, G.D., Haynes, B.F., Douek, D.C., and Kepler, T.B. (2017). Structure and Diversity of the Rhesus Macaque Immunoglobulin Loci through Multiple *De Novo* Genome Assemblies. Front. Immunol. *8*, 1407.

Reiss, S., Baxter, A.E., Cirelli, K.M., Dan, J.M., Morou, A., Daigneault, A., Brassard, N., Silvestri, G., Routy, J.P., Havenar-Daughton, C., et al. (2017). Comparative analysis of activation induced marker (AIM) assays for sensitive identification of antigen-specific CD4 T cells. PLoS ONE *12*, e0186998.

Renier, N., Adams, E.L., Kirst, C., Wu, Z., Azevedo, R., Kohl, J., Autry, A.E., Kadiri, L., Umadevi Venkataraju, K., Zhou, Y., et al. (2016). Mapping of Brain Activity by Automated Volume Analysis of Immediate Early Genes. Cell *165*, 1789–1802.

Rerks-Ngarm, S., Pitisuttithum, P., Nitayaphan, S., Kaewkungwal, J., Chiu, J., Paris, R., Premsri, N., Namwat, C., de Souza, M., Adams, E., et al.; MOPH-TAVEG Investigators (2009). Vaccination with ALVAC and AIDSVAX to prevent HIV-1 infection in Thailand. N. Engl. J. Med. *361*, 2209–2220.

Richman, D.D., Wrin, T., Little, S.J., and Petropoulos, C.J. (2003). Rapid evolution of the neutralizing antibody response to HIV type 1 infection. Proc. Natl. Acad. Sci. USA *100*, 4144–4149.

Robinson, J.T., Thorvaldsdóttir, H., Winckler, W., Guttman, M., Lander, E.S., Getz, G., and Mesirov, J.P. (2011). Integrative genomics viewer. Nat. Biotechnol. *29*, 24–26.

Sanders, R.W., Derking, R., Cupo, A., Julien, J.P., Yasmeen, A., de Val, N., Kim, H.J., Blattner, C., de la Peña, A.T., Korzun, J., et al. (2013). A next-generation cleaved, soluble HIV-1 Env trimer, BG505 SOSIP.664 gp140, expresses multiple epitopes for broadly neutralizing but not non-neutralizing antibodies. PLoS Pathog. *9*, e1003618.

Sanders, R.W., van Gils, M.J., Derking, R., Sok, D., Ketas, T.J., Burger, J.A., Ozorowski, G., Cupo, A., Simonich, C., Goo, L., et al. (2015). HIV-1 VACCINES. HIV-1 neutralizing antibodies induced by native-like envelope trimers. Science *349*, aac4223–aac4223.

Scheres, S.H.W. (2012). RELION: implementation of a Bayesian approach to cryo-EM structure determination. J. Struct. Biol. *180*, 519–530.

Schwickert, T.A., Victora, G.D., Fooksman, D.R., Kamphorst, A.O., Mugnier, M.R., Gitlin, A.D., Dustin, M.L., and Nussenzweig, M.C. (2011). A dynamic T cell-limited checkpoint regulates affinity-dependent B cell entry into the germinal center. J. Exp. Med. *208*, 1243–1252.

Shi, Y., HogenEsch, H., and Hem, S.L. (2001). Change in the degree of adsorption of proteins by aluminum-containing adjuvants following exposure to interstitial fluid: freshly prepared and aged model vaccines. Vaccine *20*, 80–85.

Sorzano, C.O.S., Bilbao-Castro, J.R., Shkolnisky, Y., Alcorlo, M., Melero, R., Caffarena-Fernández, G., Li, M., Xu, G., Marabini, R., and Carazo, J.M. (2010). A clustering approach to multireference alignment of single-particle projections in electron microscopy. J. Struct. Biol. *171*, 197–206.

Stewart-Jones, G.B.E., Soto, C., Lemmin, T., Chuang, G.Y., Druz, A., Kong, R., Thomas, P.V., Wagh, K., Zhou, T., Behrens, A.J., et al. (2016). Trimeric HIV-1-Env Structures Define Glycan Shields from Clades A, B, and G. Cell *165*, 813–826.

Suloway, C., Pulokas, J., Fellmann, D., Cheng, A., Guerra, F., Quispe, J., Stagg, S., Potter, C.S., and Carragher, B. (2005). Automated molecular microscopy: the new Leginon system. J. Struct. Biol. *151*, 41–60.

Sundling, C., Li, Y., Huynh, N., Poulsen, C., Wilson, R., O'Dell, S., Feng, Y., Mascola, J.R., Wyatt, R.T., and Karlsson Hedestam, G.B. (2012). High-resolution definition of vaccine-elicited B cell responses against the HIV primary receptor binding site. Sci. Transl. Med. *4*, 142ra96.

Tam, H.H., Melo, M.B., Kang, M., Pelet, J.M., Ruda, V.M., Foley, M.H., Hu, J.K., Kumari, S., Crampton, J., Baldeon, A.D., et al. (2016). Sustained antigen

availability during germinal center initiation enhances antibody responses to vaccination. Proc. Natl. Acad. Sci. USA *113*, E6639–E6648.

Tange, O. (2011). Gnu parallel: the command-line power tool. login *36*, 42–47.

Tas, J.M.J., Mesin, L., Pasqual, G., Targ, S., Jacobsen, J.T., Mano, Y.M., Chen, C.S., Weill, J.C., Reynaud, C.A., Browne, E.P., et al. (2016). Visualizing antibody affinity maturation in germinal centers. Science *351*, 1048–1054.

Thorvaldsdóttir, H., Robinson, J.T., and Mesirov, J.P. (2013). Integrative Genomics Viewer (IGV): high-performance genomics data visualization and exploration. Brief. Bioinform. *14*, 178–192.

Torrents de la Peña, A., Julien, J.P., de Taeye, S.W., Garces, F., Guttman, M., Ozorowski, G., Pritchard, L.K., Behrens, A.J., Go, E.P., Burger, J.A., et al. (2017). Improving the Immunogenicity of Native-like HIV-1 Envelope Trimers by Hyperstabilization. Cell Rep *20*, 1805–1817.

Turner, J.S., Benet, Z.L., and Grigorova, I.L. (2017). Antigen Acquisition Enables Newly Arriving B Cells To Enter Ongoing Immunization-Induced Germinal Centers. J. Immunol. *199*, 1301–1307.

Upadhyay, A.A., Kauffman, R.C., Wolabaugh, A.N., Cho, A., Patel, N.B., Reiss, S.M., Havenar-Daughton, C., Dawoud, R.A., Tharp, G.K., Sanz, I., et al. (2018). BALDR: a computational pipeline for paired heavy and light chain immunoglobulin reconstruction in single-cell RNA-seq data. Genome Med. *10*, 20.

Vander Heiden, J.A., Yaari, G., Uduman, M., Stern, J.N.H., O'Connor, K.C., Hafler, D.A., Vigneault, F., and Kleinstein, S.H. (2014). pRESTO: a toolkit for processing high-throughput sequencing raw reads of lymphocyte receptor repertoires. Bioinformatics *30*, 1930–1932.

Victora, G.D., and Wilson, P.C. (2015). Germinal center selection and the antibody response to influenza. Cell *163*, 545–548.

Victora, G.D., Schwickert, T.A., Fooksman, D.R., Kamphorst, A.O., Meyer-Hermann, M., Dustin, M.L., and Nussenzweig, M.C. (2010). Germinal center dynamics revealed by multiphoton microscopy with a photoactivatable fluorescent reporter. Cell *143*, 592–605.

Voss, N.R., Yoshioka, C.K., Radermacher, M., Potter, C.S., and Carragher, B. (2009). DoG Picker and TiltPicker: software tools to facilitate particle selection in single particle electron microscopy. J. Struct. Biol. *166*, 205–213.

Watson, C.T., and Breden, F. (2012). The immunoglobulin heavy chain locus: genetic variation, missing data, and implications for human disease. Genes Immun. *13*, 363–373.

Watson, C.T., Glanville, J., and Marasco, W.A. (2017). The Individual and Population Genetics of Antibody Immunity. Trends Immunol. *38*, 459–470.

Wei, X., Decker, J.M., Wang, S., Hui, H., Kappes, J.C., Wu, X., Salazar-Gonzalez, J.F., Salazar, M.G., Kilby, J.M., Saag, M.S., et al. (2003). Antibody neutralization and escape by HIV-1. Nature *422*, 307–312.

Weissburg, R.P., Berman, P.W., Cleland, J.L., Eastman, D., Farina, F., Frie, S., Lim, A., Mordenti, J., Nguyen, T.T., and Peterson, M.R. (1995). Characterization of the MN gp120 HIV-1 vaccine: antigen binding to alum. Pharm. Res. *12*, 1439–1446.

West, A.P., Jr., Scharf, L., Scheid, J.F., Klein, F., Bjorkman, P.J., and Nussenzweig, M.C. (2014). Structural insights on the role of antibodies in HIV-1 vaccine and therapy. Cell *156*, 633–648.

Wu, X., Parast, A.B., Richardson, B.A., Nduati, R., John-Stewart, G., Mbori-Ngacha, D., Rainwater, S.M.J., and Overbaugh, J. (2006). Neutralization escape variants of human immunodeficiency virus type 1 are transmitted from mother to infant. J. Virol *80*, 835–844.

Yamamoto, T., Lynch, R.M., Gautam, R., Matus-Nicodemos, R., Schmidt, S.D., Boswell, K.L., Darko, S., Wong, P., Sheng, Z., Petrovas, C., et al. (2015). Quality and quantity of TFH cells are critical for broad antibody development in SHIVAD8 infection. Sci. Transl. Med. *7*, 298ra120.

Ye, J., Ma, N., Madden, T.L., and Ostell, J.M. (2013). IgBLAST: an immunoglobulin variable domain sequence analysis tool. Nucleic Acids Res. *41*, W34-40.

Yeh, C.H., Nojima, T., Kuraoka, M., and Kelsoe, G. (2018). Germinal center entry not selection of B cells is controlled by peptide-MHCII complex density. Nat. Commun. *9*, 928.

Zhou, T., Doria-Rose, N.A., Cheng, C., Stewart-Jones, G.B.E., Chuang, G.Y., Chambers, M., Druz, A., Geng, H., McKee, K., Kwon, Y.D., et al. (2017). Quantification of the Impact of the HIV-1-Glycan Shield on Antibody Elicitation. Cell Rep. *19*, 719–732.

STAR★METHODS

KEY RESOURCES TABLE

REAGENT or RESOURCE	SOURCE	IDENTIFIER
Antibodies		
Fixable Viability Dye eFluor506	Thermo Fisher Scientific	Cat # 65-0866-18
Fixable Viability Dye eFluor780	Thermo Fisher Scientific	Cat # 65-0865-18
Mouse anti-human CD20 PE-Texas Red (clone: 2H7)	Beckman Coulter	Cat # IM3607U; RRID: AB_10645191
Mouse anti-human CD4 BV650 (clone: OKT-4)	BioLegend	Cat # 317436; RRID: AB_2563050
Mouse anti-human CD8a Qdot705 (clone: 3B5)	Thermo Fisher Scientific	Cat # Q10059; RRID: AB_11180330
Mouse anti-human IgG PE-Cy7 (clone: G18-145)	BD Biosciences	Cat # 561298; RRID: AB_10611712
Mouse anti-human CXCR5 PE (clone: MU5UBEE)	Thermo Fisher Scientific	Cat # 12-9185-42; RRID: AB_11219877
Mouse anti-human PD1 BV605 (clone: EH12.2H7)	BioLegend	Cat # 329924; RRID: AB_2563212
Mouse anti-human CD3 BV786 (clone: SP34-2)	BD Biosciences	Cat # 563918; RRID: AB_2738487
Mouse anti-human IgM PerCP-Cy5.5 (clone:G20-127)	BD Biosciences	Cat # 561285; RRID: AB_10611998
Mouse anti-human Ki67 Alexa Fluor 700 (clone: B56)	BD Biosciences	Cat # 561277; RRID: AB_10611571
Mouse anti-human Ki67 Alexa Fluor 488 (clone: B56)	BD Biosciences	Cat # 558616; RRID: AB_647087
Mouse anti-human Bcl6 Alexa Fluor 488 (clone: K112-91)	BD Biosciences	Cat # 561524; RRID: AB_10716202
Mouse anti-human CD4 APC eFluor 780 (clone: SK3)	Thermo Fisher Scientific	Cat # 47-0047-42; RRID: AB_10804505
Mouse anti-human CD8 APC eFluor 780 (clone: RPA-T8)	Thermo Fisher Scientific	Cat # 47-0088-42; RRID: AB_1272046
Mouse anti-human CD16 APC eFluor 780 (clone: ebioCB16)	Thermo Fisher Scientific	Cat # 47-0168-42; RRID: AB_11220086
Mouse anti-human CD20 Alexa Fluor 488 (clone: 2H7)	BioLegend	Cat # 302316; RRID: AB_493227
Mouse anti-human CD38 PE (Clone: OKT)	NHP Reagents	Cat # PR-3802
Mouse anti-human CD71 PE-CF594 (Clone: L01.1)	BD Biosciences	Custom conjugate
Mouse anti-human CD4 BV650 (Clone: OKT4)	BioLegend	Cat # 317436; RRID: AB_2563050
Mouse anti-human CD20 BV570 (Clone: 2H7)	BioLegend	Cat # 302332; RRID: AB_2563805
Mouse anti-human PD1 BV785 (Clone: EH12.2H7)	BioLegend	Cat # 329930; RRID: AB_2563443
Mouse anti-human CXCR5 PE-Cy7 (Clone: MU5UBEE)	Thermo Fisher Scientific	Cat # 25-9185-42; RRID: AB_2573540
Mouse anti-human CD25 FITC (Clone: BC96)	BioLegend	Cat # 302604; RRID: AB_314274
Mouse anti-human OX40 PE (Clone: L106)	BD Biosciences	Cat # 340420; RRID: AB_400027

(*Continued on next page*)

Continued

REAGENT or RESOURCE	SOURCE	IDENTIFIER
Mouse anti-human 4-1BB APC (Clone:4B4-1)	BioLegend	Cat # 309810; RRID: AB_830672
Mouse anti-human CD14 APC/Cy7 (Clone: M5E2)	BioLegend	Cat # 301820; RRID: AB_493695
Mouse anti-human CD16 APC/Cy7 (Clone: 3G8)	BioLegend	Cat # 302018; RRID: AB_314218
Mouse anti-human CD20 BV650 (Clone: 2H7)	BioLegend	Cat # 302336; RRID: AB_2563806
Mouse anti-human CD4 APC (Clone: OKT4)	BioLegend	Cat # 317416; RRID: AB_571945
Mouse anti-human Bcl6 BV421 (Clone: K112-91)	BD Biosciences	Cat # 563363; RRID: AB_2738159
Mouse anti-human Bcl6 Alexa Fluor 647 (Clone: K112-91)	BD Biosciences	Cat # 561525; RRID: AB_10898007
Mouse anti-human IgM BV421 (Clone: G20-127)	BD Biosciences	Cat # 562618; RRID: AB_2737681
Mouse anti-human IgG PE (Clone: G18-145)	BD Biosciences	Cat # 560951; RRID: AB_10563761
Mouse anti-human IgD Alexa Fluor 488	Southern Biotech	Cat # 2030-30; RRID: AB_2795631
Mouse anti-human Lambda biotin (Clone: IS7-24C7)	Miltenyi	Cat # 130-093-025; RRID: AB_1036075
Mouse anti-human CD35 BV421 (Clone: E11)	BD Biosciences	Cat # 565327; RRID: AB_2739184
Streptavidin-Alexa Fluor 647	Thermo Fisher Scientific	Cat # S32357
Streptavidin-BV421	BioLegend	Cat # 405225
Streptavidin-BV711	BioLegend	Cat # 405241
Goat anti-rhesus IgG (H+L) - HRP	Southern Biotech	Cat # 6200-05; RRID: AB_2796268
Goat anti-Human IgG, Fcγ fragment specific-HRP	Jackson ImmunoResearch	Cat # 109-035-098; RRID: AB_2337586
19R	Thermo Fisher Scientific, unpublished	Custom
BDA1 HC:QVQLQESGPGLVKPSETLSLTCAVSG ASISIYWWGWIRQPPGKGLEWIGEIIGSSGSTNS NPSFKSRVTISKDASKNQFSLNLNSVTAADTAVY YCVRVGAAISLPFDYWGQGVLVTVSS LC:SYELT QPPSVSVSPGQTARITCSGDALPKKYAYWFQQKP GQSPVLIIYEDNKRPSGIPERFSGSSSGTVATLTIS GAQVEDEGDYYCYSRHSSGNHGLFGGGTRLTVL	Genscript	Custom
BDA2 HC:QVQLQESGPGLLKPSETLSLTCAVSG GSFSSYWWSWIRQPPGKGLEWIGEINGNSGSTH YNPSLKSRVTISKDASKNQFSLKLNSVTAADTAVY YCARWGPTGVTQGEPDFDYWGQGVLVTVSS LC:SYELTQPPSVSVSPGQTARITYSGDALPKRY AYWFQQKPGQSPVLIIYEDSKRPSGIPERFSGSS SGTVATLTISGAQVEDEADYYCYSTDSSGNHFF GAGTRLTVL	Genscript	Custom
BDA3 HC:QVQLQESGPGLVKPSETLSLTCAVS GHSVSSGYGWGWIRQPPGKGLEWIGQIYGYSG STSYNPSLKSRVTVSTDTSKNQFSLRLSSLTAAD TAVYYCARWHHGSFDIWGPGTPITISS LC:SYEL TQPPSVSVSPGQTARITCSGDALPKKYAYWFQQ KPGQSPVLIIYEDNKRPSGIPERFSGSSSGTVATL TINGAQVEDEGDYYCYSRHSSGNHGLFGGGTRLTVL	Genscript	Custom

(*Continued on next page*)

Continued

REAGENT or RESOURCE	SOURCE	IDENTIFIER
BDA4 HC:QVQLQESGPGLVKPSETLSLTCAVSG ASIRIYWWGWIRQPPGKGLEWIGEIIGSSGSTNS NPSFKSRVTISKDASKNQFSLNLNSVTAADTAVY YCVRVGAAISFPFDYWGQGVLVTVSS LC:SSELTQ PPSVSVSPGQTARITCSGDALPKKYAYWFQQKPG QSPVLIIYEDNKRPSGIPERFSGSSSGTVATLTISGA QVEDEGDFYCYSRHSSGNHGLFGGGTRLTVL	Genscript	Custom
BDA5 HC:QVQLQESGPGLLKPSETLSLTCAVSG GSFSSYWWSWIRQPPGKGLEWIGEINGNSGNT HYNPSLKSRVTISKDASKNHFSLKLSSVTAADTA VYYCARWGPTGVTQGEPDFDYWGQGVLVTVSS LC:SYELTQPPSVSVSPGQTARITYSGDALPKKYA YWFQQKPGQSPVLIIYEDNKRPSGIPERFSGSSSG TVATLTISGAQVEDEADYYCYSTDSSGNHFFGAG TRLTVL	Genscript	Custom
BDA6 HC:QVQLQESGPGLLKPSETLSLTCAVSGG SFSSYWWSWIRQPPGKGLEWIGEINGNSGSTHYN PSLKSRVTISKDASKNQFSLKLNSVTAADTAVYYCA RWGPTGVTQGEPDFDYWGQGVLVTVSS LC:SYEL TQPPSVSVSPGQTARITCSGDALPKKYVYWFQQK PGQSPVLIIYEDSKRPSGIPERFSGSSSGTVATLTIS GAQVEDEADYYCYSTISSGNDRIFGAGTRLTVL	Genscript	Custom
BDA7 HC:QVQLQESGPGLVKPSETLSLTCAVSGAS ISIYWWSWIRQPPGKGLEWIGEIIGNSGSTNSNPSF KSRVTISKDASKNQFSLKLSSVTAADTAVYYCVRVG AAISLPYDYWGQGVLVTVSS LC:SYELTQPPSVSVS PGQTARITCSGDALPKKYAYWFQQKPGQSPVLIIY EDNKRPSGIPERFSGSSSGTVATLTISGAQVEDEG DYYCYSRHSSGNHGLFGGGTRLTVL	Genscript	Custom
BDA8 HC:QVQLQESGPGLLKPSETLSLTCAVSGG SFSSYWWSWIRQPPGKGLEWIGEINGNSGNTHYN PSLKSRVTISKDASKNQFSLKLSSVTAADTAVYYCA RWGPTGVTQGEPEFDYWGQGVLVTVSS LC:SYEL TQPPSVSVSPGQTARITYSGDALPKKYAYWFQQK PGQSPVLIIYEDNKRPSGIPERFSGSSSGTVATLTIS GAQVEDEADYYCYSTDSSGNHFFGAGTRLTVL	Genscript	Custom
BDA9 HC:QVQLQESGPGLLKPSETLSLTCAVSGG SFSNYWWSWIRQPPGKGLEWIGEINGNSGSTHYN PSLKSRVTISKDASKNQFSLKLNSVTAADTAVYYCA RWGPTGVTQGEPDFDFWGQGVLVTVSS LC:SYEL TQPPSVSVSPGQTARITYSGDALPKRYAYWFQQK PGQSPVLIIYEDSKRPSGIPERFSGSSSGTVATLTIS GAQVEDEADYYCYSTDSSGNHFFGVGTRLTVL	Genscript	Custom
BDA10 HC:QVQLQESGPGLVKPSETLSLTCAVSGVSI SIYWWSWIRQPPGKGLEWIGEIIGNSGNTNSSPSFKS RVTISKDASKNQFSLKLSSVTAADTAVYYCVRVGAAI SLPFDYWGQGVLVTVSS LC:SYELTQPPSVSVSPGQ TARITCSGDALPEKYAYWFQQKPGQSPVLIIYDDNIR PSGIPERFSGSSSGTVATLTISGAQVEDEGDYYCYSR HSSGNHGLFGGGTRLTVL	Genscript	Custom
BDA11 HC:QVQLQESGPGLVKPSETLSLTCAVSGGS FSSYWWSWIRQPPGKGLEWIGEINGNSGSTNYNPS LKSRVTISKDASKNQFSLKLSSVTAADTAVYYCARVR VGAAISLPFDYWGQGVLVTVSS LC:SYELTQPPSVSV SPGQTARITCSGDALPKKYAYWFQQKPGQSPVLIIYE DNKRPSGIPERFSGSSSGTVATLTISGAQVEDEGDYY CYSRHISGNHGLFGGGTRLTVL	Genscript	Custom

(*Continued on next page*)

Continued

REAGENT or RESOURCE	SOURCE	IDENTIFIER
BDA12 HC: BDA1HC LC:SYELTQPPSVSVSPGQTAR ITCSGDALPKKYAYWFQQKPGQSPVLIIYEDNKRPSG IPERFSGSSSGTVATLTISGAQVEDEGDYYCFSRHSS GNHGLFGGGTRLTVL	Genscript	Custom
BDA13 HC: BDA1 HC LC:SYELTQPPSVSVSPGQTA RITCSGDALPKKYAYWFQQKPGQSPVLIIYDDSQRP SGIPERFSGSSSGTVATLTISGAQVEDEGDYYCFSRH SSGNHGLFGGGTRLTVL	Genscript	Custom
Bacterial and Virus Strains		
BG505.W6M.ENV.C2	Wu et al., 2006 / NIH AIDS Reagent Program	Cat # 11518
12 virus panel – global isolates	(deCamp et al., 2014)	
Chemicals, Peptides, and Recombinant Proteins		
BG505 Olio6	Produced inhouse (Kulp et al., 2017)	
BG505 Olio6CD4-KO	Produced inhouse (Kulp et al., 2017)	
BG505 MD39	Produced inhouse (Kulp et al., 2017)	
BG505 Olio6CD4-KO – Biotin	Produced inhouse	
BG505 Olio6 – Biotin	Produced inhouse	
BG505 MD39 – Biotin	Produced inhouse	
BG505 SOSIP – Biotin	Produced inhouse	
BG505 gp120 - Biotin	Produced inhouse	
BG505 SOSIP.664 v5.2	Produced inhouse (Torrents de la Peña et al., 2017)	
His-Tag biotin peptide biotin - ALDGGGG SHHHHHHHH	A&A Labs LLC	N/A
Recombinant Protein A Sepharose	GE Healthcare	Cat # 17127902
Lectin from *Galanthus nivalis* (snowdrop), lyophilized powder	Sigma-Aldrich	Cat # L9275-5mg
Olio6-CD4ko peptide megapool	A&A Labs LLC	N/A
Staphylococcal enterotoxin B (SEB)	Toxin Technology	Cat # BT202
DNase I Solution	StemCell Technologies	Cat # 07900
Streptavidin	Jackson ImmunoResearch Laboratories, Inc	Cat # 016-000-084
TMB Substrate	Thermo Fisher Scientific	Cat # 34021
Cholesterol	Avanti Polar Lipids	Cat # 700000
1,2-dipalmitoyl-sn-glycero-3-phosphocholine (16:0 PC (DPPC))	Avanti Polar Lipids	Cat # 850355
N-Decanoyl-*N*-methylglucamine (MEGA-10)	Sigma-Aldrich	Cat # D6277
Quil-A saponin	InvioGen	Cat # vac-quil
Critical Commercial Assays		
Pierce Fab Preparation Kit	Thermo Fisher Scientific	Cat # 44985
eBioscience FoxP3/ Transcription Factor Staining Buffer Set	Thermo Fisher Scientific	Cat # 00-5523-00
QCL-1000 Endpoint Chromogenic LAL Assay	Lonza	Cat # 50-647U
BirA biotin-protein ligase standard reaction kit	Avidity Inc	Cat # BirA500
Cholesterol Quantitation Kit	Sigma- Aldrich	Cat # MAK043-1KT
AMPure XP beads	Beckman Coulter	Cat # A63882
KAPA HiFi HotStart Real-time PCR Master Mix (2X)	Kapa Biosystems	Cat # KK2702

(*Continued on next page*)

Continued

REAGENT or RESOURCE	SOURCE	IDENTIFIER
Deposited Data		
Rhesus macaque genomic raw sequences	NCBI SRA	PRJNA509445
Rhesus macaque genome assembly	NCBI Assembly	SBKD01000000
Week 7 single-cell RNA-seq sequences	NCBI SRA	PRJNA520929
IgG BCR sequence reads from 224-13 (bolus) right LN	NCBI SRA, GenBank	PRJNA520929, KCVI00000000
IgG BCR sequence reads from 224-13 (bolus) left LN	NCBI SRA, GenBank	PRJNA520929, KCVJ00000000
IgK BCR sequence reads from 224-13 (bolus) left LN	NCBI SRA, GenBank	PRJNA520929, KCVK00000000
IgL BCR sequence reads from 224-13 (bolus) left LN	NCBI SRA, GenBank	PRJNA520929, KCVL00000000
IgG BCR sequence reads from RCn16 (bolus) right LN	NCBI SRA, GenBank	PRJNA520929, KCVM00000000
IgK BCR sequence reads from RCn16 (bolus) right LN	NCBI SRA, GenBank	PRJNA520929, KCVN00000000
IgL BCR sequence reads from RCn16 (bolus) right LN	NCBI SRA, GenBank	PRJNA520929, KCVO00000000
IgG BCR sequence reads from RCn16 (bolus) left LN	NCBI SRA, GenBank	PRJNA520929, KCVP00000000
IgK BCR sequence reads from RCn16 (bolus) left LN	NCBI SRA, GenBank	PRJNA520929, KCVQ00000000
IgL BCR sequence reads from RCn16 (bolus) left LN	NCBI SRA, GenBank	PRJNA520929, KCVR00000000
IgG BCR sequence reads from RRk16 (bolus) right LN	NCBI SRA, GenBank	PRJNA520929, KCWO00000000
IgK BCR sequence reads from RRk16 (bolus) right LN	NCBI SRA, GenBank	PRJNA520929, KCWP00000000
IgL BCR sequence reads from RRk16 (bolus) right LN	NCBI SRA, GenBank	PRJNA520929, KCWQ00000000
IgG BCR sequence reads from RRk16 (bolus) left LN	NCBI SRA, GenBank	PRJNA520929, KCWR00000000
IgK BCR sequence reads from RRk16 (bolus) left LN	NCBI SRA, GenBank	PRJNA520929, KCWS00000000
IgL BCR sequence reads from RRk16 (bolus) left LN	NCBI SRA, GenBank	PRJNA520929, KCWT00000000
IgG BCR sequence reads from RVh16 (2w pumps) right LN	NCBI SRA, GenBank	PRJNA520929, KCVS00000000
IgK BCR sequence reads from RVh16 (2w pumps) right LN	NCBI SRA, GenBank	PRJNA520929, KCVT00000000
IgL BCR sequence reads from RVh16 (2w pumps) right LN	NCBI SRA, GenBank	PRJNA520929, KCVU00000000
IgG BCR sequence reads from RVh16 (2w pumps) left LN	NCBI SRA, GenBank	PRJNA520929, KCVV00000000
IgK BCR sequence reads from RVh16 (2w pumps) left LN	NCBI SRA, GenBank	PRJNA520929, KCVW00000000
IgL BCR sequence reads from RVh16 (2w pumps) left LN	NCBI SRA, GenBank	PRJNA520929, KCVX00000000
IgG BCR sequence reads from RYm16 (2w pumps) right LN	NCBI SRA, GenBank	PRJNA520929, KCXA00000000
IgK BCR sequence reads from RYm16 (2w pumps) right LN	NCBI SRA, GenBank	PRJNA520929, KCXB00000000
IgL BCR sequence reads from RYm16 (2w pumps) right LN	NCBI SRA, GenBank	PRJNA520929, KCXC00000000
IgG BCR sequence reads from RYm16 (2w pumps) left LN	NCBI SRA, GenBank	PRJNA520929, KCXD00000000
IgK BCR sequence reads from RYm16 (2w pumps) left LN	NCBI SRA, GenBank	PRJNA520929, KCXE00000000
IgL BCR sequence reads from RYm16 (2w pumps) left LN	NCBI SRA, GenBank	PRJNA520929, KCXF00000000
IgG BCR sequence reads from RWr16 (2w pumps) right LN	NCBI SRA, GenBank	PRJNA520929, KCWU00000000
IgK BCR sequence reads from RWr16 (2w pumps) right LN	NCBI SRA, GenBank	PRJNA520929, KCWV00000000
IgL BCR sequence reads from RWr16 (2w pumps) right LN	NCBI SRA, GenBank	PRJNA520929, KCWW00000000
IgG BCR sequence reads from RWr16 (2w pumps) left LN	NCBI SRA, GenBank	PRJNA520929, KCWX00000000
IgK BCR sequence reads from RWr16 (2w pumps) left LN	NCBI SRA, GenBank	PRJNA520929, KCWY00000000
IgL BCR sequence reads from RWr16 (2w pumps) left LN	NCBI SRA, GenBank	PRJNA520929, KCWZ00000000
IgG BCR sequence reads from RQq16 (2w pumps) right LN	NCBI SRA, GenBank	PRJNA520929, KCVY00000000
IgG BCR sequence reads from RQq16 (2w pumps) left LN	NCBI SRA, GenBank	PRJNA520929, KCVZ00000000
IgK BCR sequence reads from RQq16 (2w pumps) left LN	NCBI SRA, GenBank	PRJNA520929, KCWA00000000
IgL BCR sequence reads from RQq16 (2w pumps) left LN	NCBI SRA, GenBank	PRJNA520929, KCWB00000000
IgG BCR sequence reads from RWh16 (4w pumps) right LN	NCBI SRA, GenBank	PRJNA520929, KCXG00000000
IgK BCR sequence reads from RWh16 (4w pumps) right LN	NCBI SRA, GenBank	PRJNA520929, KCXH00000000
IgL BCR sequence reads from RWh16 (4w pumps) right LN	NCBI SRA, GenBank	PRJNA520929, KCXI00000000
IgG BCR sequence reads from RWh16 (4w pumps) left LN	NCBI SRA, GenBank	PRJNA520929, KCXJ00000000
IgK BCR sequence reads from RWh16 (4w pumps) left LN	NCBI SRA, GenBank	PRJNA520929, KCXK00000000

(*Continued on next page*)

Continued

REAGENT or RESOURCE	SOURCE	IDENTIFIER
IgL BCR sequence reads from RWh16 (4w pumps) left LN	NCBI SRA, GenBank	PRJNA520929, KCXL00000000
IgG BCR sequence reads from ROw16 (4w pumps) right LN	NCBI SRA, GenBank	PRJNA520929, KCXM00000000
IgK BCR sequence reads from ROw16 (4w pumps) right LN	NCBI SRA, GenBank	PRJNA520929, KCXN00000000
IgL BCR sequence reads from ROw16 (4w pumps) right LN	NCBI SRA, GenBank	PRJNA520929, KCXO00000000
IgG BCR sequence reads from ROw16 (4w pumps) left LN	NCBI SRA, GenBank	PRJNA520929, KCXP00000000
IgK BCR sequence reads from ROw16 (4w pumps) left LN	NCBI SRA, GenBank	PRJNA520929, KCXQ00000000
IgL BCR sequence reads from ROw16 (4w pumps) left LN	NCBI SRA, GenBank	PRJNA520929, KCXR00000000
IgG BCR sequence reads from RTh16 (4w pumps) right LN	NCBI SRA, GenBank	PRJNA520929, KCWI00000000
IgK BCR sequence reads from RTh16 (4w pumps) right LN	NCBI SRA, GenBank	PRJNA520929, KCWJ00000000
IgL BCR sequence reads from RTh16 (4w pumps) right LN	NCBI SRA, GenBank	PRJNA520929, KCWK00000000
IgG BCR sequence reads from RTh16 (4w pumps) left LN	NCBI SRA, GenBank	PRJNA520929, KCWL00000000
IgK BCR sequence reads from RTh16 (4w pumps) left LN	NCBI SRA, GenBank	PRJNA520929, KCWM00000000
IgL BCR sequence reads from RTh16 (4w pumps) left LN	NCBI SRA, GenBank	PRJNA520929, KCWN00000000
IgG BCR sequence reads from RFr16 (4w pumps) right LN	NCBI SRA, GenBank	PRJNA520929, KCWC00000000
IgK BCR sequence reads from RFr16 (4w pumps) right LN	NCBI SRA, GenBank	PRJNA520929, KCWD00000000
IgL BCR sequence reads from RFr16 (4w pumps) right LN	NCBI SRA, GenBank	PRJNA520929, KCWE00000000
IgG BCR sequence reads from RFr16 (4w pumps) left LN	NCBI SRA, GenBank	PRJNA520929, KCWF00000000
IgK BCR sequence reads from RFr16 (4w pumps) left LN	NCBI SRA, GenBank	PRJNA520929, KCWG00000000
IgL BCR sequence reads from RFr16 (4w pumps) left LN	NCBI SRA, GenBank	PRJNA520929, KCWH00000000
Negative stain EM map of polyclonal serum in complex with BG505 SOSIP.664 from RM 224-13 (bolus)	EMDataBank	EMD-9175
Negative stain EM map of polyclonal serum in complex with BG505 SOSIP.664 from RM RCn16 (bolus)	EMDataBank	EMD-9176
Negative stain EM map of polyclonal serum in complex with BG505 SOSIP.664 from RM RRk16 (bolus)	EMDataBank	EMD-9180
Negative stain EM map of polyclonal serum in complex with BG505 SOSIP.664 from RM RVh16 (2w pumps)	EMDataBank	EMD-9181
Negative stain EM map of polyclonal serum in complex with BG505 SOSIP.664 from RM RYm16 (2w pumps)	EMDataBank	EMD-9185
Negative stain EM map of polyclonal serum in complex with BG505 SOSIP.664 from RM RWr16 (2w pumps)	EMDataBank	EMD-9184
Negative stain EM map of polyclonal serum in complex with BG505 SOSIP.664 from RM RQq16 (2w pumps)	EMDataBank	EMD-9179
Negative stain EM map of polyclonal serum in complex with BG505 SOSIP.664 from RM RWh16 (4w pumps)	EMDataBank	EMD-9183
Negative stain EM map of polyclonal serum in complex with BG505 SOSIP.664 from RM ROw16 (4w pumps)	EMDataBank	EMD-9178, EMD-9186
Negative stain EM map of polyclonal serum in complex with BG505 SOSIP.664 from RM RTh16 (4w pumps)	EMDataBank	EMD-9182
Negative stain EM map of polyclonal serum in complex with BG505 SOSIP.664 from RM RFr16 (4w pumps)	EMDataBank	EMD-9177
Negative stain EM map of polyclonal serum in complex with BG505 SOSIP.664 from RM 145-11 (bolus)	EMDataBank	EMD-0571
Negative stain EM map of polyclonal serum in complex with BG505 SOSIP.664 from RM RHw16(bolus)	EMDataBank	EMD-0580
Negative stain EM map of polyclonal serum in complex with BG505 SOSIP.664 from RM RAa14 (bolus)	EMDataBank	EMD-0575
Negative stain EM map of polyclonal serum in complex with BG505 SOSIP.664 from RM 5N6 (bolus)	EMDataBank	EMD-0569
Negative stain EM map of polyclonal serum in complex with BG505 SOSIP.664 from RM REj15 (bolus)	EMDataBank	EMD-0578

(*Continued on next page*)

Continued

REAGENT or RESOURCE	SOURCE	IDENTIFIER
Negative stain EM map of polyclonal serum in complex with BG505 SOSIP.664 from RM REv16 (bolus)	EMDataBank	EMD-0579
Negative stain EM map of polyclonal serum in complex with BG505 SOSIP.664 from RM RAv16 (ED)	EMDataBank	EMD-0576, EMD-0577
Negative stain EM map of polyclonal serum in complex with BG505 SOSIP.664 from RM B077(ED)	EMDataBank	EMD-0573, EMD-0574
Negative stain EM map of polyclonal serum in complex with BG505 SOSIP.664 from RM BM57 (ED)	EMDataBank	EMD-0572
Negative stain EM map of polyclonal serum in complex with BG505 SOSIP.664 from RM 99-13(ED)	EMDataBank	EMD-0570
Negative stain EM map of polyclonal serum in complex with BG505 SOSIP.664 from RM RMI15 (ED)	EMDataBank	EMD-0581
Negative stain EM map of polyclonal serum in complex with BG505 SOSIP.664 from RM RWo15 (ED)	EMDataBank	EMD-0582
Negative stain EM map of BDA1 in complex with BG505 SOSIP.664	EMDataBank	EMD-9138
Experimental Models: Cell Lines		
TZM-bl cells	NIH AIDS Reagent Program	Cat #8129
Experimental Models: Organisms/Strains		
Indian-origin rhesus macaques (outbred)	Yerkes National Primate Research Center	
Olionucleotides		
CDS Oligo (dT): TTTTTTTTTTTTTTTTTTTTTTTTTTVN	Integrated DNA Technologies	
SMARTer II A Oligo: AAGCAGTGGTATCAACGCA GAGTACATrGrGrG	Integrated DNA Technologies	
IgG Constant Primer: GCCAGGGGGAAGACCGATGG GCCCTTGGTGGA	Integrated DNA Technologies	
IgK Constant Primer: GCGGGAAGATGAAGACAGA TGGTGCAGCCACAG	Integrated DNA Technologies	
IgL Constant Primer: GGCCTTGTTGGCTTGAAGC TCCTCAGAGGAGGG	Integrated DNA Technologies	
P5_Seq BC_XX 5PIIA: CACGACGCTCTTCCGATCT 4-8xN AACCACTA AAGCAGTGGTATCAACGCAGAGT	Integrated DNA Technologies	
P7_ i7_XX IgG: CAAGCAGAAGACGGCATACGAGA TTAGTGGTT GCCAGGGGGAAGACCGATGGGCCC TTGGTGGA	Integrated DNA Technologies	
P7_ i7_XX IgK: CAAGCAGAAGACGGCATACGAG ATTAGTGGTT GCGGGAAGATGAAGACAGATGGTGC AGCCACAG	Integrated DNA Technologies	
P7_ i7_XX IgL: CAAGCAGAAGACGGCATACGAGATT AGTGGTT GGCCTTGTTGGCTTGAAGCTCCTCAG AGGAGGG	Integrated DNA Technologies	
P5_Graft P5_seq: AATGATACGGCGACCACCGAGA TCTACAC TCTTTCCCTACACGACGCTCTTCCGATCT	Integrated DNA Technologies	N/A
Software and Algorithms		
Prism v7.0/v8.0	GraphPad	https://www.graphpad.com/scientific-software/prism/
FlowJo v10.4	FlowJo LLC	https://www.flowjo.com
Appion database	(Lander et al., 2009)	
Leginon	(Suloway et al., 2005)	
DoG Picker	(Voss et al., 2009)	
Relion	(Scheres, 2012)	

(*Continued on next page*)

Continued

REAGENT or RESOURCE	SOURCE	IDENTIFIER
FALCON-Unzip	(Chin et al., 2016)	
IMGT		http://www.imgt.org
BLAT	(Kent, 2002)	
BLASR	(Chaisson and Tesler, 2012)	
BLAST		https://blast.ncbi.nlm.nih.gov/Blast.cgi
MsPAC		https://bitbucket.org/oscarlr/mspac
Integrated Genomics Viewer	(Robinson et al., 2011; Thorvaldsdóttir et al., 2013)	https://software.broadinstitute.org/software/igv/
BALDR	(Upadhyay et al., 2018)	
FastQC v0.11.5	(Andrew, 2010)	
Immcantation	(Gupta et al., 2015; Vander Heiden et al., 2014)	
IgBLAST v1.6.1	(Ye et al., 2013)	
MUSCLE v3.8.1551	(Edgar, 2004)	
CD-HIT v4.7	(Fu et al., 2012)	
IMGT DomainGAPAlign	(Ehrenmann and Lefranc, 2011; Ehrenmann et al., 2010)	
MAFFT	(Katoh and Standley, 2013)	
FastTree2	(Price et al., 2010)	
FigTree		http://tree.bio.ed.ac.uk/software/figtree/
ImageJ		https://imagej.nih.gov/ij/
Other		
Mini-osmotic pumps (0.5uL/hr, 14 day release)	ALZET	Model 2002
Mini-osmotic pumps (0.25uL/hr, 28 day release)	ALZET	Model 2004
Costar Assay Plate, 96 well flat-bottom, half area, high binding	Corning	Cat # 3690

CONTACT FOR REAGENT AND RESOURCE SHARING

Further information and requests for resources and reagents should be directed to and will be fulfilled by the Lead Contact, Shane Crotty (shane@lji.org).

EXPERIMENTAL MODEL AND SUBJECT DETAILS

Rhesus Macaques

Outbred Indian RMs (*Macaca mulatta*) were sourced and housed at the Yerkes National Primate Research Center and maintained in accordance with NIH guidelines. This study was approved by the Emory University Institutional Animal Care and Use Committee (IACUC). When osmotic pumps were implanted, animals were kept in single, protected contact housing. At all other times, animals were kept in paired housing. Animals were treated with anesthesia and analgesics for procedures as per veterinarian recommendations and IACUC approved protocols. In all studies, animals were grouped to divide age, weight and gender as evenly as possible.

OP study: Animals were between 2.5 – 3 years of age at time of 1st immunization. Bolus group 2: 2 males (M), 1 female (F); 2w OP group: 3M, 1F; 4w OP group: 3M, 1F.

ED study: Animals were between 3 – 6.5 years of age at time of 1st immunization. Bolus group 1: 3M, 3F; ED group: 2M, 4F.

Antigen tracking study: animals were between 3 – 6 years of age at time of immunization. Bolus group: 2M, 1F; OP group: 3M; ED group: 3M.

METHOD DETAILS

Immunizations

Osmotic pump study: Animals were immunized at 2 time points: week 0 and week 8. All immunizations were administered subcutaneously (SubQ) divided between the left and right mid-thighs. Bolus animals were given two SubQ injections of 50 μg of

Olio6$_{CD4ko}$ + 187.5 units (U) of saponin adjuvant in PBS, for a total of 100 μg Olio6$_{CD4ko}$ trimer protein + 375U of saponin adjuvant. At week 0, osmotic pumps (Alzet, models −2002 and −2004) were loaded with 50 μg Olio6$_{CD4ko}$ + 187.5U saponin adjuvant, for a total of 100 μg Olio6$_{CD4ko}$ trimer + 375U of saponin adjuvant. Pumps were implanted SubQ in the same location as bolus immunizations. At week 8, osmotic pump animals were immunized with osmotic pumps loaded each with 25 μg Olio6$_{CD4ko}$ + 93.75U saponin adjuvant. At the end of the osmotic pump delivery, a SubQ bolus immunization of 25 μg Olio6$_{CD4ko}$ + 93.75U was given in each leg, totaling 50 μg Olio6$_{CD4ko}$ + 187.5U saponin adjuvant at weeks 12 and 14 for 2 week and 4 week osmotic pump groups, respectively. Each pump was loaded with Olio6$_{CD4ko}$ and saponin adjuvant in a total volume of 200ul. During the 1st immunization, each 2w and 4w OP released 3.57ug Olio6$_{CD4ko}$ + 13.4U saponin adjuvant and 1.78ug Olio6$_{CD4ko}$ + 6.7U saponin adjuvant per day, respectively. During the 2nd immunization, each 2w and 4w OP released 1.78ug Olio6$_{CD4ko}$ + 6.7U saponin and 0.89ug Olio6$_{CD4ko}$ + 3.35U saponin adjuvant per day, respectively.

Dose escalation study: Animals were immunized at 3 time points: weeks 0, 10, and 24. All immunizations were administered SubQ in the left and right mid-thighs. Bolus animals were given two injections of 50 μg of Olio6 + 187.5U of saponin adjuvant in PBS, for total of 100 μg immunogen and 375U saponin adjuvant at weeks 0 and 8. At week 24, two injections of 150 μg of Olio6 + 187.5U saponin adjuvant were administered for a total of 300 μg Olio6 + 375U saponin adjuvant. For each immunization, escalating dose animals were given seven injections of Olio6 and saponin adjuvant in each thigh over 12 days (on days 0, 2, 4, 6, 8, 10, 12 for each immunization). The total doses of Olio6 at each injection during the first two immunizations were: 0.2, 0.43, 1.16, 3.15, 8.56, 23.3, 63.2 μg (the doses per immunization site were 0.1, 0.215, 0.58, 1.575, 4.28, 11.65, 31.6 μg). The total doses of Olio6 at each injection during the third immunization were: 0.6, 1.29, 3.48, 9.45, 25.68, 69.9, 189.6 μg (the doses per immunization site were 0.3, 0.645, 1.74, 4.725, 12.84, 34.95, 94.8 μg). The total doses of saponin adjuvant at each injection during all immunizations were: 0.75, 1.61, 4.35, 11.81, 32.1, 87.38, 237.0U (the doses per immunization site were 0.375, 0.805, 2.175, 5.905, 16.05, 43.69, 118.5U).

Antigen tracking study: Animals were immunized at week 0 with a total dose of 100ug untagged MD39 conjugated to Alexa Fluor 647. All immunizations were administered SubQ in the left and right mid-thighs. Bolus animals were given 2 injections of 50 μg MD39 + 187.5U of saponin adjuvant in PBS. Osmotic pumps (Alzet, models 2002) were loaded with 50 μg MD39 + 187.5U saponin adjuvant. Escalating dose animals were given a series of 7 injections over 12 days (on days 0, 2, 4, 6, 8, 10, 12 for each immunization). The total dose of MD39 at each injection were: 0.2, 0.43, 1.16, 3.15, 8.56, 23.3, 63.2 μg (the doses per immunization site were 0.1, 0.215, 0.58, 1.575, 4.28, 11.65, 31.6 μg). The total doses of saponin adjuvant at each injection were: 0.75, 1.61, 4.35, 11.81, 32.1, 87.38, 237.0U (the doses per immunization site were 0.375, 0.805, 2.175, 5.905, 16.05, 43.69, 118.5U). Animals were sacrificed at 2 or 7 days (3 animals per group per day) after immunization (bolus, d2 and d7; pumps, d16 and d21; escalating dose, d14 and d19). All inguinal LNs were harvested and fixed in PLP buffer (pH7.4 50mM PBS + 100mM lysine, 1% paraformaldehyde, 2mg/mL sodium periodate) for 1 week at 4°C and then washed and stored in PBS with 0.05% sodium azide at 4°C until used for imaging.

Lymph node fine needle aspirates, whole LN biopsy tissue, blood collection and processing

LN FNAs were used to sample at both right and left inguinal LNs. FNAs were performed by a veterinarian. Draining lymph nodes were identified by palpitation. Cells were collected by passing a 22-gauge needle attached to a 3mL syringe into the lymph node 4 times. Samples were expelled into RPMI containing 10% fetal bovine serum, 1X penicillin/streptomycin. Samples were centrifuged and Ammonium-Chloride-Potassium (ACK) lysing buffer was used if sample was contaminated with red blood cells. Excisional LNs were conducted at weeks 12 (bolus) or 14 (osmotic pump groups). LNs were dissociated through 70 μM strainers and washed with PBS. Blood was collected at various time points into CPT tubes for PBMC and plasma isolation. Serum was isolated using serum collection tubes and frozen.

ISCOMs-class saponin adjuvant

The adjuvant used for all the described studies was a ISCOM-like saponin nanoparticle comprised of self-assembled cholesterol phospholipid, and quillaja saponin prepared as previously described (Plotkin, 2010). Briefly, 10 mg each of cholesterol (Avanti Polar Lipids) and DPPC (Avanti Polar Lipids) were dissolved separately in 20% MEGA-10 (Sigma-Aldrich) detergent at a final concentration of 20 mg/mL and 50 mg Quil-A saponin (InvivoGen) was dissolved in MilliQ H_2O at a final concentration of 100 mg/mL. Next, DPPC solution was added to cholesterol followed by addition of Quil-A saponin in rapid succession and the volume was brought up with PBS for a final concentration of 1 mg/mL cholesterol and 2% MEGA-10. The solution was allowed to equilibrate at 25°C overnight, followed by 5 days of dialysis against PBS using a 10k MWCO membrane. The adjuvant solution was filter sterilized using a 0.2 μm Supor syringe filter, concentrated using 50k MWCO Centricon filters, and further purified by FPLC using a Sephacryl S-500 HR size exclusion column. Each adjuvant batch was finally characterized by negative stain transmission electron microscopy (TEM) and dynamic light scattering (DLS) to confirm uniform morphology and size and validated for low endotoxin content by Limulus Amebocyte Lysate assay (Lonza). Final adjuvant concentration was determined by cholesterol quantification (Sigma-Aldrich).

Immunogen and probe generation

Olio6, Olio6$_{CD4ko}$, and MD39 Env trimers were generated as previously described. Avi-tagged Olio6, Olio6$_{CD4ko,}$ and MD39 DNA constructs were synthesized, protein was produced and purified, and the proteins were then biotinylated using BirA-500 (Avidity) and assessed for biotin conjugation efficiency using SDS-PAGE. All Env immunogens and probes contained a six histidine tag (His tag) for purification. Immunogens were tested for endotoxin contamination with Endosafe PTS (Charles River). Proteins with an

endotoxin level < 10 EU/mg were used in immunizations. Immunogens and probes were aliquoted and kept frozen at −80°C until immediately before use.

Flow cytometry and cellular analyses

Biotinylated protein were individually premixed with fluorochrome-conjugated streptavidin (SA-Alexa Fluor 647 [Ax647] or SA-Brilliant Violet 421 [BV421]) at RT for 20 minutes. Olio6$_{CD4ko}$ probes were used in Figures 1, 3, 6, and S1 (osmotic pump study) from weeks −1 to 8. Olio6 probes were used from weeks 9 to 14. Olio6 and Olio6$_{CD4ko}$ differ by a single amino acid . MD39 probes were used in Figures 7 and S7 (dose escalation study). MD39 is closely related to Olio6.

For the full LN GC panel, cells were incubated with probes for 30 minutes at 4°C, washed twice and then incubated with surface antibodies for 30 minutes at 4°C. Cells were fixed and permeabilized for 30 minutes using FoxP3/Transcription Factor Staining Buffer Set (Thermo Scientific) according to manufacturer's protocols. Cells were stained with intranuclear antibodies in 1X permeabilization buffer for 30 minutes, 4°C. Cells were washed twice with 1x permeabilization buffer and acquired on an LSR I (BD Biosciences). For Ag-specific B cell sort panels, cells were incubated with probes for 30 minutes at 4°C, washed twice and then incubated with surface antibodies for 30 minutes at 4°C. Cells were sorted on a FACSAria II.

For the osmotic pump study, full LN GC panel was used on fresh cells at weeks −2, 1-7, 9-12, 14. At weeks 7,12, and 14, cells were sorted using the Ag-specific B cell sort panel. Cells were stained fresh at week 7 and single cell sorted. At weeks 12 (bolus) and week 14 (osmotic pump animals), biopsied LNs were thawed, stained and bulk sorted for BR sequencing. Sorted cells were defined as Viability dye$^-$ CD4$^-$ CD8a$^-$ CD16$^-$ CD20$^+$ (IgM$^+$ IgG$^+$)$^-$ Olio6-Alexa647$^+$ Olio6-BV421$^+$. For the dose escalation study, the full LN GC panel was used at every time point. Data reported are raw flow cytometry values at each time point.

Validation of CD38 and CD71 as surface markers of B_{GC} cells: frozen, biopsied mesenteric LNs were used. Cells were stained as described above.

B cell analysis: LN FNA samples 3% of the LN on average. Because of the nature of the technique, some samples do not have enough cells to be included in the analyses. Generally, for GC and Env-specific B cell gating, a threshold of 1,000 and 10,000 B cells, respectively, is used. For Env-specific B_{GC} cell gating, a threshold of 1,000 B_{GC} cells is used.

B_{Mem} cells: B_{Mem} cells (% Env$^+$ or Env^{hi}) were calculated as the percentage of Env-specific or high-affinity Env-specific B cells that were not BCL6$^+$ KI67$^+$ or CD38$^-$ CD71$^+$. B_{Mem} Env$^+$ and Env^{hi} (% B) cells were calculated as % Env$^+$ (% B cells) - % Env$^+$ B_{GC} (% B) and % Env^{hi} (% B cells) - % Env^{hi} B_{GC} (% B), respectively.

Area under the curve [AUC]: AUC was calculated for individual LNs. For Figures 1 and S1, AUC was calculated from weeks 1, 3 to 7. Bolus gr1 did not have FNA data at week 1. For these samples, the median of the week 1 values from bolus gr2 was used. Raw values were used at other time points. For Figure 2, AUC was calculated from weeks 1, 3 to 6. GC-T_{FH} frequencies were not collected for bolus grp2, 2w pumps or 4w pump animals at week 7. For Figure 3, AUC was calculated between weeks 9 and 12 because of poor cell recovery at weeks 8 and 14. For Figures 7 and S7, AUC was calculated between weeks 3-7 (1st immunization) and between weeks 11-15 (2nd immunization) using raw values. Parameters used: baseline = 0; peaks less than 10% of distance from minimum to maximum y were ignored.

Antigen-specific CD4$^+$ T cell assay

AIM assays were conducted as previously described (Dan et al., 2016; Havenar-Daughton et al., 2016b; Reiss et al., 2017).

Osmotic pump study: Frozen macaque lymph nodes from week 12 (bolus animals) or week 14 (osmotic pump animals) were thawed. Cells were treated with DNase (StemCell Technologies, Inc.) for 15 minutes, 37°C washed and then rested for 3 hours. Cells were cultured under the following conditions: media only (RPMI containing 10% fetal bovine serum, 1X penicillin/streptomycin, 2mM L-glutamine), 5ug/mL Olio6$_{CD4ko}$ peptide megapool, or 1ng/mL SEB (positive control, Toxin Technology, Inc.). After 18 hours, cells were stained and acquired on FACSCelesta (BD Biosciences).

Dose escalation study: About 50% of lymphocytes are lost during the freeze-thaw process. To maximize the number of viable cells to identify Env-specific CD4$^+$ cells, cells were shipped overnight at 4°C to LJI. Cells were centrifuged and treated with DNase for 15 minutes, 37°C. Cells were washed, cultured for 18 hours under the conditions described above. All values reported are background subtracted ((% OX40$^+$ 4-1BB$^+$ CD4$^+$ (Env-stimulated condition) – % OX40$^+$ 4-1BB$^+$ CD4$^+$ (unstimulated condition)).

Whole genome sequencing and genome assembly

High molecular weight (> 50kb) genomic DNA was isolated from the kidney of a perfused, female rhesus macaque. A full genome 30kb library was prepared according to manufacturer's protocols. Sequencing was performed on a PacBio RS II (Pacific Biosciences). Genome assembly was performed using FALCON and FALCON-Unzip (Pacific Biosciences) (Chin et al., 2016). The final assembly contained 1633 contigs made up of 2.83 Gbp. The N50 contig length is 8.4Mbp, with a maximum contig length of 28.8Mbp.

Immunoglobulin loci annotation

Primary contigs from FALCON/FALCON-Unzip assemblies containing IG sequences were identified by aligning V, D, and J sequences from multiple sources, including sequences for RM and the crab-eating macaque (*Macaca fascicularis*) from the IMGT reference directory (http://www.imgt.org/vquest/refseqh.html) and using BLAT (Corcoran et al., 2016; Kent, 2002). Gene annotation of primary contigs was carried out in two stages: (1) rough coordinates in each contig harboring putative V, D, and J segments were

identified by mapping existing sequences (i.e., those noted above for contig identification, as well as human IG D and J gene sequences from IMGT); followed by (2) manual curation, during which precise 5′ and 3′ gene segment boundaries were determined for each annotation, based on alignments to previously reported sequences, as well as the identification of flanking recombination signal sequence (RSS) heptamers within the contig assembly. Each gene annotation was assigned to a given subfamily based on the closest matching published sequence. Only ORF annotations lacking premature stop codons and/or insertion-deletions resulting in drastic frameshifts were considered.

Additional V gene allelic variants in the IGH, IGK, and IGL loci were identified by mapping PacBio raw reads back to IG-associated primary and alternate contigs from the FALCON/FALCON-Unzip assemblies using BLASR (Chaisson and Tesler, 2012). Putative heterozygous ORF genes were identified based on variants present in PacBio reads mapping to a given ORF locus (Figure 6C). To characterize putative alternate alleles, raw reads were partitioned and assembled locally at heterozygous ORFs using MsPAC (O.L.R., unpublished data; https://bitbucket.org/oscarlr/mspac). Raw reads and assembled allelic variants were visually inspected in the context of primary and alternate FALCON/FALCON-Unzip contigs and confirmed using the Integrated Genomics Viewer (Robinson et al., 2011; Thorvaldsdóttir et al., 2013). To classify genes/alleles annotated from PacBio assembly data as "known" or "novel," sequences were cross-referenced with the RM IMGT reference database and publicly available sequences annoted as Ig sequences in the NCBI nucleotide collection using BLAT and BLAST (https://blast.ncbi.nlm.nih.gov/Blast.cgi), respectively. The number of annotated RM per IGHV, IGLV, and IGKV subfamilies were compared to counts collated from human gene tables available from IMGT.

Bulk BCR sequencing

The protocol for rhesus macaque repertoire sequencing was obtained by courtesy of Dr. Daniel Douek, NIAID/VRC (Huang et al., 2016). Bulk Env-specific B cells were sorted into 350uL QIAGEN RLT buffer. RNA was extracted using the RNeasy Micro-DNase Digest protocol (QIAGEN) on QIAcube automation platforms (Valencia, CA). Reverse transcription (RT) was performed using Clontech SMARTer cDNA template switching: 5′ CDS oligo(dT) (12 μM) was added to RNA and incubated at 72°C for 3 minutes and 4°C for at least 1 minute. The RT mastermix (5x RT Buffer (250 mM Tris-HCl (pH 8.3), 375 mM KCl, 30 mM $MgCl_2$), Dithiothreitol, DTT (20 mM), dNTP Mix (10 mM), RNase Out (40U/μL), SMARTer II A Oligo (12 μM), Superscript II RT (200U/μL)) was added to the reaction and incubated at 42°C for 90 minutes and 70°C for 10 minutes. First-strand cDNA was purified using AMPure XP beads (Beckman Coulter). Following RT, two PCR rounds were carried out to generate immunoglobulin amplicon libraries compatible with Illumina sequencing. All oligos were ordered from Integrated DNA Technologies. The first PCR amplification was carried out using KAPA Real-Time Library Amplification Kit (Kapa Biosciences). cDNA was combined with master mix (2X KAPA PCR Master Mix, 12 μM μL 5PIIA and 5 μL IgG/IgK/IgL Constant Primer (2 μM)). The amplification was monitored using real-time PCR and was stopped during the exponential phase. The amplified products were again purified using AMPure XP beads. A second round of PCR amplification was carried out for addition of barcodes and Illumina adaptor sequences: master mix (2X KAPA PCR Master Mix 2x, SYBR Green 1:10K, Nuclease-free water), 10 μM of P5_Seq BC_XX 5PIIA, 10 μM of P7_ i7_XX IgG/IgK/IgL and were combined with amplified Immunoglobulin from the first round PCR and amplified using real-time PCR monitoring. The P5_Seq BC_XX 5PIIA primers contain a randomized stretch of four to eight random nucleotides. This was followed by purification with AMPure XP beads. A final PCR step was performed for addition of remaining Illumina adaptors by mixing master mix (2X KAPA PCR Master Mix, 10 μM P5_Graft P5_seq, Nuclease-free water), 10 μM of P7_ i7_XX IgG/IgK/IgL oligo and amplified products from the previous PCR step followed by purification with AMPure XP beads. The quality of library was assessed using Agilent Bioanalyzer. The amplicon libraries were pooled and sequenced on an Illumina MiSeq as a 309 paired-end run.

Single cell RNA-seq

Single cells were sorted by flow cytometry into 10 uL of QIAGEN RLT buffer. RNA was purified using RNACleanXP Solid Phase Reversible Immobilization (SPRI) beads (Beckman Coulter). Full-length cDNA amplification of single-cells was performed using a modified version of the SMART-Seq II protocol (Picelli et al., 2014), as described previously (Upadhyay et al., 2018). Amplified cDNA was fragmented using Illumina Nextera XT DNA Library Preparation kits and dual-indexed barcodes were added to each sample. Libraries were validated using an Agilent 4200 Tapestation, pooled, and sequenced at 101 SR on an Illumina HiSeq 3000 to an average depth of 1M reads in the Yerkes NHP Genomics Core (http://www.yerkes.emory.edu/nhp_genomics_core/).

V gene and somatic hypermutation analyses

Illumina bcl files from IgG, IgK and IgL amplicons were converted to fastq files usng the bcl2fastq tool. FastQC v0.11.5 (Andrew, 2010) was used to check the quality of fastq files. The repertoire sequence analysis was carried out using the pRESTO 0.5.6, Change-O 0.3.12, Alakazam 0.2.10.999 and SHazaM 0.1.9 packages from the Immcantation pipeline (Gupta et al., 2015; Vander Heiden et al., 2014). Pre-processing was performed using tools in the pRESTO package. Paired-end reads were first assembled with AssemblePairs tool. Reads with a mean quality score of less than 20 were filtered out using FilterSeq. The MaskPrimers tool was used to remove the forward primers and the random nucleotides from the assembled sequences. Data from each of two technical replicates were combined. Duplicates were removed and the duplicate counts were obtained for each unique sequence using CollapseSeq. SplitSeq was used to select sequences that had duplicate counts of at least two to eliminate singletons that may arise due to sequencing errors. The pre-processed sequences were then annotated using IgBLAST v1.6.1 (Ye et al., 2013).

Since the IMGT database (Lefranc and Lefranc, 2001) is lacking several V genes, a custom IgBLAST database was created for V genes using sequences from the genomic assembly in this study. The sequences were aligned using MUSCLE v3.8.1551 (Edgar, 2004) and only the V genes with complete sequence and no unknown amino acid (X) were selected. The corresponding nucleotide sequences of these V genes were clustered using CD-HIT v4.7(Fu et al., 2012) to remove 100% redundant sequences. The protein sequences for this non-redundant set were submitted to the IMGT DomainGapAlign tool (Ehrenmann and Lefranc, 2011; Ehrenmann et al., 2010) to obtain gapped V sequences. Corresponding gaps were introduced in the nucleotide sequences and the positions for framework (FR) and complementarity-determining regions (CDR) regions determined using custom scripts. These sequences were used to create the IgBLAST database for V genes. The databases for J and D genes was obtained from the IgBLAST ftp site (ftp://ftp.ncbi.nih.gov/blast/executables/igblast/release/internal_data/rhesus_monkey/). The annotations from IgBLAST were saved into a Change-O database and functional sequences were selected using Change-O. The gene usage and clonal frequencies were obtained from the Alakazam package and SHM estimations were obtained from the SHazaM package.

To obtain paired heavy and light chain sequences from single cell RNA-Seq data, we used the BALDR pipeline, as previously described (Upadhyay et al., 2018), with the Unfiltered method for rhesus macaques. Parallel instances of BALDR were run using the gnu parallel utility (Tange, 2011). The reads were trimmed using Trimmomatic v0.36 (Bolger et al., 2014). The trimmed reads were assembled using Trinity v2.6.5 (Grabherr et al., 2011). The assembled transcripts were annotated with the sequenced V(D)J genes in this study using IgBLAST v1.6.1. Reads greater than 50 bp were aligned to the assembled transcripts using bowtie2-2.3.0 (Langmead and Salzberg, 2012) to rank assembled transcripts based on the number of mapped reads. The assembled transcripts were filtered to remove non-productive sequences and those with the same V(D)J and CDR3 sequence as a higher ranked transcript. Out of the remaining sequences, the top ranking transcript sequence was chosen for the heavy and light chains.

Lineage analysis

For the quantification of B cell lineages, two independent analyses were performed with largely equivalent results.

Lineage analyses in Figures 5 and S4 utilized only the sequences from the genomic assembly generated in this study. The annotations from IgBLAST were saved into a Change-O database and functional sequences were selected using Change-O. The functional sequences were assigned to a clone using a custom script based on the following criteria: (i) same V gene, (ii) same J gene, (iii) same CDR3 length and (iv) percentage identity of CDR3 nucleotide sequence > 85%. The analysis was also performed with the larger IgBLAST database with comparable results.

Phylogenetic trees were generated using a larger IgBLAST database created for V genes using sequences from the genomic assembly in this study or by combining sequences from previously published studies (Corcoran et al., 2016; Lefranc and Lefranc, 2001; Ramesh et al., 2017; Sundling et al., 2012) and the sequences from the assembly in this study. Lineage assignment was performed using a clustering procedure that exploited both germline inference and sequence similarity. Two sequences were deemed to potentially belong to the same lineage when: (i) their inferred UCA sequences (ignoring the junction and D region) are within 1% of each other (using a kmer-based distance approximation from (Kumar et al., 2018) for computational efficiency), tolerating calls to closely related V and J genes; and (ii) when the length-normalized Levenshtein distance between their junction+D sequences is within 10%. The clustering algorithm itself maintains a set of candidate lineages, storing all sequences for each lineage, and each new sequence in turn is added to the lineage where the largest proportion of sequences match the above two criteria. If no existing candidate cluster has > 50% of its reads match the new sequence, then that sequence is used to seed a new candidate cluster containing this sequence as its sole member. Where members of a lineage had different inferred UCA sequences, the modal UCA was chosen as the UCA for the entire lineage. This lineage clustering algorithm was implemented in the Julia language for scientific computing (v0.6.2). Each lineage was aligned with MAFFT (Katoh and Standley, 2013), and phylogenetic trees were inferred using FastTree2 (Price et al., 2010). Phylogenies were visualized using FigTree (http://tree.bio.ed.ac.uk/software/figtree/), using automated coloring and annotation scripts implemented in Julia.

ELISAs

BG505 trimer, gp120 and His ELISAs: Half-area 96-well high binding plates (Corning) were coated with streptavidin at 2.5 μg/mL (Thermo Fisher Scientific) overnight at 4°C. Plates were washed with PBS + 0.05% Tween (PBS-T) three times. Biotinylated BG505, biotinylated His peptide conjugated to mouse CD1d or biotinylated gp120 was diluted to 1.0 μg/mL in PBS + 1% BSA were captured for 2 hours, 37°C. Plates were washed three times and then blocked with PBS+ 3% BSA for 1 hour, RT. Plasma samples or monoclonal antibodies were serially diluted in PBS + 1% BSA and incubated for 1 hour, RT. Plates were washed three times and horseradish peroxidase goat anti-rhesus IgG (H+L) secondary (Southern Biotech) was added at 1:3000 dilution in PBS + 1% PBS for 1 hour, RT. Plates were washed three times with PBS-T and absorption was measured at 450nm following addition of TMB substrate (Thermo Scientific). Endpoint titers were calculated as dilution at which O.D. signal was 0.1 above background using GraphPad Prism v7.0 or 8.0. Antibody data panels show geometric mean titers with geometric SD.

Lectin-capture BG505 trimer ELISA: To maximize access to the base of the trimer, we utilized a lectin-capture assay. Env trimer is heavily glycosylated, except at the base. Capture with a lectin, which binds glycans, increases the likelihood that the base will be exposed more than in a streptavidin-capture ELISA. Half-area 96- well high binding plates (Corning) were coated with 5 μg/mL lectin from *Galanthus nivalis* (snowdrop) (Sigma) in PBS overnight at 4°C. Plates were washed with 0.05% PBS-Tween (PBS-T) three times. 1ug/ml BG505 trimer in PBS + 1% BSA was bound to plates for 2 hours at 37°C and then washed three times. Plates were blocked with

PBS + 3% BSA for 1 hour, RT. Monoclonal antibodies were serially diluted in PBS + 1% BSA and incubated for 1.5 hours at RT. Plates were washed three times with PBS-T before incubation with horseradish peroxidase goat anti-human IgG, Fcγ fragment specific (Jackson ImmunoResearch) at 1:5000 in PBS + 1% BSA for 1hr, RT. Plates were washed five times with PBS-T and absorption was measured at 450nm following addition of TMB substrate (Thermo Fisher Scientific). O.D. values presented are background subtracted.

Cross-competition trimer ELISA: We used a modified lectin capture ELISA for this assay. Plates were coated with GNL and BG505 and blocked as previously described. Plates were incubated with 0 or 10 μg/mL 19R (fab) in PBS + 1% BSA for 1.5 hours at RT. Plates were washed three times with PBS-T. 2.5 μg/mL of whole monoclonal antibody was added for 1 hour at RT and then washed three times with PBS-T before incubation with horseradish peroxidase goat anti-human IgG, Fcγ fragment specific (Jackson ImmunoResearch) at 1:5000 in PBS + 1% BSA for 1hr, RT. Plates were washed five times with PBS-T and absorption was measured at 450nm following addition of TMB substrate (Thermo Fisher Scientific). Data presented are background (no fab or mAb) subtracted. As an additional background control, 19R fab was incubated without mAb.

Pseudovirus neutralization assay

Autologous neutralization assays were performed as previously described (Pauthner et al., 2017). BG505 pseudovirus neutralization was tested using the BG505.W6M.ENV.C2 isolate (AIDS Reagents Program), carrying the T332N mutation to restore the N332 glycosylation site.

Heterologous neutralization breadth was tested on a panel of 12 cross-clade isolates, representative of larger virus panels composed of isolated from diverse geography and clades (deCamp et al., 2014). All viruses in this panel are Tier 2. Week 10 (bolus), w12 (2w OPs), and w14 (4w OPs) were tested in osmotic pump study. Limit of detection (LOD) for heterologous viruses is 1:50 (dotted line). Titers below LOD are set at 1:40. Week 26 (bolus) and w27 (ED) were tested in ED study.

Neutralization titers are reported as ID_{50} titers. All neutralization Ab data panels show geometric mean titers with geometric SD.

19R

The genes encoding the 19R rhesus macaque IgG1 heavy chain and kappa light chain were synthesized and separately cloned into the pcDNA3.4 plasmid by Thermo Fisher Scientific. The 19R IgG was expressed in Expi293 cells and purified using Protein A by Thermo Fisher Scientific. 19R Fab was generated by digesting 19R IgG using the Pierce Fab Preparation Kit (Thermo Fisher Scientific).

Monoclonal EM analysis

The heavy and light chains of the BDA monoclonal antibodies were codon-optimized, synthesized and cloned into pFUSE2ss-CHIg-hG1 and pFUSE2ss-CLIg-hl2, respectively, by GenScript. Antibodies were expressed and purified by GenScript. Antibody sequences are available in the Key Resources Table.

Fab was generated using Pierce Fab preparation kit (Thermo Fisher Scientific). 15 μg of BG505 SOSIPv5.2 Env trimer (untagged) was complexed with 41 μg BDa1 Fab at room temperature overnight in a total reaction volume of 50 μL. The complex was diluted 1:20 with TBS and 3 μL was applied to a glow-discharged, carbon-coated 400-mesh copper grid and blotted off after 15 s. 3 μL of 2% (w/v) uranyl formate stain was applied and immediately blotted off, followed by another application of 3 μL of stain for 45 s, blotted once more, and allowed to air-dry. Images were collected via Leginon (Potter et al., 1999) using an FEI Talos microscope (1.98 A/pixel; 72,000 × magnification; 25 e^{-}/A^{2}). Particles were picked from the raw images using DoG Picker (Voss et al., 2009). 2D classification, 3D sorting and refinement of the complex was conducted using RELION 3.0b0 (Nakane et al., 2018).

Polyclonal EM analysis

Plasma (Pump study: week 10 (bolus), week 12 (2 week pumps) or week 14 (4 week pumps); Dose escalation study: weeks 13 and 15 pooled) was diluted 4X with PBS and incubated with protein A Sepharose beads (GE Healthcare) overnight at 4C. Resin was washed 3X with PBS and eluted with 0.1M glycine pH2.5 and immediately neutralized with 1M Tris-HCL pH 8. Fabs were purified using Pierce Fab preparation kit (Thermo). Fab was generated using Pierce Fab Preparation Kit (Thermo Scientific). Reaction was incubated with protein A Sepharose resin for 1 hour, RT. Fabs were buffer exchanged using Amicon ultra 0.5ml centrifugal filters (Millipore Sigma).

Upon buffer exchange into TBS, 0.5 to 0.8 mg of total Fab was incubated overnight with 10 μg BG505 trimers at RT in ~36 μL total volume. The formed complexes were then separated from unbound Fab via size exclusion chromatography (SEC) using Superose 6 Increase 10/300 column (GE Healthcare) equilibrated with TBS. The flow-through fractions containing the complexes were pooled and concentrated using 100 kDa cutoff centrifugal filters (EMD Millipore). The final trimer concentration was adjusted to approximately 0.04 mg/mL prior to application onto carbon-coated copper grids.

Complexes were applied to glow-discharged, carbon-coated 400-mesh copper grids, followed by applying 3 μL of 2% (w/v) uranyl formate stain that was immediately blotted off, and followed by application of another 3 μL of stain for 45–60 s, and blotted once more. Stained grids were allowed to air-dry and stored under ambient conditions until imaging. Images were collected via Leginon using a Tecnai T12 electron microscopes operated at 120 kV; × 52,000 magnification; 2.05 A/pixel. In all cases, the electron dose was 25 e^{-}/A^{2}. Particles were picked from the raw images using DoG and placed into stacks using Appion software (Lander et al., 2009). 2D reference-free alignment was performed using iterative MSA/MRA) (Sorzano et al., 2010). Finally, the particle stacks were then converted from IMAGIC to RELION-formatted MRC stacks and subjected to RELION 2.1 2D and 3D classification (Scheres, 2012).

Epitopes are pseudocolored as: base (purple), glycan hole-I (light blue), C3/V5 (dark blue), fusion peptide (orange), V1/V3 apex (green).

Whole LN Imaging

All NHP LNs were harvested and immediately placed in PLP buffer (pH 7.4 50 mM PBS + 100 mM lysine, 1% paraformaldehyde, 2 mg/mL sodium periodate) for fixation. After 4-5 days at 4°C, the tissues were washed and stored in PBS with 0.05% sodium azide at 4°C until taken for imaging.

Total antigen signal within LNs from the antigen tracking study was measured by placing the tissues directly on the glass scanning surface of a Typhoon FLA 9500 biomolecular imager (GE Healthcare Life Sciences) and using a 635 nm excitation laser and a $\geq$ 665 nm long-pass filter. The integrated signal density corresponding to Alexa Fluor 647-labeled MD39 in each LN was calculated using ImageJ and plotted using GraphPad Prism 8.

Selected LNs were clarified via a combination / modification of the iDISCO (Renier et al., 2016) and CUBIC (Kubota et al., 2017) organ-clearing methods. The LNs were first delipidated based on the iDISCO methanol incubation protocol. First, the tissues were washed in water for 1 hour, followed by 20% methanol in water for 2 hours. A series of step increases in methanol percentage (40%, 60%, 100%, 100%) followed, each step for 2 hours. The LNs were then placed into 2:1 MeOH:DCM overnight, and the next day were rehydrated with the following series of methanol solutions for 2 hours each: 100%, 100%, 80%, 60%, 40%, 20%, 0%, 0%. Next, the LNs were placed into 10-20 mL of a 1:1 mixture of CUBIC-R solution for 1 day, followed by at least 20 mL of undiluted CUBIC-R for 2 days or as long as needed for adequate clarification. Larger organs were moved into a fresh 20 mL of CUBIC-R solution to ensure that the refractive index of the solution would not be significantly lowered by residual water in the tissue.

Clarified LNs were imaged in CUBIC-R using the LaVision Ultramicroscope II focused beam ligh tsheet using Olympus MVPLAPO 2x Dry lens, magnification: 2.0x, NA: 0.50, WD: 10 mm with short dipping cap. The Alexa Fluor 647-labeled SOSIP was imaged using the 640 nm laser at 100 ms exposure time on an Andor Neo camera with focus magnification: 1.25x. Snapshots and movies were generated using the 3D viewer in the FIJI package of ImageJ.

Histology

Selected LNs were embedded in 3% low melting temperature agarose (Sigma-Aldrich), and then sliced into 350 μm-thick sections using a vibratome. The slices were blocked and permeabilized for 2 days in PBS with 10% goat serum and 0.2% Triton X-100, followed by staining for 3 days with BV421-labeled mouse anti-human CD35 (E11,BD Biosciences) and Alexa Fluor 488-labeled mouse anti-Ki67 (B56, BD Biosciences) in the blocking buffer. Stained slices were then washed for 3 days with PBS containing 0.2% Tween-20, and then mounted onto glass slides with coverslips. Images were captured using an automated spinning disc confocal slide scanner (TissueFAXS Confocal SL, TissueGnostics USA) utilizing a Zeiss Axio Imager Z2 equipped with a Zeiss 20x Plan-Apochromat 0.8NA objective, Lumencor Spectra X light engine, Maerzhauser motorized stage and 120 slide loader, and a Crest Optics X Light V2 confocal imager, along with TissueFAXS slide scanning software.

QUANTIFICATION AND STATISTICAL ANALYSIS

Graphpad Prism v7.0 or 8.0 was used for all statistical analyses. Significance of differences in neutralization, BG505 binding titers, cellular frequencies and mean fluorescent intensities were calculated using unpaired, two-tailed Mann-Whitney U tests. Differences in mutation frequencies and CDR3 length between groups were calculated using unpaired Student's t tests. Significance of differences in V gene use between groups and between Env MFIs (q value) were calculated using multiple t tests, corrected for multiple comparisons with a false discovery rate (FDR) of 5% (Benjamini, Krieger, and Yekutieli). Differences in BCR expression of GC versus non-B_{GC} cells were calculated using paired, Wilcoxon test. Correlations between neutralization and cell frequencies were calculated using log transformed Ab titer values in two-tailed Pearson correlation tests. Differences in fluorescence intensity in LNs were calculated using two-way ANOVA.

DATA AND SOFTWARE AVAILABILITY

Env-specific B cell BCR and whole genome raw reads used in this paper are available at NCBI Sequence Read Archive (https://www.ncbi.nlm.nih.gov/sra). The accession number for the Whole Genome Shotgun project reported in this paper is DDBJ/ENA/GenBank: SBKD00000000. The version described in this paper is version SBKD01000000. The accession number for the raw genomic reads is SRA: PRJNA509445. Raw reads and genome assembly are available under BioProject ID: PRJNA509445. The accession numbers for Env-specific BCR sequences are DDBJ/ENA/GenBank: KCVI00000000, KCVJ00000000, KCVK00000000, KCVL00000000, KCVM00000000, KCVN00000000, KCVO00000000, KCVP00000000, KCVQ00000000, KCVR00000000, KCVS00000000, KCVT00000000, KCVU00000000, KCVV00000000, KCVW00000000, KCVX00000000, KCVY00000000, KCVZ00000000, KCWA00000000, KCWB00000000, KCWC00000000, KCWD00000000, KCWE00000000, KCWF00000000, KCWG00000000, KCWH00000000, KCWI00000000, KCWJ00000000, KCWK00000000, KCWL00000000, KCWM00000000, KCWN00000000, KCWO00000000, KCWP00000000, KCWQ00000000, KCWR00000000, KCWS00000000, KCWT00000000, KCWU00000000, KCWV00000000, KCWW00000000, KCWX00000000, KCWY00000000, KCWZ00000000, KCXA00000000, KCXB00000000,

KCXC00000000, KCXD00000000, KCXE00000000, KCXF00000000, KCXG00000000, KCXH00000000, KCXI00000000, KCXJ00000000, KCXK00000000, KCXL00000000, KCXM00000000, KCXN00000000, KCXO00000000, KCXP00000000, KCXQ00000000, KCXR00000000. Env-specific BCR sequences are available under BioProject ID: PRJNA520929.

The accession numbers for the 3D EM reconstructions are Electron Microscopy DataBank (https://www.emdatabank.org/): EMD-9175, EMD-9176, EMD-9177, EMD-9178, EMD-9179, EMD-9180, EMD-9181, EMD-9182, EMD-9183, EMD-9184, EMD-9185, EMD-9186, EMD-0569, EMD-0570, EMD-0571, EMD-0572, EMD-0573, EMD-0574, EMD-0575,EMD-0576, EMD-0577, EMD-0578, EMD-0579, EMD-0580, EMD-0581, EMD-0582, EMD-9138.

Lymph node GC Panel

Marker	Fluorochrome	Company	Clone
Env probe-biotin	Alexa Fluor 647	Invitrogen	
Env probe-biotin	Brilliant Violet 421	BioLegend	
Viability	efluor506	Thermo Fisher	
CD20	PE-Texas Red	Beckman Coulter	2H7
CD4	Brilliant Violet 650	Biolegend	OKT-4
CD8a	Qdot 705	Thermo Fisher	3B5
IgG	PE-Cy7	BD Biosciences	G18-145
CXCR5	PE	Thermo Fisher	MU5UBEE
PD1	Brilliant Violet 605	Biolegend	EH12.2H7
CD3	Brilliant Violet 786	BD Biosciences	SP34-2
IgM	PerCP-Cy5.5	BD Biosciences	G20-127
KI67	Alexa Fluor 700	BD Biosciences	B56
BCL6	Alexa Fluor 488	BD Biosciences	K112-91

Antigen-specific B cell sorts

Marker	Fluorochrome	Company	Clone
Env probe-biotin	Alexa Fluor 647	Invitrogen	
Env probe-biotin	Brilliant Violet 421	BioLegend	
Viability	efluor780	Thermo Fisher	
CD4	APC efluor780	Thermo Fisher	SK3
CD8a	APC efluor780	Thermo Fisher	RPA-T8
CD16	APC efluor780	Thermo Fisher	ebioCD16
CD20	Alexa Fluor 488	BioLegend	2H7
IgG	PE-Cy7	BD Biosciences	G18-145
IgM	PerCP-Cy5.5	BD Biosciences	G20-127
CD38	PE	NHP Reagents	OKT
CD71	PE-CF594	BD Biosciences (custom)	L01.1

AIM Assay Panel

Marker	Fluorochrome	Company	Clone
CD4	Brilliant Violet 650	BioLegend	OKT4
CD20	Brilliant Violet 570	BioLegend	2H7
PD1	Brilliant Violet 785	BioLegend	EH12.2H7
CXCR5	PE-Cy7	Thermo Fisher	MU5UBEE
CD25	FITC	BioLegend	BC96
OX40	PE	BD Biosciences	L106
4-1BB	APC	BioLegend	4B4-1
Viability	efluor780	Thermo Fisher	
CD8a	APC efluor780	Thermo Fisher	RPA-T8
CD14	APC/Cy7	BioLegend	M5E2
CD16	APC/Cy7	BioLegend	3G8

B_{GC} cell surface marker validation

Marker	Fluorochrome	Company	Clone
Viability	efluor780	Thermo Fisher	
CD20	Brilliant Violet 650	BioLegend	2H7
CD8a	APC efluor780	Thermo Fisher	RPA-T8
CD4	APC	BioLegend	OKT4
CD38	PE	NHP Reagents	OKT
CD71	PE-CF594	BD Biosciences (custom)	L01.1
BCL6	BV421	BD Biosciences	K112-91
KI67	Alexa Fluor 700	BD Biosciences	B56

Macaque BCR expression

Marker	Fluorochrome	Company	Clone
Viability	efluor780	Thermo Fisher	
CD4	APC efluor780	Thermo Fisher	SK3
CD8a	APC efluor780	Thermo Fisher	RPA-T8
CD16	APC/Cy7	BioLegend	3G8
CD20	Brilliant Violet 650	BioLegend	2H7
BCL6	Alexa Fluor 647	BD Biosciences	K112-91
KI67	Alexa Fluor 700	BD Biosciences	B56
IgM	BV421	BD Biosciences	G20-127
IgG	PE	BD Biosciences	G18-145
IgD	Alexa Fluor 488	Southern Biotech	
Lambda	Biotin	Miltenyi	IS7-24C7
Streptavidin	Brilliant Violet 711	BioLegend	

Supplemental Figures

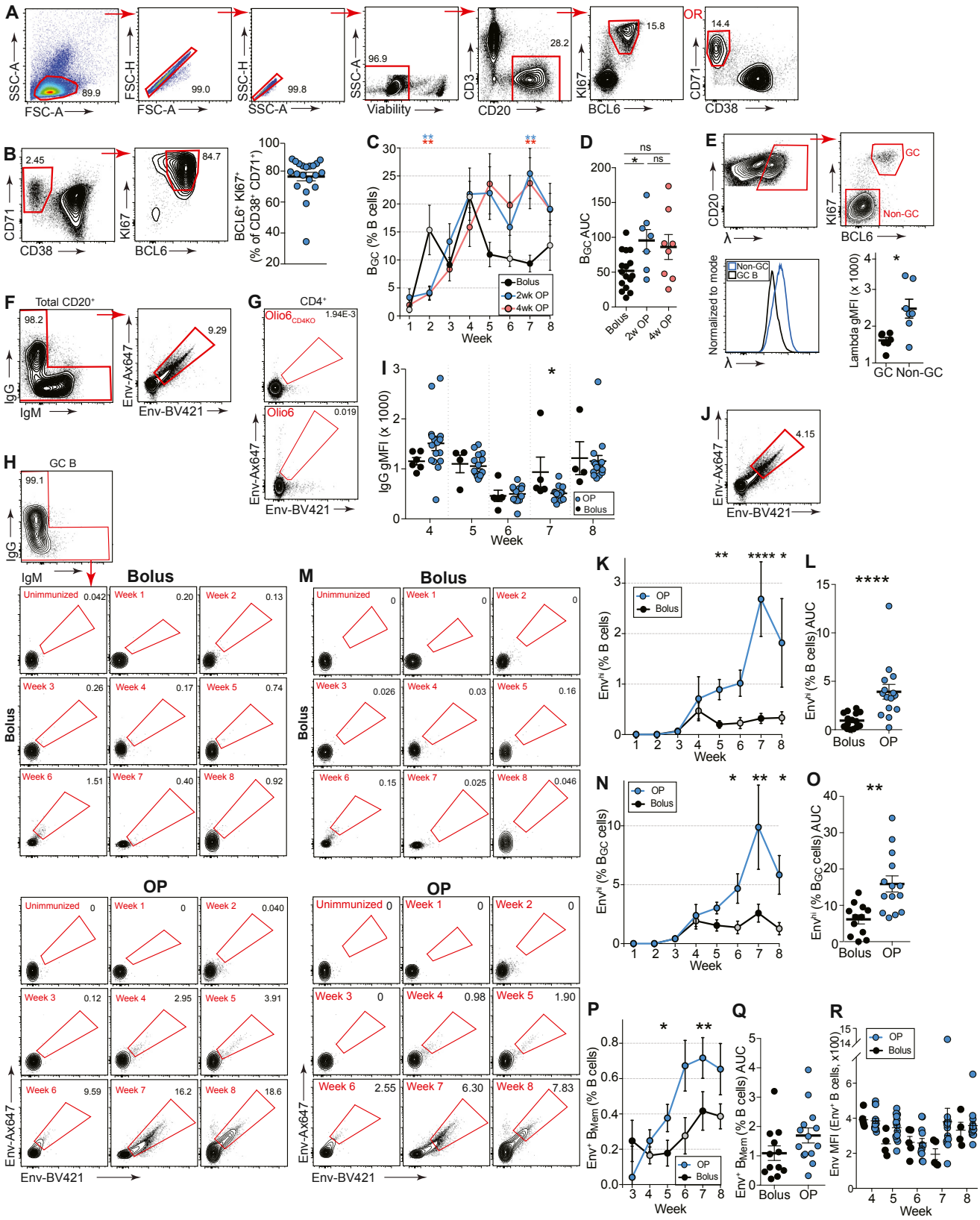

(legend on next page)

Figure S1. B Cell Responses after One Immunization, Related to Figure 1

(A) Full gating strategy of B_{GC} cells. KI67$^+$ BCL6$^+$ expression was used at weeks −1-6, 8-14. CD38$^-$CD71$^+$ expression used at week 7.

(B) Validation of CD38 and CD71 as surface markers for bona fide B_{GC} cells in mesenteric LNs of RM.

(C) B_{GC} frequencies of bolus and individual OP groups. **$p < 0.01$. Blue asterisks, 2w OP versus bolus. Pink asterisks, 4w OP versus bolus.

(D) Cumulative B_{GC} cell responses to first immunization of individual groups between w1 plus w3-7.

(E) Lambda expression in B_{GC} and non-B_{GC} cells. Top panel, gating strategy for B_{GC} and non-B_{GC} cells in LNs. Lower panel, histogram and quantification of lambda expression in lambda$^+$ B_{GC} and non-B_{GC} cells.

(F) Gating strategy of Env trimer-specific B cells, gated on CD20$^+$ cells as per (A).

(G) $Olio6_{CD40ko}$ differs from Olio6 by a single amino acid, to prevent binding to human CD4. Neither trimer binds RM CD4.

(H) Gating strategy and flow cytometry analysis of Env trimer-specific B_{GC} cells over time within an individual LN, gated on CD20$^+$ cells as per (A).

(I) Quantification of IgG gMFI of Env$^+$ B_{GC} cells. Differences in gMFI between weeks is due to use of different panels or flow cytometers for acquisition.

(J) Representative flow cytometry plot of high-affinity Env trimer-specific B cells, gated on CD20$^+$ cells.

(K) Quantification of high-affinity Env trimer-specific B cells over time.

(L) Cumulative high-affinity Env trimer-specific B cell response between w1 and w3-7 [AUC].

(M) Flow cytometry analysis of high-affinity Env-specific B_{GC} cells in a bolus-immunized animal between w-1 and 8.

(N) Quantification of high-affinity Env trimer-specific B_{GC} cells over time.

(O) Cumulative high-affinity Env-specific B_{GC} cell responses within individual LNs between w2 and w7.

(P) Quantification of Env trimer-specific B_{Mem} cells. B_{Mem} were defined as the non-GC (BCL6$^-$ KI67$^-$ or CD38$^+$ CD71$^-$) B cells within the Env-specific B cell gate as per (E).

(Q) Cumulative Env trimer-specific B_{Mem} cell response between w3 and w7 [AUC].

All data represent mean ± SEM.*$p < 0.05$, **$p < 0.01$, ***$p < 0.001$, ****$p < 0.0001$

(R) Mean fluorescent intensities (MFIs) of Env trimer-specific B cells over time. Value calculated as: average of Env_{Ax647} and Env_{BV421} MFIs (Env$^+$ B cells) – average of Env_{Ax647} and Env_{BV421} MFIs (Env$^-$ B cells). As bolus Gp1 was not stained at same time as other groups, Gp1 was not included in these analyses. Number of LNs graphed are: bolus, 6 (w4), 4 (w5), 5 (w6), 5 (w7), 4 (w8); OP, 15 (w4), 15 (w5), 12 (w6), 15 (w7), 15 (w8). Statistical significance was tested using multiple t tests with 5% FDR.

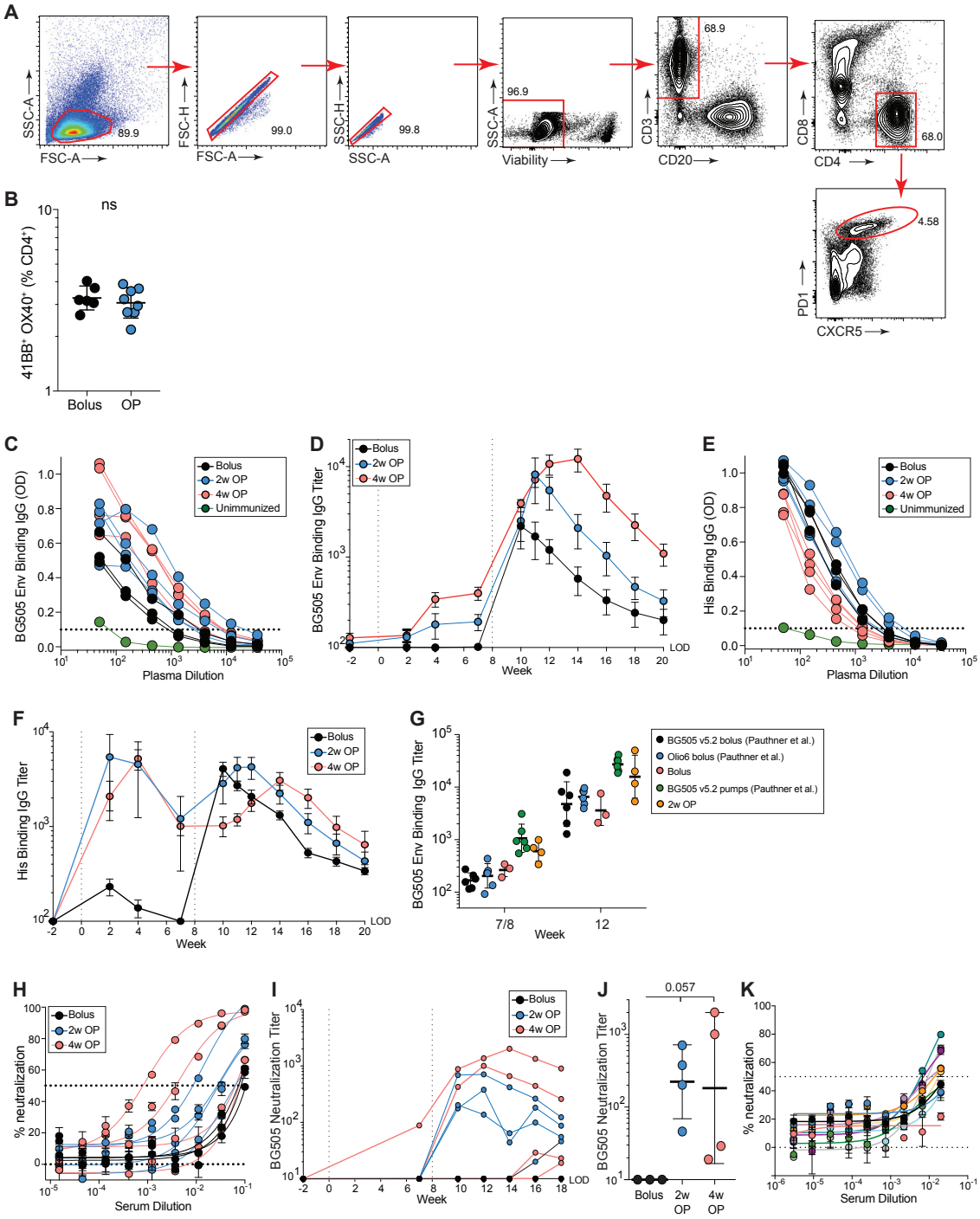

Figure S2. Full GC-T_{FH} Cell Gating Strategy and Serology, Related to Figures 1 and 3

(A) Full gating strategy of GC-T_{FH} cells. GC-T_{FH} cells were measured at all time points, except for w7.

(B) Bolus and OP immunized animals have comparable frequencies of 4-1BB$^+$ OX40$^+$ CD4$^+$ T cells under SEB stimulation of AIM_{OB} assay. SEB stimulation serves as a positive control for the overall health of the cells.

(C) Representative BG505 Env IgG binding IgG curves at w11. Unimmunized control is at w-2.

(D) BG505 Env trimer endpoint binding IgG titers over time.

(E) Representative anti-His binding IgG curves at w11. Unimmunized control is at w-2.

(F) Quantification of anti-His endpoint binding IgG titers over time.

(legend continued on next page)

(G) Direct comparison of BG505 binding IgG titers of animals in this study versus animals in Pauthner et al. For Pauthner et al. groups, plasma from w8 and w12 was used. For bolus and 2w OP groups, plasma from w7 and w12 was used.
(H) Representative BG505 pseudovirus TZM-bl neutralization curves at w14.
(I) Quantification of BG505 neutralization titers between groups over time.
(J) Peak autologous neutralization titers of each animal after two immunizations.
(K) Representative TRO11 pseudovirus TZM-bl neutralization curves at w10 (bolus), w12 (2w OP group, and w14 (4w OP group).
ELISA endpoint titers calculated as dilution at which the O.D. is 0.1 above background. Neutralization titers are reported as ID_{50} titers. All BG505 binding and neutralization data represent geometric mean titers ± geometric SD using BG505 N332.

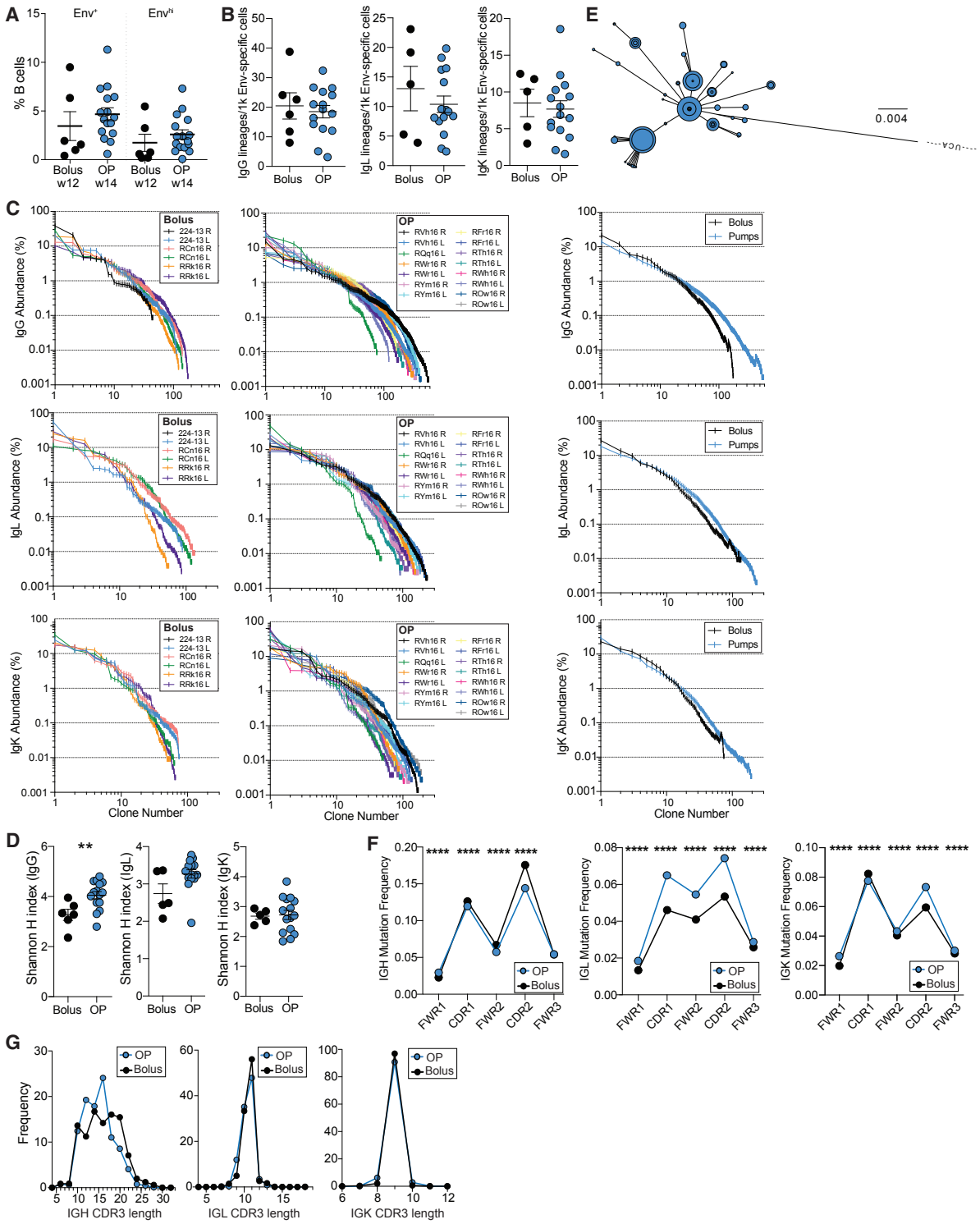

Figure S3. Slow Delivery Immunization Results in More B Cell Diversity, Related to Figure 4

A) Frequencies of Env^{+} and Env^{hi} B cells at sorted time points (bolus, w12 and OP, w14). Env^{+} cells were used for BCR sequencing.

(B) Quantification of IgG, IgL, and IgK lineages normalized by number of cells sorted. Each data point is an individual LN.

(C) Representative phylogenetic analysis of a single Env-specific lineage found in only one LN.

(legend continued on next page)

(D) IgG, IgL, and IgK clonal abundance in individual LNs and within each group.
(E) Shannon H indices of individual LNs. Statistical significance tested using unpaired, two-tailed Mann-Whitney *U* test. **p < 0.01
(F) Comparison of mutation frequencies across BCR. Statistical significance tested using Student's t test, ****p < 0.0001
(G) Comparison of length of CDR3 in heavy and light chains.

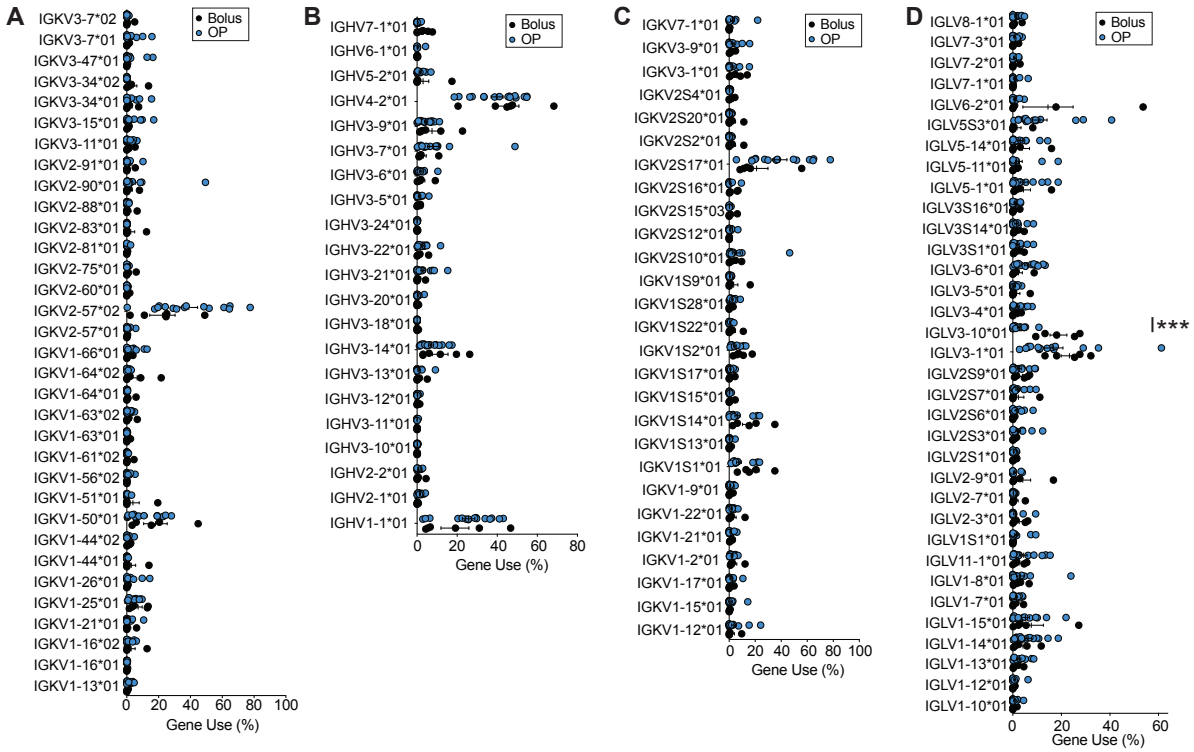

Figure S4. Slow Delivery Alters the Env-Specific B Cell Repertoire, Related to Figure 5

(A) Frequency of IGKV gene use, assessed using genomic RM reference in this study.

(B) Frequency of IGHV genes used by BCRs sequenced in Figure 6, assessed using IMGT database.

(C) Frequency of IGKV gene use, assessed using IMGT database.

(D) Frequency of IGLV gene use, assessed using IMGT database. ***q < 0.001, FDR = 5%.

Mean ± SEM are graphed.

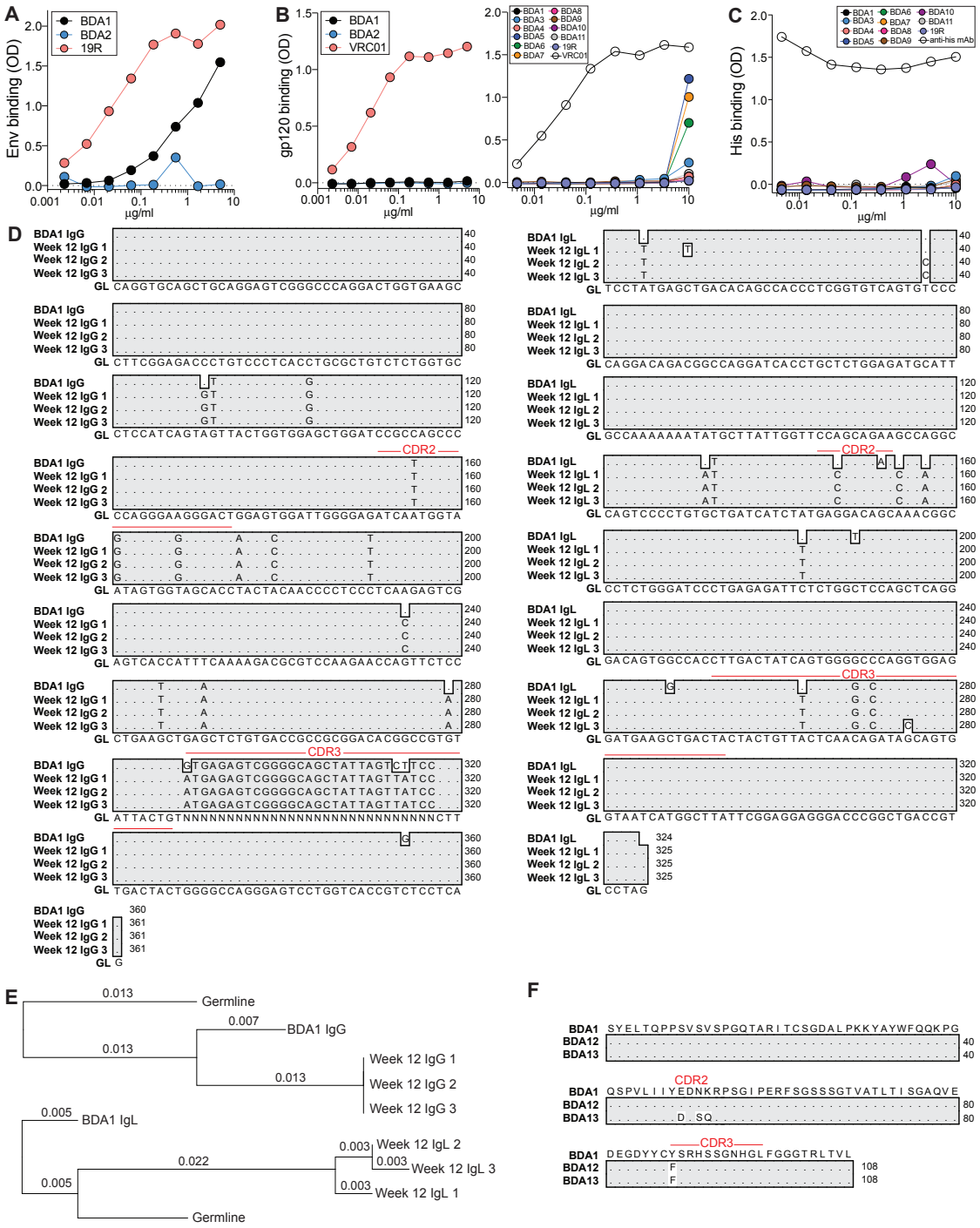

Figure S5. IGLV3-15*01-Utilizing mAbs Recognize the Base of the Env Trimer, Related to Figure 5

(A) Binding curves of BDA2, and control mAb, 19R to Env trimer. 19R is a high-affinity base-binding mAb. BDA2 showed no binding to Env trimer.

(B) Binding curves of isolated mAbs and control VRC01 and 19R mAbs to gp120. VRC01 is an HIV-1 bnAb that recognizes the CD4 binding site and gp120 monomer.

(C) Binding curves of isolated mAbs and control anti-His mAb to His peptide.

(D) Nucleotide alignment of week 7 BDA1 heavy and light chains, its inferred germline sequences and three closest w12 Env-specific BCR sequences.

(E) Phylogenetic analyses of sequences in B.

(F) Protein alignment of BDA1 and related mAbs.

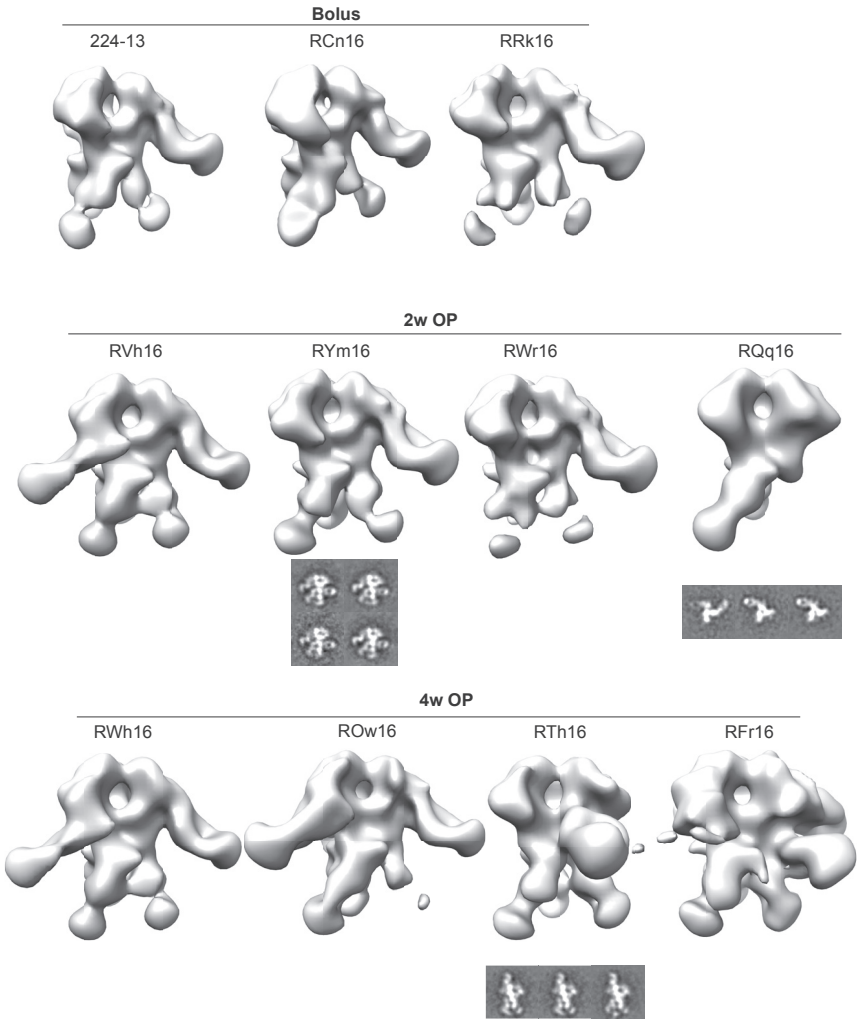

Figure S6. Pump-Immunized Animals Recognize a Diverse Set of Epitopes, Related to Figure 5

3D reconstructions of Fab-binding in individual animals. Fabs targeting regions in some animals were rare and were not included in individual 3D reconstructions, but are presented in the 2D images.

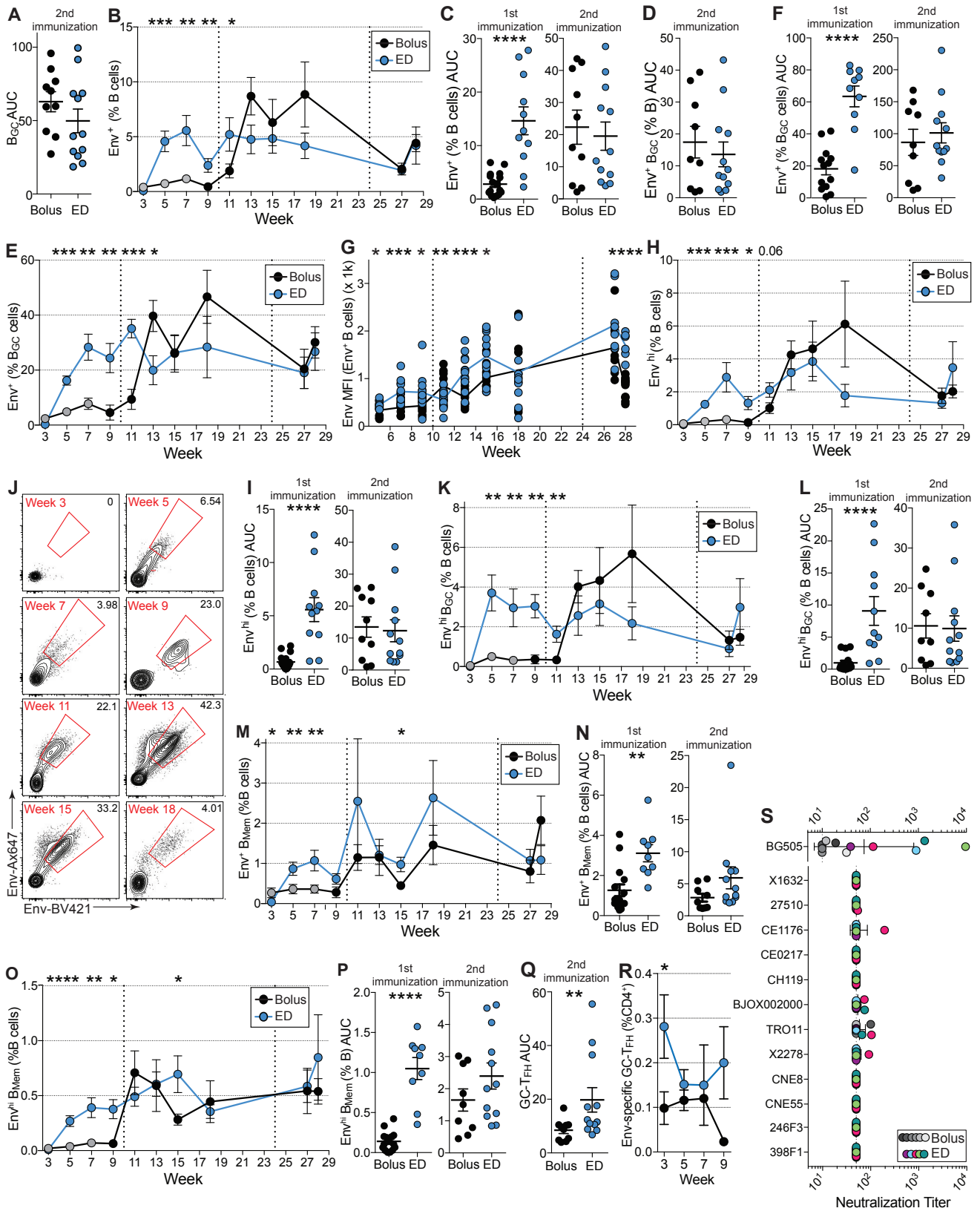

(legend on next page)

Figure S7. Dose Escalation Immunization Enhances Ag-Specific B and CD4$^+$ Responses, Related to Figure 6

(A) Cumulative B_{GC} cell responses to the 2nd immunizations [AUC]. AUC was calculated between w11- 15.
(B) Quantification of Env trimer-specific B cells over time.
(C) Cumulative Env trimer-specific B cell responses to one and two immunizations [AUC].
(D) Cumulative Env trimer-specific B_{GC} cell responses to the 2nd immunization [AUC].
(E) Frequency of Env trimer-specific B_{GC} cells over time.
(F) Cumulative Env trimer-specific B_{GC} cell responses to one and two immunizations [AUC].
(G) Mean fluorescent intensities (MFIs) of Env trimer-specific B cells over time. Value calculated as: average of Env_{Ax647} and Env_{BV421} MFIs (Env^+ B cells) – average of Env_{Ax647} and Env_{BV421} MFIs (Env^- B cells). Number of LNs graphed are: bolus, 12 (w5), 11 (w7), 11 (w9), 10 (w11), 11 (w13), 11 (w15), 7 (w18), 9 (w27), 12 (w28); ED, 10 (w5), 12 (w7), 12 (w9), 12 (w11), 12 (w13), 12 (w15), 10 (w18), 8 (w27), 6 (w28). Statistical significance was tested using multiple t tests with 5% FDR. *q < 0.05, **q < 0.01, ***q < 0.001, ****q < 0.0001.
(H) Frequency of high-affinity Env trimer-specific B cells over time.
(I) Cumulative high-affinity B cell responses to one and two immunizations [AUC].
(J) Flow cytometry analysis of high-affinity Env trimer-specific B_{GC} cells in a bolus immunized animal between w-1 and w8.
(K) Frequency of high-affinity Env trimer-specific B_{GC} cells over time.
(L) Cumulative high-affinity B_{GC} cell response to one and two immunizations [AUC].
(M) Quantification of Env-specific B_{Mem} cells over time.
(N) Cumulative Env trimer-specific B_{Mem} cells to one and two immunizations [AUC].
(O) Quantification of high-affinity Env trimer-specific B_{Mem} cells over time.
(P) Cumulative high-affinity Env trimer-specific B_{Mem} cells responses to one and two immunizations [AUC].
(Q) Cumulative GC-T_{FH} cell responses to the 2nd immunization [AUC].
(R) Quantification of Env trimer-specific GC-T_{FH} cells after 1 immunization.
(S) Neutralization breadth using 12-virus panel at w26 (bolus) and w27 (ED).
Cell-frequency data represent mean ± SEM. Statistical significance was tested using unpaired, two-tailed Mann-Whitney *U* tests, unless otherwise noted. *p < 0.05, **p < 0.01, ***p < 0.001, ****p < 0.0001.

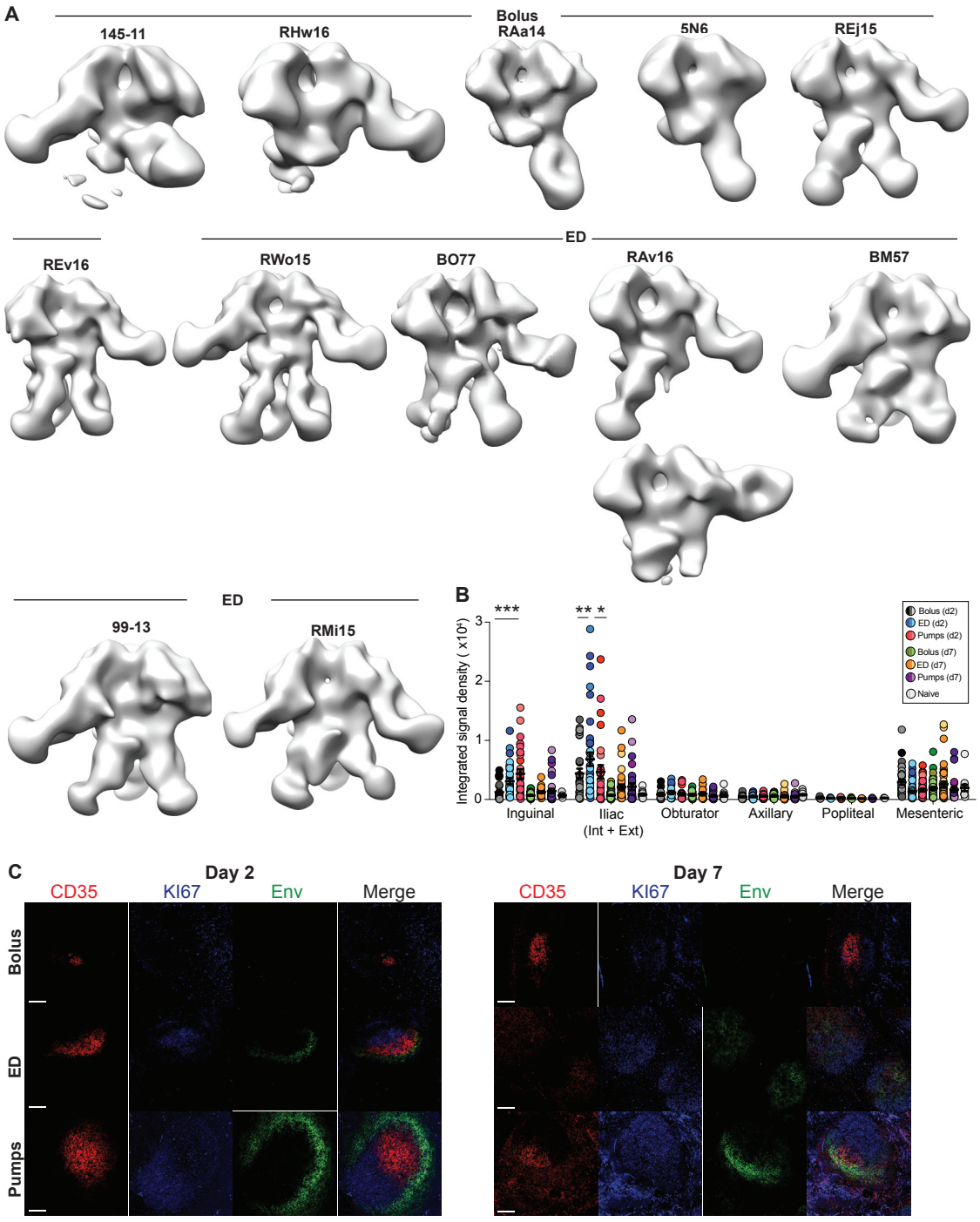

Figure S8. Slow Delivery Immunization Results in Enhanced Ag Retention in LNs, Related to Figures 6 and 7

(A) 3D reconstructions of Fab-binding in individual animals.

(B) Quantitation of Env_{AX647} (Alexa647-labeled MD39) in all harvested LNs from RMs immunized via conventional bolus, 2w OP, or an ED regimen. Mean ± SEM are graphed. Statistical significance was tested using two-way ANOVA. *adjusted $p < 0.05$, **$p < 0.01$, ***$p < 0.001$

(C) Histology of draining LNs at d2 and d7 of all three immunization groups. Green, Env; red, CD35; blue, KI67. Scale bars, 100 μm. D7 bolus image panel is same as that in Figure 7C.